PFC/RR-89-14 DOE/ET-51013-275

Simulation of Drift Wave Turbulence: Trapped Structures and a New Nonadiabatic Electron Model

James Allen Crotinger

March 1989

Plasma Fusion Center
and the
Department of Nuclear Engineering
Massachusetts Institute of Technology
Cambridge, Massachusetts 02139 USA

SIMULATION OF DRIFT WAVE TURBULENCE: TRAPPED STRUCTURES AND A NEW NONADIABATIC ELECTRON MODEL

by

JAMES ALLEN CROTINGER

B.S., Nuclear Engineering
Kansas State University
(1983)

Submitted to the Department of Nuclear Engineering
in partial fulfillment of the requirements for the degree of

Doctor of Philosophy

at the

MASSACHUSETTS INSTITUTE OF TECHNOLOGY

March 1989

Signature of Author..
Department of Nuclear Engineering
March 15, 1989

Certified by..
Thomas H. Dupree
Professor of Nuclear Engineering and Physics
Thesis Supervisor

Accepted by..
Allan F. Henry
Chairman, Departmental Committee on Graduate Students

SIMULATION OF DRIFT WAVE TURBULENCE: TRAPPED STRUCTURES AND A NEW NONADIABATIC ELECTRON MODEL

by

JAMES ALLEN CROTINGER

Submitted to the Department of Nuclear Engineering
on March 15, 1989, in partial fulfillment of the
requirements for the degree of
Doctor of Philosophy

Abstract

The development of trapped structures in decaying and saturated drift wave turbulence is studied via computer simulation. A two-dimensional electrostatic fluid model is used. The turbulence which evolves in the pure decay runs (no nonadiabatic electrons) is characterized by tightly bound monopole vortices and a very narrow frequency spectrum. These results are qualitatively similar to results found in two dimensional Navier-Stokes simulations. For the studies of saturated turbulence, rather than simply introducing the linear growth rate, a new nonadiabatic electron model is used. This model takes into account the effects of broadening and shifting of the frequency spectrum which results from the strongly nonlinear character of the problem—effects which are found to be very important in the turbulent states which are studied. These states are characterized by broadened frequency spectra, with strong damping on the nonadiabatic electrons at high-k and along the k_x-axis. Trapped structures are observed in many of the saturated simulations, even in the presence of moderately broad frequency spectra. The extent of the trapping varied dramatically, becoming a much stronger effect as the RMS electric field increased.

Thesis Supervisor: Thomas H. Dupree
Title: Professor of Nuclear Engineering and Physics

Acknowledgements

I would like to thank my advisor, Prof. Thomas H. Dupree, for his assistance, supervision, and support. Tom's insight into the problems of plasma turbulence, and his talents for conveying his ideas to others, have been invaluable elements in my education. He is truly a remarkable teacher.

I would also like to thank the many members of the Plasma Fusion Center community with whom I've interacted. I would especially like to mention Prof. Jeffrey P. Freidberg, Prof. Dieter Sigmar, Prof. Kim Molvig, Dr. Scott W. Haney, Dr. Pekka Hakkarainen, Dr. Abdelhaq Hamza, Dave Humphreys, and Ken Kupfer. These folks have greatly enriched my experience at M.I.T.

I would like to acknowledge the financial support I received from the U.S. Department of Energy: this research was performed in part in conjunction with the Magnetic Fusion Energy Science Fellowship Program which is administered for the United States Department of Energy by Oak Ridge Associated Universities.

I would also like to thank the Institute for Fusion Studies—especially Prof. Wendell Horton, Prof. Toshi Tajima, Prof. Richard Hazeltine, and Carolyn Valentine—for their hospitality during my summer practicum in 1986.

This thesis was typeset with AmigaTEX, an extraodinary implementation of Don Knuth's TEX program for the Commodore Amiga personal computer. I would like to thank Don Knuth for this wonderful program, and Tomas Rokicki, the author of AmigaTEX, for his even more wonderful implementation.

Finally, I would like to thank my wife, Tamara, for her patience, love, and support, and my sons, Jamie and Jeffrey, whose smiles and love have kept us going.

James Allen Crotinger

Contents

List of Tables

List of Figures

Chapter 1

Introduction

1.1 Goals

Do coherent "trapped" structures exist in saturated drift wave turbulence? Or is the turbulence more properly characterized as a collection of waves with random phases? In this thesis, I will try to address this question via direct numerical simulation of a two dimensional model equation.

Several other authors (Hasegawa and Mima[1, 2], Terry and Horton [3, 4, 5, 6], and Waltz [7]) have studied two dimensional drift wave turbulence using equations similar to the one used in this work. This thesis has a somewhat different focus, however, in its concentration on trapped structures in fully developed turbulence. Furthermore, a new model for the nonadiabatic electron response is used, which is necessary to correctly simulate the interaction of the electrons with a coherent structure. The effects of this new model are studied in some detail.

1.2 Motivation

The most pressing problem in fusion plasma physics today is that of *anomalous* transport of particles and energy in tokamak confinement experiments. The goal of the fusion program is to confine a plasma at a sufficient density and for an adequate time such that a significant number of particles will fuse. Early estimates indicated that there should have been no problem in attaining the necessary confinement conditions. Experiments, however, have been plagued by anomalous transport processes, drastically reducing the energy and particle confinement time. The electron heat transport, for instance, is measured to be a factor of 10–100 above the expected value. The particle transport is also found to be anomalously high, although not to the same degree [8].

Anomalous transport processes are believed to be primarily due to low frequency turbulence driven by the density and temperature gradients necessary to have a confined plasma. Experimental measurements of the the density and potential indicate that there is a continuous spectrum of fluctuations characterized by an average scale size $k^{-1} \sim \rho_s$, and an average frequency $\omega \sim \omega_{*e}$ [8]. Here ρ_s is the ion Larmor radius at the electron temperature, and ω_{*e} is the electron diamagnetic drift frequency. These scale sizes are consistent with various types of drift waves, all of which have frequencies of approximately ω_{*e}, and whose linear growth rates peak at $k\rho_s \sim 1$.

The density and potential fluctuations are found to have spectral characteristics which indicate that the system is in a strongly turbulent state: The frequency and wave number spectra are found to be continuous. The frequency spectrum is characterized by a broad width, $\Delta\omega \sim \omega$, and the wave number spectrum is observed to be nearly isotropic perpendicular to the magnetic field. The fluctuation levels are a few percent:

$$\frac{e\phi}{T_e} \sim \frac{\tilde{n}}{n_0} \sim \frac{\rho_s}{L_n} \sim 3\text{–}5\%.$$

We shall see in Chapter 2 that these fluctuation levels are sufficiently large to make our model equation strongly nonlinear.

1.3 Turbulence Theory

Turbulence, by its very nature, is not predictable. Rather one must form a theory for the statistical properties of the turbulence, which ultimately would lead to an estimate of the average transport. For such a theory to be believable, it must be consistent with the underlying dynamical equations.

The usual approach to these statistical theories is to derive moment equations for the various correlation functions from the original dynamical equation. Due to the nonlinearity, this process results in an infinite hierarchy of moment equations, with the evolution equation for each moment depending on moments of a higher order. This is exactly analogous to the B.B.G.K.Y. hierarchy in plasma physics. The question, then, is how to truncate this hierarchy and obtain a finite set of equations which give a good approximation to reality. Unlike the familiar closure problems in plasma transport theory, there is no good expansion parameter in a strongly turbulent system—the very definition of *strong* turbulence implies that the nonlinear terms are just as big as, or bigger than, the linear terms.

If this is the case, then regular perturbation theory, or *weak turbulence theory*, makes no sense at all. Indeed, these expansions contain time secularities which cause them to diverge with time, leading to nonphysical results.

Weak turbulence theory has been extended to give resonance broadening theory [9, 10], the Direct Interaction Approximation (DIA) [11, 12], and clump theory [13, 14, 15, 16, 17]. These theories result from summing an infinite subset of the perturbation expansion in an attempt to remove the worst secularities, a technique known as renormalized perturbation theory.

The resonance broadening theory may be derived by adding a random, diffusive perturbation to the particle's linear orbit, which essentially renormalizes the linear propagator. Thus it has a simple and elegant physical interpretation. Unfortunately, in certain cases (including the drift wave problem) this theory has some serious flaws in that it fails to conserve energy and does not reduce to the weak turbulence equations in the limit of small fluctuations [15, 18].

In contrast, the equations of the DIA are complicated in the extreme, and are very hard to understand from a physical point of view. They consist of coupled nonlinear integro-differential (non-Markovian) equations for the spectrum and the response function. The full equations have never been solved for the plasma problem, although several simplified versions have been studied [7, 18]. The theory does, however, possess an interesting property: it can be shown to be an exact statistical description of a certain contrived model problem [19, 20, 21]. Thus it satisfies all the necessary realizability conditions and, in essence, must be well behaved. Many people have taken this fact as implying that the DIA must also be a good approximation. This is not necessarily the case. In spite of all the wonderful renormalization, the DIA is still a perturbation theory. If the fluctuations are truly large, then the non-secular terms which the DIA has neglected are not small.

When is the plasma turbulence too strong for the DIA? There is no easy answer to this question since the DIA always gives a well behaved result. But from a physical point of view, the perturbation theory will break down completely when the turbulence gets sufficiently strong to *trap* particles. In the fluid model of drift wave turbulence this means that the fluctuations are sufficiently strong that the $\mathbf{E}\times\mathbf{B}$ drift of the particles is larger than the diamagnetic drift, which results in the formation of eddies whose lifetimes are longer than a drift wave period. Once these coherent structures form, the orbits of the fluid particles can no longer be described by perturbation theory, invalidating the assumptions of the DIA.

The clump theory is a physically motivated turbulence theory which concentrates on the formation and dynamics of semi-coherent blobs of charge [13, 14, 15]. It incorporates in a readily understandable way the ideas of mixing and orbit instability. The clump theory may be derived via a renormalization procedure [16, 17], although this derivation, as with the DIA's, is without foundation if the clump lifetime becomes on the order of, or larger than, the trapping time. In this case, the clump becomes a phase space density hole, and a more phenomenological approach is needed in order to make the clump picture fit.

Thus we are led to our problem: Do trapped structures form in saturated drift wave turbulence? We will try to answer this question by solving the dynamical equation for the potential fluctuations. We shall see that trapped structures can form and last for many drift periods, even in driven turbulence with a moderately broad frequency spectrum.

1.4 Outline

Some fairly drastic assumptions have been made in deriving our model equation. The ions are treated as cold, so there are no finite Larmor radius effects. The electrons are treated as being nearly adiabatic with a constant temperature. The equilibrium density profile is taken to be exponential so that diamagnetic drift speed is a constant. The ion dynamics are treated in two dimensions (perpendicular to the magnetic field), and there is no magnetic shear. These assumptions neglect a great deal of important physics. However they maintain the main nonlinearity in the problem, and are sufficiently simple that we can afford to solve them many times with a fairly high resolution.

The model equation based on these assumptions is derived in Chapter 2. To lowest order, this equation is just the Hasegawa-Mima equation [1]. Terry and Horton [3, 4, 5], and Waltz [7] have also studied extensions to this equation. However they made use of rather *ad hoc* expressions for the nonadiabatic electron response which are plainly wrong in the presence of coherent structures. We derive a form for the nonadiabatic response which approximates the correct behavior of the electrons in the limit of coherent structures, and which also reduces to the linear growth rate in the limit of small amplitude fluctuations.

Chapter 3 contains a discussion of the numerical technique used to solve the equations derived in Chapter 2. We employ a spectral approximation for the spatial derivatives, with all the aliasing terms removed. A high order Runge-Kutta algorithm is used to advance the equations in time. The resulting code is free of aliasing instabilities, and is found to give accurate solutions to an exact test problem.

Chapters 4 and 5 deal with solutions to the Hasegawa-Mima equation. This equation is essentially correct on a short time scale, and is about a factor of 5 less expensive to simulate. We try to learn as much as possible about its solutions before moving on to our more complicated model. In Chapter 4 we look at the simulation of isolated trapped structures. The Hasegawa-Mima equation possesses a family of exact solutions. We derive the simplest member of this family, the *modon* or dipole vortex, and study its properties. Several reasons are given as to why it is unlikely that such structures would actually evolve in a turbulent system. Next we look at the evolution of isolated monopole vortices. These are not exact solutions to the equations, but it is shown that they can have very long lifetimes and that they are generally more robust than the modon.

The turbulence of the Hasegawa-Mima equation is studied in Chapter 5. Here we attempt to understand how trapped structures might evolve in a turbulent system. Like the two-dimensional Navier-Stokes equations, this equation exhibits a *dual cascade*—energy tends to flow to long wavelengths, and enstrophy, to short wavelengths. In the presence of viscous damping, the dual cascade results in a quick decay of the total enstrophy relative to the decay of the energy. This leads us to the *selective decay* model, in which we derive an equation for the final state of the system by minimizing the enstrophy with the constraint of fixed energy. It is shown that another variational principle, which may be interpreted as maximizing the local entropy, leads us back to the equation for an isolated structure, derived in Chapter 4.

Simulations of the Hasegawa-Mima equation show that the system relaxes quickly to a state consisting of many monopole structures with sizes on the order of a few ρ_s. This quick relaxation is followed by a quasistationary state in which the average scale length slowly increases as monopoles slowly merge and grow larger. These structures are seen to have extremely long lifetimes, and the turbulence is observed to have a very narrow frequency spectrum. It is conjectured that these structures are somehow local solutions to the variational principle described above.

A comparison is made with a similar model in which no density gradient is present. The spectral evolution of the two systems is found to be similar. However the tendency to form isolated monopole vortices is much stronger in the zero-gradient case, where monopole structures are exact isolated solutions.

Finally, in Chapter 6, we look at the changes which occur when our nonadiabatic electron model is included. The resulting turbulence has a broadened frequency spectrum, which causes the nonadiabatic electrons to act as a sink, as well as a source, of energy. We calculate a nonlinear growth rate due to the nonadiabatic electrons. It is found to be strongly negative at high-k and along the k_x-axis. In spite of the broadened spectrum, we still find that trapped structures tend to form. Their behavior is modified significantly, however. Their motion is now much more dynamic. They tend to wander about in the x direction and to undergo strong shape changes on a time scale somewhat longer than the eddie turnover time. The extent of their dominance—the number of vortices and the fraction of the fluid which is trapped—depends on the input parameters to the problem.

Chapter 2

The Model

Several related model equations for describing drift waves are derived in the following sections. We are primarily interested in obtaining a simple model equation that contains the essential nonlinear dynamics. Thus we will consider only the case of the electrostatic universal mode in an unsheared slab. This simplification neglects a great deal of very important physics: magnetic shear, ion kinetic and gyrokinetic effects, electron and ion motions along the field lines (although these will be touched upon during the derivation), trapped electrons, the effects of temperature and magnetic field fluctuations, etc. Certainly we cannot expect to make accurate predictions of tokamak transport using our model! But there is still a great deal to be learned from the simpler turbulent systems, and the simulations are much more practical, given todays level of computers.

2.1 General Assumptions

2.1.1 Geometry

We consider a slab plasma as shown in Fig. 2.1, where the magnetic field is constant and in the $\hat{\mathbf{z}}$ direction, and the density gradient is in the $-\hat{\mathbf{x}}$ direction.

2.1.2 Length and Time Scales

The plasma will be treated in the low frequency, long wavelength regime:

$$\frac{\omega}{k_{\|}v_{th_i}} \gg 1, \tag{2.1}$$

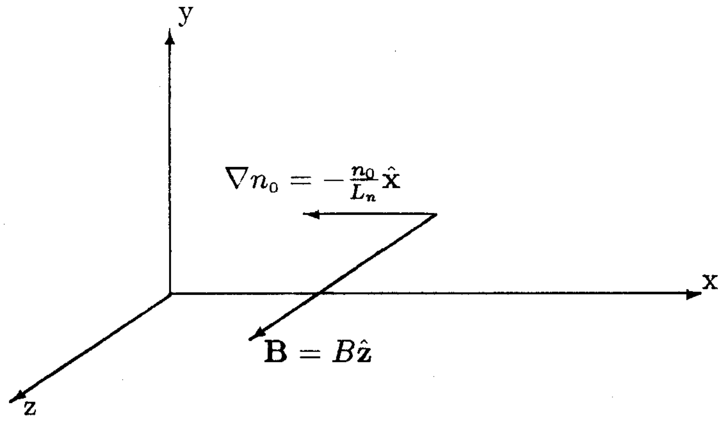

Figure 2.1: *Coordinate system for our slab plasma.*

$$\frac{\omega}{k_\parallel v_{th_e}} \ll 1, \tag{2.2}$$

and

$$k^2 \lambda_{\mathrm{Debye}}^2 \ll 1, \tag{2.3}$$

where ω is a characteristic frequency for the turbulence, $\mathbf{k} = k_\parallel \hat{\mathbf{z}} + \mathbf{k}_\perp$ is a characteristic wave vector, k is its magnitude, v_{th_i} and v_{th_e} are the ion and electron thermal velocities, and λ_{Debye} is the Debye length. These assumptions allow us to treat the ions as a fluid, to treat the electrons as being nearly adiabatic, and to treat the plasma as being quasineutral. This is still a fairly complex system. We further restrict the problem with an ordering that is appropriate for drift waves and ion acoustic waves:

$$\frac{\omega}{\Omega_i} \sim \frac{\rho_s}{L_n} \equiv \epsilon \ll 1, \tag{2.4}$$

$$k_\perp \rho_s \sim 1, \tag{2.5}$$

and

$$\frac{k_\parallel}{k_\perp} \sim \epsilon, \tag{2.6}$$

where Ω_i is the ion gyrofrequency, ρ_s is the ion gyroradius at the electron temperature, L_n is the density scale length, and $k_\perp = |\mathbf{k}_\perp|$. This ordering allows us to greatly simplify the ion fluid equations. The ordering for $k_\parallel$ given in Eq. (2.6) will later be changed to $k_\parallel \ll \epsilon k_\perp$, allowing us to handle the ion dynamics in two dimensions.

2.1.3 Field Amplitudes

Experimental measurements of the electric potential fluctuations in tokamak plasmas show that [22, 23, 8]

$$\frac{e\phi}{T_e} \approx 5\%,$$

where ϕ is the potential, e is the magnitude of the electron charge, and T_e is the electron temperature. To a good approximation the fluctuation levels scale as ρ_s/L_n. We shall assume all fluctuating quantities to be of this order:

$$\frac{e\phi}{T_e} \sim \frac{n_1}{n_0} \sim \frac{v_\parallel}{c_s} \sim \frac{\rho_s}{L_n}, \tag{2.7}$$

where n_1 is the ion density fluctuation, $v_\parallel$ is the parallel component of the ion velocity, n_0 is the equilibrium density, and $c_s = \rho_s \Omega_i$ is the ion sound speed.

2.2 The Ion Fluid Equations

Under the assumptions stated in Eqs. (2.1)–(2.3), the ions obey the following continuity and momentum equations:

$$\frac{\partial n_i}{\partial t} + \nabla \cdot (n_i \mathbf{v}_i) = 0, \tag{2.8}$$

$$n_i m_i \left(\frac{\partial \mathbf{v}_i}{\partial t} + \mathbf{v}_i \cdot \nabla \mathbf{v}_i \right) = -\nabla p_i + \nu \nabla^2 \mathbf{v}_i + n_i q_i \left(\mathbf{E} + \frac{1}{c} \mathbf{v}_i \times \mathbf{B} \right). \tag{2.9}$$

where n_i is the ion density, m_i, the mass, q_i, the charge, $\mathbf{v}_i$, the fluid velocity, p_i, the ion pressure, and $\nu = \nu_{ii} p_i / \Omega_i^2$, the viscosity [24], ν_{ii} being the ion-ion collision frequency.

2.2.1 The Parallel Velocity Equation

We proceed by separating the ion continuity equation into its parallel and perpendicular components. The parallel component of Eq. (2.9) is simply

$$n_i m_i \left(\frac{\partial v_\parallel}{\partial t} + \mathbf{v}_i \cdot \nabla v_\parallel \right) = -\frac{\partial p_i}{\partial z} + \nu \nabla^2 v_\parallel - n_i q_i \frac{\partial \phi}{\partial z}. \tag{2.10}$$

2.2.2 The Perpendicular Velocity Equation

The perpendicular component of Eq. (2.9) is found by taking the cross product of $\hat{\mathbf{z}}$ with Eq. (2.9), and then solving for $\mathbf{v}_\perp$:

$$\begin{aligned} \mathbf{v}_\perp &= \frac{e}{nqB}\,\hat{\mathbf{z}}\times\nabla p_i + \frac{c}{B}\,\hat{\mathbf{z}}\times\nabla\phi \\ &\quad + \frac{\nu}{nm}\frac{1}{\Omega_i}\nabla^2\,\hat{\mathbf{z}}\times\mathbf{v}_\perp + \frac{1}{\Omega_i}\left(\frac{\partial}{\partial t} + \mathbf{v}_i\cdot\nabla\right)\hat{\mathbf{z}}\times\mathbf{v}_\perp . \end{aligned} \tag{2.11}$$

We recognize that $\mathbf{v}_\perp$ is composed of the diamagnetic drift, $\mathbf{E}\times\mathbf{B}$ drift, and the inertial and viscous drifts. The latter are down by ω/Ω_i, and so they may be calculated perturbatively. This leads to

$$\mathbf{v}_\perp = \mathbf{v}_* + \mathbf{v}_{\mathrm{E}} + \mathbf{v}_\nu + \mathbf{v}_m, \tag{2.12}$$

where

$$\begin{aligned} \mathbf{v}_* &= \frac{c}{nqB}\,\hat{\mathbf{z}}\times\nabla p_i, \\ &= \frac{\rho_s c_s}{\tau}\,\hat{\mathbf{z}}\times\nabla\log n, \end{aligned} \tag{2.13}$$

$$\mathbf{v}_{\mathrm{E}} = \frac{c}{B}\,\hat{\mathbf{z}}\times\nabla\phi, \tag{2.14}$$

$$\begin{aligned} \mathbf{v}_\nu &= \frac{\nu}{nm}\frac{1}{\Omega_i}\nabla_\perp^2\,\hat{\mathbf{z}}\times\mathbf{v}_\perp, \\ &= -\frac{\nu_{ii}}{\Omega_i}c_s\rho_s^3\nabla_\perp^2\nabla_\perp\left(\frac{e\phi}{T_e}\right), \end{aligned} \tag{2.15}$$

and

$$\begin{aligned} \mathbf{v}_m &= \frac{1}{\Omega_i}\left(\frac{\partial}{\partial t} + (v_\parallel\hat{\mathbf{z}} + \mathbf{v}_* + \mathbf{v}_{\mathrm{E}})\cdot\nabla\right)\hat{\mathbf{z}}\times(\mathbf{v}_* + \mathbf{v}_{\mathrm{E}}), \\ &\approx \frac{1}{\Omega_i}\left(\frac{\partial}{\partial t} + (\mathbf{v}_* + \mathbf{v}_{\mathrm{E}})\cdot\nabla\right)\hat{\mathbf{z}}\times(\mathbf{v}_* + \mathbf{v}_{\mathrm{E}}), \end{aligned} \tag{2.16}$$

and where $\tau = T_e/T_i$ is the ratio of the electron to ion temperatures. The parallel convective derivative has been neglected in Eq. (2.16) since it is down by an order in magnitude.

Throughout this thesis the temperature profile shall be taken to be flat and independent of time. For now we will also assume that $T_e \sim T_i$, although we will later only consider cold ions. With T_i constant, the diamagnetic and $\mathbf{E} \times \mathbf{B}$ velocities may be combined by defining

$$\begin{aligned} \mathbf{v}_\psi &= \mathbf{v}_* + \mathbf{v}_{\mathrm{E}}, \\ &= \rho_s c_s \, \hat{\mathbf{z}} \times \nabla \left(\tau^{-1} \log n + \frac{e\phi}{T_e} \right), \\ &= \rho_s c_s \, \hat{\mathbf{z}} \times \nabla \psi, \end{aligned} \tag{2.17}$$

where

$$\psi \equiv \frac{1}{\tau} \log n + \frac{e\phi}{T_e}. \tag{2.18}$$

In terms of $\mathbf{v}_\psi$, we have

$$\mathbf{v}_m = \frac{1}{\Omega_i} \left(\frac{\partial}{\partial t} + \mathbf{v}_\psi \cdot \nabla \right) \hat{\mathbf{z}} \times \mathbf{v}_\psi, \tag{2.19}$$

but

$$\begin{aligned} \hat{\mathbf{z}} \times \mathbf{v}_\psi &= \rho_s c_s \, \hat{\mathbf{z}} \times (\hat{\mathbf{z}} \times \nabla_\perp \psi), \\ &= -\rho_s c_s \nabla_\perp \psi, \end{aligned}$$

so that Eq. (2.19) becomes

$$\mathbf{v}_m = -\rho_s^2 \left(\frac{\partial}{\partial t} + \mathbf{v}_\psi \cdot \nabla \right) \nabla_\perp \psi. \tag{2.20}$$

2.2.3 The Continuity Equation

The perpendicular component of the velocity was found above explicitly in terms of ψ, ϕ, $v_\parallel$, and n_1. We now eliminate it from the continuity equation in terms of of these variables. To do this, we rewrite Eq. (2.8) as

$$\left(\frac{\partial}{\partial t} + \mathbf{v}_i \cdot \nabla\right) \log n + \frac{\partial v_\parallel}{\partial z} + \nabla \cdot (\mathbf{v}_m + \mathbf{v}_\nu) = 0, \tag{2.21}$$

where use has been made of the fact that $\nabla \cdot \mathbf{v}_\psi = 0$. Then using Eq. (2.20) in Eq. (2.21) we get

$$\begin{aligned} \left(\frac{\partial}{\partial t} + \mathbf{v}_\psi \cdot \nabla\right) \left(\log n - \rho_s^2 \nabla_\perp^2 \psi\right) + \frac{\partial v_\parallel}{\partial z} + \nu_{ii} \rho_s^4 \nabla_\perp^4 \left(\frac{e\phi}{T_e}\right) & \\ = \; -\left(\mathbf{v}_m + \mathbf{v}_\nu\right) \cdot \nabla \log n, & \qquad (2.22) \end{aligned}$$

where again we have ignored the parallel convective derivative.

2.2.4 Applying the Amplitude Ordering

To further simplify the equations we must separate the equilibrium from the fluctuations so that we may apply the ordering presented in Section 2.1.3. Thus we write

$$\log n \; = \; \log\left(n_o + n_1\right) \; \approx \; \log n_o + \frac{n_1}{n_o}, \tag{2.23}$$

and

$$\psi = \psi_0 + \psi_1, \tag{2.24}$$

where

$$\psi_0 = \frac{1}{\tau} \log n_o, \tag{2.25}$$

$$\psi_1 = \frac{1}{\tau} \frac{n_1}{n_o} + \frac{e\phi}{T_e}. \tag{2.26}$$

Assuming only that $\nabla_\perp^2\psi_0 \ll \nabla_\perp^2\psi_1$ (it is identically zero for the exponential density profile) we can, after a bit more algebra, write Eq. (2.22) as

$$\begin{aligned}\left(\frac{\partial}{\partial t} + \rho_s c_s\, \hat{\mathbf{z}}\times\nabla_\perp\psi_1\cdot\nabla_\perp\right)\left(\frac{n_1}{n_0} - \rho_s^2\nabla_\perp^2\psi_1\right) + \nu_{ii}\rho_s^4\nabla_\perp^4\left(\frac{e\phi}{T_e}\right)&\\ -\rho_s c_s \frac{\partial \log n_0}{\partial x}\frac{\partial}{\partial y}\left(\frac{e\phi}{T_e} + \frac{1}{\tau}\rho_s^2\nabla_\perp^2\psi_1\right) + \frac{\partial v_\parallel}{\partial z}&\\ = -\left(\mathbf{v}_m + \mathbf{v}_\nu\right)\cdot\nabla\log n.& \qquad (2.27)\end{aligned}$$

Up to this point nothing has been said about the ordering of the viscous terms in these equations. Rigorously, these terms are quite small in the collisionless regime and should be neglected. However some damping in necessary to properly simulate saturated turbulence. In a real plasma this damping would come from both collisional effects and from Landau damping on the ions. The latter effect is neglected entirely in this model as it would require a three dimensional kinetic simulation of the ions, which is not feasible. So, in somewhat of an *ad hoc* manner, we will keep linear damping term but will neglect the nonlinear term on the right hand side of Eq. (2.27). We shall find later that our results are not very sensitive to the value of ν_{ii}, which to some extent justifies our cavalier handling of this term.

The remaining term on the right hand side of Eq. (2.27) scales as $\epsilon^3\Omega_i$. The terms on the left hand side all are of order $\epsilon^2\Omega_i$. Keeping only these second order terms, we obtain

$$\begin{aligned}\left(\frac{\partial}{\partial t} + \rho_s c_s\, \hat{\mathbf{z}}\times\nabla_\perp\psi_1\cdot\nabla_\perp\right)\left(\frac{n_1}{n_0} - \rho_s^2\nabla_\perp^2\psi_1\right) + \nu_{ii}\rho_s^4\nabla_\perp^4\left(\frac{e\phi}{T_e}\right)&\\ -\rho_s c_s \frac{\partial \log n_0}{\partial x}\frac{\partial}{\partial y}\left(\frac{e\phi}{T_e} + \frac{1}{\tau}\rho_s^2\nabla_\perp^2\psi_1\right) + \frac{\partial v_\parallel}{\partial z} = 0.& \qquad (2.28)\end{aligned}$$

Similarly, the parallel momentum equation, Eq. (2.10), may be written as:

$$\left(\frac{\partial}{\partial t} + \frac{\rho_s c_s}{\tau}\frac{\partial \log n_0}{\partial x}\frac{\partial}{\partial y} + \rho_s c_s\, \hat{\mathbf{z}}\times\nabla_\perp\psi_1\cdot\nabla_\perp\right) v_\parallel + c_s^2\frac{\partial\psi_1}{\partial z} = 0. \qquad (2.29)$$

2.3 The Electrons

2.3.1 The Drift-kinetic Equation

The extreme smallness of the electron gyroradius and the low frequency of the drift wave allow us to treat the electrons using the drift-kinetic equation. In our slab plasma this equation may be written as:

$$\frac{\partial f_e}{\partial t} + v_\parallel \frac{\partial f_e}{\partial z} + \mathbf{v}_{\mathrm{E}} \cdot \nabla_\perp f_e + \frac{e}{m_e} \frac{\partial \phi}{\partial z} \frac{\partial f_e}{\partial v_\parallel} = 0. \tag{2.30}$$

Note that the electron polarization drift is down by a mass ratio from the ion polarization drift, and thus is negligible. We break f_e into an equilibrium piece, an adiabatic piece, and a *nonadiabatic* piece:

$$f_e = f_0 \left(1 + \frac{e\phi}{T_e}\right) + \hat{f}, \tag{2.31}$$

where

$$f_0 = e^{-\frac{x}{L_n}} f_{MB}, \tag{2.32}$$

f_{MB} being a Maxwellian. Using Eqs. (2.31)–(2.32) in Eq. (2.30) we get the following equation

$$\begin{aligned} & f_0 \frac{\partial}{\partial t}\left(\frac{e\phi}{T_e}\right) + \frac{\partial \hat{f}}{\partial t} + f_0 v_\parallel \frac{\partial}{\partial z}\left(\frac{e\phi}{T_e}\right) + v_\parallel \frac{\partial \hat{f}}{\partial z} \\ & \qquad + \left(1 + \frac{e\phi}{T_e}\right) \mathbf{v}_{\mathrm{E}} \cdot \nabla_\perp f_0 + \mathbf{v}_{\mathrm{E}} \cdot \nabla_\perp \hat{f} \\ & \qquad - f_0 v_\parallel \frac{\partial}{\partial z}\left(\frac{e\phi}{T_e}\right) - \frac{e\phi}{T_e} \frac{\partial}{\partial z}\left(\frac{e\phi}{T_e}\right) v_\parallel f_0 = 0. \end{aligned} \tag{2.33}$$

The leading order terms cancel, leaving

$$\begin{aligned} & f_0 \frac{\partial}{\partial t}\left(\frac{e\phi}{T_e}\right) + \frac{\partial \hat{f}}{\partial t} + v_\parallel \frac{\partial \hat{f}}{\partial z} + \mathbf{v}_{\mathrm{E}} \cdot \nabla_\perp \hat{f} \\ & \qquad + \left(1 + \frac{e\phi}{T_e}\right) \mathbf{v}_{\mathrm{E}} \cdot \nabla_\perp f_0 - \frac{e\phi}{T_e} \frac{\partial}{\partial z}\left(\frac{e\phi}{T_e}\right) v_\parallel f_0 = 0. \end{aligned} \tag{2.34}$$

2.3.2 The Nonadiabatic Electron Response

We assume that the nonadiabatic part of the distribution function, $\hat{f}$, is of the same order as that given by the linear theory:

$$\begin{aligned} \hat{f} &\sim \hat{f}_{\text{Linear}} = \frac{\omega - \omega_{*e}}{k_{\|} v_{th_e}} Z\left(\frac{\omega}{k_{\|} v_{th_e}}\right) \frac{e\phi_{\mathbf{k}\omega}}{T_e} f_0, \\ &\approx \frac{i\sqrt{\pi}}{k_{\|} v_{th_e}} \left(\omega - \omega_{*e}\right) \frac{e\phi_{\mathbf{k}\omega}}{T_e} f_0; \qquad \frac{\omega}{k_{\|} v_{th_e}} \ll 1, \\ &\sim \frac{\omega}{k_{\|} v_{th_e}} \frac{e\phi_{\mathbf{k}\omega}}{T_e} f_0, \end{aligned} \tag{2.35}$$

where Z is the plasma dispersion function dispersion function [25], and ω_{*e} is the electron drift frequency, given by

$$\omega_{*e} \equiv \frac{\rho_s}{L_n} k_y \rho_s \Omega_i. \tag{2.36}$$

Recall that

$$\delta \equiv \frac{\omega}{k_{\|} v_{th_e}} \ll 1, \tag{2.37}$$

and thus we order $\hat{f} \sim \epsilon \delta f_0$. Using this assumption, and Eqs. (2.4)-(2.6), to leading order Eq. (2.34) becomes

$$f_0 \frac{\partial}{\partial t}\left(\frac{e\phi}{T_e}\right) + v_{\|} \frac{\partial \hat{f}}{\partial z} + \frac{\rho_s}{L_n} f_0 c_s \frac{\partial}{\partial y}\left(\frac{e\phi}{T_e}\right) = \frac{e\phi}{T_e} \frac{\partial}{\partial z}\left(\frac{e\phi}{T_e}\right) v_{\|} f_0 \tag{2.38}$$

The terms on the left hand side of Eq. (2.38) are all $\sim \epsilon^2 \Omega_i f_0$. These terms alone give the usual low frequency, linear result expressed above. The term on the right hand side is $\sim \delta^{-1} \epsilon^3 \Omega_i f_0$, which typically is about the same size. Thus it would appear that the electrons also must be treated nonlinearly. Fortunately, the nonlinear term is odd in $v_{\|}$ and we only need the density moment, $\hat{n}_e$, which will be exactly that given by the linear theory:

$$\hat{n}_{e_{\mathbf{k}\omega}} = n_0 \frac{i\sqrt{\pi}}{k_{\|} v_{th_e}} \left(\omega - \omega_{*e}\right) \frac{e\phi_{\mathbf{k}\omega}}{T_e}. \tag{2.39}$$

This can be transformed back to the time domain, giving

$$\hat{n}_{e_{\mathbf{k}}}(t) = -n_0 \frac{\sqrt{\pi}}{k_{\parallel} v_{th_e}} \left(\frac{\partial}{\partial t} + i\omega_{*e}\right) \frac{e\phi_{\mathbf{k}}}{T_e}. \tag{2.40}$$

The total electron density fluctuation is

$$\tilde{n}_{e_{\mathbf{k}}} = n_0 \frac{e\phi_{\mathbf{k}}}{T_e} + \hat{n}_{e_{\mathbf{k}}}(t). \tag{2.41}$$

2.4 Dimensionless Variables

The final part of the manipulation of these equations is to simply rescale them. We define the following dimensionless variables

$$\begin{aligned} t' &= \frac{c_s}{L_n} t, \\ x' &= \frac{x}{\rho_s}, \\ y' &= \frac{y}{\rho_s}, \\ z' &= \frac{z}{L_n}, \\ \phi' &= \frac{L_n}{\rho_s} \frac{e\phi}{T_e}, \\ \psi' &= \frac{L_n}{\rho_s} \psi, \\ n_1' &= \frac{L_n}{\rho_s} \frac{n_1}{n_0}. \end{aligned} \tag{2.42}$$

In terms of these, Eqs. (2.28) and (2.29) become

$$\begin{aligned} &\left(\frac{\partial}{\partial t} + \hat{\mathbf{z}} \times \nabla_{\perp} \psi_1 \cdot \nabla_{\perp}\right) \left(n_1 - \nabla_{\perp}^2 \psi_1\right) + \nu \nabla_{\perp}^4 \phi \\ &\qquad + v_d(x) \frac{\partial}{\partial y} \left(\phi + \frac{1}{\tau} \nabla_{\perp}^2 \psi_1\right) + \frac{\partial v_{\parallel}}{\partial z} = 0, \end{aligned} \tag{2.43}$$

and

$$\left(\frac{\partial}{\partial t} - \frac{v_d(x)}{\tau}\frac{\partial}{\partial y} + \hat{\mathbf{z}}\times\nabla_\perp\psi_1\cdot\nabla_\perp\right) v_\parallel + \frac{\partial\psi_1}{\partial z} = 0, \tag{2.44}$$

where $\nu \equiv \nu_{ii}/\Omega_i$ and

$$v_d(x) = -\frac{L_n}{\rho_s}\frac{\partial \log n_0}{\partial x}, \tag{2.45}$$

L_n being an average (constant) scale length. Note that for the exponential density profile, $v_d(x) \equiv 1$. From now on the primes will be dropped unless it is necessary to distinguish dimensionless and dimensional variables.

The plasma is quasineutral, $\tilde{n}_i = \tilde{n}_e$, and so we may write the ion density fluctuation as

$$n_1' = \phi' + \hat{n}', \tag{2.46}$$

where n_1' and ϕ' are the dimensionless variables defined earlier, and $\hat{n}'$ is the dimensionless nonadiabatic electron density. The latter may be written as

$$\hat{n}' = \frac{L_n}{\rho_s}\frac{\hat{n}_e}{n_0} = -\delta_0\left(\frac{\partial}{\partial t} + \frac{\partial}{\partial y}\right)\phi', \tag{2.47}$$

where

$$\delta_0 = \frac{\sqrt{\pi}}{(k_\parallel L_n)\left(\frac{v_{th_e}}{c_s}\right)}. \tag{2.48}$$

Written in this form, we can gauge the size of δ_0. In a typical tokamak with minor radius a and major radius R we would have

$$k_\parallel L_n \approx k_\parallel a = k_\parallel R\,\frac{a}{R} \approx \frac{a}{R} \approx \frac{1}{4},$$

and

$$\frac{v_{th_e}}{c_s} = \sqrt{\frac{2m_i}{m_e}} \approx 60,$$

so that $\delta_0 \sim 1.77/15 \approx 0.12$. Thus δ_0 is typically somewhat larger than our expansion parameter ϵ.

Although the nonadiabatic electron response derived above is correct, it must be handled with special care: substituting Eq. (2.47) into Eq. (2.43) gives a second order equation in time which is singular in the sense that it becomes first order as $\delta_0 \to 0$. For now we shall treat $\hat{n}'$ as a separate variable and worry about the proper treatment later. This leads to the following form for our equations:

$$\left(\frac{\partial}{\partial t} + \hat{\mathbf{z}}\times\nabla_\perp\psi_1\cdot\nabla_\perp\right)\left(\phi + \hat{n} - \nabla_\perp^2\psi_1\right) + \nu\nabla_\perp^4\phi$$

$$+v_d(x)\frac{\partial}{\partial y}\left(\phi + \frac{1}{\tau}\nabla_\perp^2\psi_1\right) + \frac{\partial v_\parallel}{\partial z} = 0, \tag{2.49}$$

and

$$\left(\frac{\partial}{\partial t} - \frac{v_d}{\tau}\frac{\partial}{\partial y} + \hat{\mathbf{z}}\times\nabla_\perp\psi_1\cdot\nabla_\perp\right)v_\parallel + \frac{\partial\psi_1}{\partial z} = 0, \tag{2.50}$$

where we now have

$$\psi_1 = \frac{1}{\tau}\left(\phi + \hat{n}\right) + \phi. \tag{2.51}$$

2.5 Simplifications

2.5.1 Cold Ions

The ions will be treated as cold for the remainder of this work: $\tau \sim \epsilon^{-1}$. Actually, this is the only regime in which our derivation is truly valid. Under the assumption that $k_\perp\rho_s \sim 1$, $T_i = T_e$ implies that $k_\perp\rho_i \sim 1$ which would lead to strong ion gyrokinetic effects. These effects cannot be treated with a simple fluid model.

For cold ions, $\psi_1 = \phi$, and Eqs. (2.49)–(2.50) reduce to the following equations, similar to those studied by Meiss, *et al.*[26].

$$\left(\frac{\partial}{\partial t} + \hat{\mathbf{z}}\times\nabla_\perp\phi\cdot\nabla_\perp\right)\left(\phi - \nabla_\perp^2\phi + \hat{n}\right) + v_d(x)\frac{\partial\phi}{\partial y} + \nu\nabla_\perp^4\phi + \frac{\partial v_\parallel}{\partial z} = 0, \tag{2.52}$$

and

$$\left(\frac{\partial}{\partial t} + \hat{\mathbf{z}}\times\nabla_\perp\phi\cdot\nabla_\perp\right)v_\parallel + \frac{\partial\phi}{\partial z} = 0. \tag{2.53}$$

Note that these equations are not really all that much simpler than with the temperatures equal. In fact, since the nonlinearities are basically of the same form as before, Eqs. (2.49)–(2.50) would not be much more work to integrate than Eqs. (2.52)–(2.53) would be.

2.5.2 The Two-Dimensional Limit

Equations (2.52)–(2.53) describe the drift wave coupled to the ion-acoustic wave. This coupling may be removed, along with all the complexity involved in doing a 3-d simulation, by assuming $k_\parallel \ll \epsilon k_\perp$.

We cannot let $k_\parallel$ become too small, however, since we are limited to $k_\parallel v_{th_e} \gg \omega$. In fact this constraint makes the neglect of the parallel ion dynamics inconsistent since the coupling term is roughly the same size as the contribution from the nonadiabatic electrons. Recall that

$$\frac{\partial\hat{n}}{\partial t} \sim \delta\epsilon^2\Omega_i,$$

and

$$\begin{aligned}\frac{\partial v_\parallel}{\partial z} &\sim \epsilon k_\parallel c_s \\ &\sim \epsilon\frac{k_\parallel v_{th_e}}{\omega}\frac{\omega}{\Omega_i}\frac{c_s}{v_{th_e}}\Omega_i \\ &\sim \epsilon^2\delta^{-1}\sqrt{\frac{m_e}{2m_i}}\,\Omega_i,\end{aligned}$$

and so

$$\frac{\partial\hat{n}}{\partial t} : \frac{\partial v_\parallel}{\partial z} \approx \delta^2 : \sqrt{\frac{m_e}{2m_i}}. \tag{2.54}$$

If $\delta \approx 12\%$, as estimated earlier (Section 2.4) for a tokamak ($k_\parallel \sim \epsilon_A \epsilon k_\perp$; $\epsilon_A = a/R$), then this ratio is very close to one. Thus, in a tokamak plasma, the parallel dynamics of the *ions* may be as important to the nonlinear evolution of the collisionless drift wave as the parallel dynamics of the electrons.

For practical and pedagogical reasons, however, we will live with this inconsistency and allow Eq. (2.52) to become

$$\left(\frac{\partial}{\partial t} + \hat{\mathbf{z}}\times\nabla_\perp\phi\cdot\nabla_\perp\right)\left(\phi - \nabla_\perp{}^2\phi + \hat{n}\right) + v_d(x)\frac{\partial\phi}{\partial y} + \nu\nabla_\perp{}^4\phi = 0. \tag{2.55}$$

2.6 Treatment of the Nonadiabatic Electrons

As mentioned above, our model for the nonadiabatic electron term requires some special care. Using Eq. (2.47) directly in our ion continuity equation, Eq. (2.55), gives an equation singular in time:

$$\left(\frac{\partial}{\partial t} + \hat{\mathbf{z}}\times\nabla_\perp\phi\cdot\nabla_\perp\right)\left(\phi - \nabla_\perp{}^2\phi - \delta_0\left(\frac{\partial}{\partial t} + \frac{\partial}{\partial y}\right)\phi\right) \tag{2.56}$$

$$+v_d(x)\frac{\partial\phi}{\partial y} + \nu\nabla_\perp{}^4\phi = 0.$$

If we look at the linear dispersion relation for Eq. (2.56) we see that we are in trouble right away. There are two roots: One is the unstable drift wave and the other has a dimensionless frequency of order δ_0^{-1}, i.e. $\omega \sim k_\parallel v_{th_e}$, violating our assumptions used in deriving the nonadiabatic electron response. This second root is completely artificial and we must take special care to avoid it. We will take a look at three methods of doing this in the following three sections.

2.6.1 The Hasegawa-Mima Equation

The simplest method of treating the nonadiabatic electron response is to ignore it. If we set $\delta_0 = 0$ we get the well known Hasegawa-Mima Equation [1, 2]:

$$\left(\frac{\partial}{\partial t} + \hat{\mathbf{z}}\times\nabla_\perp\phi\cdot\nabla_\perp\right)\left(\phi - \nabla_\perp^2\phi\right) + v_d(x)\frac{\partial\phi}{\partial y} + \nu\nabla_\perp{}^4\phi = 0. \tag{2.57}$$

If the density profile is exponential, and thus $v_d = 1$, then Eq. (2.57) can be Fourier transformed in both x and y to yield the following mode coupling equation:[1]

---

[1] See Appendix A for an explanation of our Fourier transform conventions

$$\frac{\partial \phi_{\mathbf{k}}}{\partial t} = -i\omega_{\mathbf{k}}\phi_{\mathbf{k}} - \nu k^4 \phi_{\mathbf{k}} + \sum_{\mathbf{k}'+\mathbf{k}''=\mathbf{k}} V_{\mathbf{k},\mathbf{k}',\mathbf{k}''}\, \phi_{\mathbf{k}'}\phi_{\mathbf{k}''}, \tag{2.58}$$

where $\omega_{\mathbf{k}}$ is the linear frequency, given by

$$\omega_{\mathbf{k}} = \frac{k_y}{1+k^2}, \tag{2.59}$$

and $V_{\mathbf{k},\mathbf{k}',\mathbf{k}''}$ is the mode coupling coefficient, given by

$$V_{\mathbf{k},\mathbf{k}',\mathbf{k}''} = \frac{1}{2}\,\frac{\hat{\mathbf{z}}\cdot\mathbf{k}'\times\mathbf{k}''\left(k''^2 - k'^2\right)}{1+k^2}. \tag{2.60}$$

While neglecting the nonadiabatic response might seem like a perfectly valid and consistent thing to do, it is not. This assumption fundamentally changes the nature of the problem by removing the linear instability.

2.6.2 The Terry-Horton Equation

Terry and Horton [3, 4, 5] corrected this deficiency of the Hasegawa-Mima model in the following way: they assumed that $\frac{\partial}{\partial t} \approx -i\omega_{\mathbf{k}}^0$ in the expression for the nonadiabatic electron response, where $\omega_{\mathbf{k}}^0$ is the mode frequency neglecting the nonadiabatic electrons (i.e. Eq. (2.59)). Making this substitution into Eq. (2.47) leads to the following approximate form for the nonadiabatic electron response:

$$\hat{n} \approx i\delta_{\mathbf{k}}\phi_{\mathbf{k}}, \tag{2.61}$$

where[2]

$$\delta_{\mathbf{k}} = -\delta_0 \frac{k_y k^2}{1+k^2}. \tag{2.62}$$

This may be transformed back to physical space to give

$$\hat{n} \approx \delta_0 \frac{\partial}{\partial y} \nabla_\perp^2 P^{-1} \phi \tag{2.63}$$

---

[2] Terry and Horton get a somewhat different expression since they include other effects, such as finite temperature and trapped electrons (in the banana sense). The comments I make regarding Eq. (2.62) apply equally well to their expressions.

where $P \equiv 1 - \nabla_\perp{}^2$. Substituting Eq. (2.63) into Eq. (2.55) then gives

$$\left(\frac{\partial}{\partial t} + \hat{\mathbf{z}}\times\nabla_\perp\phi\cdot\nabla_\perp\right)\left(\phi - \nabla_\perp{}^2\phi + \delta_0\frac{\partial}{\partial y}\nabla_\perp{}^2 P^{-1}\phi\right) \tag{2.64}$$

$$+v_d(x)\frac{\partial\phi}{\partial y} + \nu\nabla_\perp{}^4\phi = 0.$$

Transforming Eq. (2.64) to Fourier **k**-space gives the following mode coupling equation:

$$\frac{\partial\phi_{\mathbf{k}}}{\partial t} = \left(-i\hat{\omega}_{\mathbf{k}} + \hat{\gamma}_{\mathbf{k}} - \nu k^4\right)\phi_{\mathbf{k}} + \sum_{\mathbf{k}'+\mathbf{k}''=\mathbf{k}} \hat{V}_{\mathbf{k},\mathbf{k}',\mathbf{k}''}\,\phi_{\mathbf{k}'}\phi_{\mathbf{k}''}. \tag{2.65}$$

The linear frequency and growth rate, $\hat{\omega}_{\mathbf{k}}$ and $\hat{\gamma}_{\mathbf{k}}$, are given by

$$\hat{\omega}_{\mathbf{k}} = \frac{k_y\left(1+k^2\right)}{\left(1+k^2\right)^2 + \delta_{\mathbf{k}}^2}. \tag{2.66}$$

and

$$\hat{\gamma}_{\mathbf{k}} = -\frac{k_y\delta_{\mathbf{k}}}{\left(1+k^2\right)^2 + \delta_{\mathbf{k}}^2}. \tag{2.67}$$

The modified mode coupling coefficient is given by

$$\hat{V}_{\mathbf{k},\mathbf{k}',\mathbf{k}''} = \frac{1}{2}\,\frac{\hat{\mathbf{z}}\cdot\mathbf{k}'\times\mathbf{k}''\left(\chi_{\mathbf{k}''} - \chi_{\mathbf{k}'}\right)}{1+\chi_{\mathbf{k}}}. \tag{2.68}$$

where

$$\chi_{\mathbf{k}} = k^2 + i\delta_{\mathbf{k}} \tag{2.69}$$

If we ignore the terms of order δ^2 in Eqs. (2.66) and (2.67) we get back the usual expressions for the mode frequency and the linear growth rate of the polarization destabilized drift wave. Still, the physics behind the above assumption is all wrong. It is basically a weak turbulence assumption. If the system is strongly turbulent, as is observed experimentally, then there is no reason to set $\omega = \omega_{\mathbf{k}}$. We will study this question closely with our code.

2.6.3 A New Method

The Terry-Horton equation was arrived at by doing a perturbation theory on the linear part of the equation. What I do is along the same track but I carry it one step further. First rewrite Eq. (2.55) as

$$\begin{aligned}\left(\frac{\partial}{\partial t} + \hat{\mathbf{z}}\times\nabla_\perp\phi\cdot\nabla_\perp\right)\left(\phi - {\nabla_\perp}^2\phi\right) + v_d(x)\frac{\partial\phi}{\partial y} + \nu{\nabla_\perp}^4\phi \\ = \delta_0\left(\frac{\partial}{\partial t} + \hat{\mathbf{z}}\times\nabla_\perp\phi\cdot\nabla_\perp\right)\left(\frac{\partial}{\partial t} + \frac{\partial}{\partial y}\right)\phi\end{aligned} \tag{2.70}$$

The right hand side of Eq. (2.70) is assumed small compared to the left hand side, which is recognized as the Hasegawa-Mima equation. The procedure is to approximate the $\frac{\partial}{\partial t}$ operators on the right hand side using the Hasegawa-Mima equation.

This technique is an extension of the perturbation technique that is usually applied to solve the linear dispersion relation. In the linear case this technique can be iterated and the solution can be shown to always converge to the real drift wave root. Multiple iterations could also be done in this nonlinear case, but it is not obvious that this would be worth the rather large computational expense which it would incur.

To this end we define

$$\dot{\phi}_0 \equiv \left.\frac{\partial\phi}{\partial t}\right|_{\delta_0=0} = -P^{-1}\frac{\partial\phi}{\partial y} - P^{-1}\left\{\phi, P\phi\right\} \tag{2.71}$$

where $P = 1 - {\nabla_\perp}^2$, and $\{\cdot,\cdot\}$ is the Poisson bracket, defined to be

$$\{u,v\} \equiv \frac{\partial u}{\partial x}\frac{\partial v}{\partial y} - \frac{\partial u}{\partial y}\frac{\partial v}{\partial x} \tag{2.72}$$

Now differentiate Eq. (2.71) with respect to time, and use Eq. (2.71) as necessary:

$$\begin{aligned}&\frac{\partial}{\partial t}\left(\dot{\phi}_0 + \frac{\partial\phi}{\partial y}\right) \\ &= \left(1 - P^{-1}\right)\frac{\partial}{\partial t}\frac{\partial\phi}{\partial y} - P^{-1}\frac{\partial}{\partial t}\left\{\phi, P\phi\right\} \\ &= \left(1 - P^{-1}\right)\frac{\partial\dot{\phi}_0}{\partial y} - P^{-1}\left\{\dot{\phi}_0, P\phi\right\} - P^{-1}\left\{\phi, P\dot{\phi}_0\right\} \\ &= -P^{-1}\left(1 - P^{-1}\right)\frac{\partial^2\phi}{\partial y^2} - P^{-1}\left(1 - P^{-1}\right)\frac{\partial}{\partial y}\left\{\phi, P\phi\right\} \\ &\quad -P^{-1}\left\{\dot{\phi}_0, P\phi\right\} - P^{-1}\left\{\phi, P\dot{\phi}_0\right\}\end{aligned} \tag{2.73}$$

and thus we have the following equation:

$$\begin{aligned}
&\left(\frac{\partial}{\partial t} + \hat{\mathbf{z}}\times\nabla_\perp\phi\cdot\nabla_\perp\right)\left(\phi - {\nabla_\perp}^2\phi\right) + v_d(x)\frac{\partial\phi}{\partial y} \\
&\quad = -\delta_0\Bigg(P^{-1}\left(1-P^{-1}\right)\frac{\partial^2\phi}{\partial y^2} + P^{-1}\left(1-P^{-1}\right)\frac{\partial}{\partial y}\left\{\phi, P\phi\right\} \\
&\qquad +P^{-1}\left\{\dot{\phi}_0, P\phi\right\} + P^{-1}\left\{\phi, P\dot{\phi}_0\right\} - \left\{\phi, \dot{\phi}_0 + \frac{\partial\phi}{\partial y}\right\}\Bigg)
\end{aligned} \tag{2.74}$$

The right hand side of Eq. (2.74) is only a function of ϕ and spatial operators on ϕ. The first term is exactly the linear growth term discussed above.

Transforming Eq. (2.74) to Fourier **k**-space gives the following mode coupling equation:

$$\begin{aligned}
\frac{\partial\phi_{\mathbf{k}}}{\partial t} &= \left(-i\omega_{\mathbf{k}} + \gamma_{\mathbf{k}}\right)\phi_{\mathbf{k}} + \left(\frac{1+k^2-i\delta_{\mathbf{k}}}{1+k^2}\right)\sum_{\mathbf{k}'+\mathbf{k}''=\mathbf{k}} V_{\mathbf{k},\mathbf{k}',\mathbf{k}''}\;\phi_{\mathbf{k}'}\phi_{\mathbf{k}''} \\
&+ \frac{\delta_0}{1+k^2}\sum_{\mathbf{k}'+\mathbf{k}''=\mathbf{k}} V_{\mathbf{k},\mathbf{k}',\mathbf{k}''}\;\left(\dot{\phi}^0_{\mathbf{k}'}\phi_{\mathbf{k}''} + \dot{\phi}^0_{\mathbf{k}''}\phi_{\mathbf{k}'}\right) \\
&- \delta_0\sum_{\mathbf{k}'+\mathbf{k}''=\mathbf{k}}\frac{\hat{\mathbf{z}}\cdot\mathbf{k}'\times\mathbf{k}''}{2\left(1+k^2\right)}\;\left(\dot{\phi}^0_{\mathbf{k}''}\phi_{\mathbf{k}'} - \dot{\phi}^0_{\mathbf{k}'}\phi_{\mathbf{k}''} + i\left(k''_y - k'_y\right)\;\phi_{\mathbf{k}'}\phi_{\mathbf{k}''}\right)
\end{aligned} \tag{2.75}$$

where

$$\dot{\phi}^0_{\mathbf{k}} = -i\omega_{\mathbf{k}}\phi_{\mathbf{k}} + \sum_{\mathbf{k}'+\mathbf{k}''=\mathbf{k}} V_{\mathbf{k},\mathbf{k}',\mathbf{k}''}\;\phi_{\mathbf{k}'}\phi_{\mathbf{k}''}. \tag{2.76}$$

The mode coupling coefficient, $V_{\mathbf{k},\mathbf{k}',\mathbf{k}''}$ above is the same as that for the Hasegawa-Mima equation, Eq. (2.60).

2.7 Conservation Properties

2.7.1 Conservative Form of the Equations

Observe that, in the inviscid limit, Eq. (2.55) may immediately be written in a conservative form

$$\left(\frac{\partial}{\partial t} + \hat{\mathbf{z}}\times\nabla_\perp\phi\cdot\nabla_\perp\right)\left(\frac{L_n}{\rho_s}\log n_o + \phi - \nabla_\perp^2\phi + \hat{n}\right) = 0.$$

For an exponential density profile this becomes

$$\left(\frac{\partial}{\partial t} + \hat{\mathbf{z}}\times\nabla_\perp\phi\cdot\nabla_\perp\right)\left(-x + \phi - \nabla_\perp^2\phi + \hat{n}\right) = 0, \tag{2.77}$$

which is a statement that the quantity $x-\phi+\nabla_\perp^2\phi-\hat{n}$ is conserved along the trajectory of a fluid element. In the remainder of this thesis, we will refer to *this* quantity as the density, and denote it by ρ. Since ρ depends monotonically on x, it imposes a fundamental restriction on the motion of a fluid element: a fluid element can only move far from its *equilibrium* position by creating a large fluctuation, which in turn requires a great deal of energy. Conversely, assuming that the system only has a finite amount of energy available, a fluid element can only move a finite distance from its equilibrium position.

This conservation property may be expressed as an infinite number of integral constants of the form

$$I_f[\phi] = \int_{D(t)} f(\rho)\, dx\, dy \tag{2.78}$$

where f is any function and $D(t)$ is any closed region of the $x-y$ plane whose boundary moves with the $\mathbf{E}\times\mathbf{B}$ drift velocity.

2.7.2 The Hasegawa-Mima Equation

For localized solutions on an infinite domain, several moments of Eq. (2.57) annihilate the nonlinearity. This leads to the following set of integral constants when the viscosity is neglected[27]:

$$E[\phi] = \int \left(\phi^2 + \nabla_\perp\phi\cdot\nabla_\perp\phi\right) dx\, dy \tag{2.79}$$

$$\Omega[\phi] = \int \left(\left(\nabla_\perp^2\phi\right)^2 + \nabla_\perp\phi\cdot\nabla_\perp\phi\right) dx\, dy \tag{2.80}$$

$$N[\phi] = \int \phi\, dx\, dy \tag{2.81}$$

$$\begin{aligned} X[\phi] &= \int x\,\phi\,dx\,dy && (2.82) \\ Y[\phi] &= \int y\,\phi\,dx\,dy - tN[\phi] && (2.83) \\ M[\phi] &= \int \left((y-t)^2 + x^2\right)\phi\,dx\,dy && (2.84) \end{aligned}$$

Equation (2.78) also applies here, naturally, but with $\hat{n} = 0$.

Of these constraints, the energy, E, and generalized enstrophy, Ω, are the most useful. Only these two (along with the N moment, which is somewhat trivial) survive in the periodic, turbulent system which we will be studying. They play a role in the statistical equilibrium of the turbulence as well as the cascade process, to be discussed in Chapter 5.

Effect of Viscosity

Viscosity destroys all the exact invariants mentioned above except N. Since the nonlinearity is still annihilated by these moments, however, we can obtain simple equations for their evolution. For the energy and enstrophy these equations may be written in terms of the Fourier spectrum as

$$\frac{dE}{dt} = -\sum_{\mathbf{k}} \nu_k E_k \qquad (2.85)$$

and

$$\frac{d\Omega}{dt} = -\sum_{\mathbf{k}} k^2 \nu_k E_k \qquad (2.86)$$

where

$$E_k \equiv \left(1 + k^2\right) |\phi_k|^2, \qquad (2.87)$$

$$E \equiv \frac{1}{2} \sum_{\mathbf{k}} E_k, \qquad (2.88)$$

and $\nu_k = \nu k^4$.

2.7.3 Energy and Enstrophy Conservation in General

When we introduce the nonadiabatic electron density, there are no longer any exact constants of motion other than N. Nor can simple equations of the form of Eqs. (2.85)–(2.86) be written. However we can write simple equations which are valid on a slow time scale, $\tau \gg \omega_{*e}^{-1}$.

We start by writing our general equation, Eq. (2.55), in terms of the fluctuating part of the density:

$$\psi \equiv \phi - \nabla_\perp^2 \phi + \hat{n}. \tag{2.89}$$

Then Eq. (2.55) may be written as

$$\frac{\partial \psi}{\partial t} + \frac{\partial \phi}{\partial y} + \{\phi, \psi\} = -\nu \nabla_\perp^4 \phi \tag{2.90}$$

For any sufficiently differentiable functions f and g on a periodic domain (or an infinite one, provided f, g vanish sufficiently quickly) it is easy to show that

$$\int f \{f, g\}\, dx\, dy = 0. \tag{2.91}$$

Thus the ψ and ϕ moments of Eq. (2.90) will annihilate the nonlinearity. Taking these moments leads to the following equations:

$$\int \phi \frac{\partial \psi}{\partial t} = -\nu \int \phi \nabla_\perp^4 \phi \tag{2.92}$$

and

$$\int \psi \frac{\partial \psi}{\partial t} + \int \psi \frac{\partial \phi}{\partial y} = -\nu \int \psi \nabla_\perp^4 \phi. \tag{2.93}$$

Note that the term $\int \phi \frac{\partial \phi}{\partial y}$ vanishes since the integrand is an exact differential. In terms of the Fourier coefficients, these equations become

$$\mathrm{Re} \sum_{\mathbf{k}} \phi_{\mathbf{k}}^* \frac{\partial \psi_{\mathbf{k}}}{\partial t} = -\nu \sum_{\mathbf{k}} k^4 |\phi_{\mathbf{k}}|^2 \tag{2.94}$$

and

$$\frac{1}{2}\frac{\partial}{\partial t}\sum_{\mathbf{k}}|\psi_{\mathbf{k}}|^2 + \mathrm{Re}\sum_{\mathbf{k}}\psi_{\mathbf{k}}^* i k_y \phi_k = -\nu\sum_{\mathbf{k}} k^4|\phi_{\mathbf{k}}|^2 \tag{2.95}$$

Using the definition of ψ, and introducing the energy E and mode energy $E_{\mathbf{k}}$ as defined in Eqs. (2.87)–(2.88), Eq. (2.94) may be written as

$$\frac{\partial E}{\partial t} = -\sum_{\mathbf{k}}\nu_k E_{\mathbf{k}} - \mathrm{Re}\sum_{\mathbf{k}}\phi_{\mathbf{k}}\frac{\partial \hat{n}_{\mathbf{k}}^*}{\partial t} \tag{2.96}$$

Similarly, if we define

$$C_k = |\psi_k|^2 \tag{2.97}$$

and

$$C = \frac{1}{2}\sum_{\mathbf{k}} C_k, \tag{2.98}$$

we may rewrite Eq. (2.95) as

$$\frac{\partial C}{\partial t} = -\sum_{\mathbf{k}}\left(1+k^2\right)\nu_k E_{\mathbf{k}} - \mathrm{Re}\sum_{\mathbf{k}}\left(\nu_k + i k_y\right)\hat{n}_{\mathbf{k}}^*\phi_{\mathbf{k}} \tag{2.99}$$

In the limit as $\hat{n} \to 0$, $C - E \to \Omega$, the generalized enstrophy defined in Eq. (2.79). We make this the general definition of the enstrophy:

$$\Omega = C - E. \tag{2.100}$$

Then Ω obeys the following equation:

$$\frac{\partial \Omega}{\partial t} = -\sum_{\mathbf{k}}\left(k^2\nu_k E_{\mathbf{k}} + \mathrm{Re}\left(\hat{n}_{\mathbf{k}}^*\phi_{\mathbf{k}}\right)\right) + \mathrm{Re}\sum_{\mathbf{k}}\left(\frac{\partial \hat{n}_{\mathbf{k}}^*}{\partial t} - i k_y \hat{n}_{\mathbf{k}}^*\right)\phi_{\mathbf{k}}. \tag{2.101}$$

Slow Time Scale Equations

Equations (2.96)–(2.99) are completely general, but are complicated in that they involve the nonadiabatic electron density and its time derivative. Let us assume that we can separate the time behavior into a slow time scale, τ, such that $\omega_{*e}\tau \gg 1$. If most of the energy in the fluctuations is at frequencies on the order of ω_{*e}, then we can expand the fast time scale in a Fourier series:

$$\phi_{\mathbf{k}}(t) = \sum_{\omega} \phi_{\mathbf{k}_\omega}(\tau) e^{-i\omega t} \tag{2.102}$$

and

$$\hat{n}_{\mathbf{k}} = \sum_{\omega} \hat{n}_{\mathbf{k}_\omega}(\tau) e^{-i\omega t} \tag{2.103}$$

Substituting these into Eqs. (2.96)–(2.101) we get

$$\frac{\partial E}{\partial t} = -\sum_{\mathbf{k}} \nu_k E_{\mathbf{k}} - \mathrm{Re} \sum_{\mathbf{k},\omega,\omega'} i\omega' \hat{n}^*_{\mathbf{k}_{\omega'}} \phi_{\mathbf{k}_\omega} e^{-i(\omega-\omega')t} \tag{2.104}$$

and

$$\begin{aligned}\frac{\partial \Omega}{\partial t} &= -\sum_{\mathbf{k}} k^2 \nu_k E_{\mathbf{k}} - \mathrm{Re} \sum_{\mathbf{k},\omega,\omega'} \hat{n}^*_{\mathbf{k}_{\omega'}} \phi_{\mathbf{k}_\omega} e^{-i(\omega-\omega')t} \\ &\quad + \mathrm{Re} \sum_{\mathbf{k},\omega,\omega'} (i\omega' - ik_y)\, \hat{n}^*_{\mathbf{k}_{\omega'}} \phi_{\mathbf{k}_\omega} e^{-i(\omega-\omega')t}.\end{aligned}$$

Finally, averaging over the short time scale picks out only the frequency $\omega = \omega'$, giving us the following equations:

$$\frac{dE}{d\tau} = -\sum_{\mathbf{k}} \nu_k E_{\mathbf{k}} - \mathrm{Re} \sum_{\mathbf{k},\omega} i\omega \hat{n}^*_{\mathbf{k}_\omega} \phi_{\mathbf{k}_\omega} \tag{2.105}$$

and

$$\frac{d\Omega}{d\tau} = -\sum_{\mathbf{k}} k^2 \nu_k E_{\mathbf{k}} - \mathrm{Re} \sum_{\mathbf{k},\omega} \hat{n}^*_{\mathbf{k}_\omega} \phi_{\mathbf{k}_\omega} + \mathrm{Re} \sum_{\mathbf{k},\omega} (i\omega - ik_y)\, \hat{n}^*_{\mathbf{k}_\omega} \phi_{\mathbf{k}_\omega}. \tag{2.106}$$

For our specific problem, the nonadiabatic electron response is given by Eq. (2.47), or

$$\hat{n}_{\mathbf{k}_\omega} = i\delta_0 \left(\omega - k_y\right) \phi_{\mathbf{k}_\omega}.$$

Using this expression in Eqs. (2.105)-(2.106) gives the final form for our slow time scale equations:

$$\frac{dE}{d\tau} = -\sum_{\mathbf{k}} \nu_k E_{\mathbf{k}} - \delta_0 \sum_{\mathbf{k},\omega} \omega \left(\omega - k_y\right) \left|\phi_{\mathbf{k}_\omega}\right|^2 \tag{2.107}$$

and

$$\frac{d\Omega}{d\tau} = -\sum_{\mathbf{k}} k^2 \nu_k E_{\mathbf{k}} + \delta_0 \sum_{\mathbf{k},\omega} \left(\omega - k_y\right)^2 \left|\phi_{\mathbf{k}_\omega}\right|^2. \tag{2.108}$$

The first equation is fairly straight forward, just being an obvious balance between energy going to the nonadiabatic electrons and energy being dissipated via viscosity. Since Ω has no clear physical meaning, however, it is difficult to interpret the second equation. It could, however, be a source of trouble: the term due to the nonadiabatic electrons is positive, so if the viscosity is not sufficiently large, the system might never settle into a steady state.

2.7.4 The Terry-Horton Equation

The Terry-Horton equation is somewhat special in that the equation for C takes on a pleasingly simple form without having to resort to the fast time average. In this case we have

$$C_k = \sum_{\mathbf{k}} \left|1 + k^2 + i\delta_{\mathbf{k}}\right|^2 \left|\phi_{\mathbf{k}}\right|^2. \tag{2.109}$$

and

$$\frac{\partial C}{\partial t} = -\sum_{\mathbf{k}} \left(1 + k^2\right) \left(\nu_k - \hat{\gamma}_{\mathbf{k}}\right) E_{\mathbf{k}} \tag{2.110}$$

where $\hat{\gamma}_{\mathbf{k}}$ is just their linear growth rate, as given by Eq. (2.67).

2.7.5 Our Model Equation

Examination of Poisson brackets in Eq. (2.74) shows that there is no single moment of that equation which will simultaneously annihilate all of the nonlinearities. Thus Eqs. (2.107)-(2.108) are only approximations for our model, even on the long time scale.

Chapter 3

The Numerical Method

I have written a Fourier spectral/pseudospectral code [28, 29, 30, 31] for solving the two dimensional mode coupling equations derived in Chapter 1. This type of numerical method was chosen for a variety of reasons: First, Fourier methods are a natural choice for homogeneous turbulence simulations. Much of the theoretical analysis of these problems is done using Fourier analysis [32, 33]. Second, spectral methods have been used a great deal in simulating homogeneous fluid turbulence, where they have been found to be both efficient and accurate [34, 29, 28, 35, 36].

In the following sections I give a derivation of the spectral and pseudospectral methods for a simple one-dimensional equation (Burger's equation) and describe the straight-forward extension to our problem. I'll explain subtle differences between spectral and pseudospectral methods for nonlinear problems such as these. Finally I give some numerical results from an accuracy test, the simulation of the dipole vortex solution to the Hasegawa-Mima equation.

3.1 Spectral and Pseudospectral Methods

Spectral and pseudospectral methods are a subset of a more general class of methods known as the Method of Weighted Residuals (MWR) [37]. These methods approximate the solutions to an equation, say $L(u) = 0$, by a finite series expansion using a suitable set of basis functions, $\{\phi_j\}$:

$$\hat{u} = u_0 + \sum_{j=1}^{N} a_j \phi_j \tag{3.1}$$

where u_0 is generally chosen to satisfy the boundary conditions so that the expansion functions only have to satisfy homogeneous boundary conditions. The *residual*, $L(\hat{u})$, is then required to be orthogonal to the space spanned by a set of weight functions, $\{w_j\}$. This gives the following set of N equations for the N coefficients a_j:

$$\langle L(\hat{u}), w_j \rangle = 0, \qquad j = 1, 2, \ldots, N, \tag{3.2}$$

where $\langle \cdot, \cdot \rangle$ is an appropriate inner product.

The spectral and pseudospectral methods differ in the choice of the weight functions, $\{w_j\}$. The spectral method takes $\{w_j\} = \{\phi_j\}$. The pseudospectral method takes $\{w_j\} = \{2\pi\delta(x - x_j)\}$, where the $\{x_j\}$ are called the *collocation points*, and are usually chosen to bring out certain properties of the basis functions. The coefficients for the pseudospectral method are thus found by requiring that the differential equation be satisfied at the collocation points, $L(\hat{u}_j) = 0$.

If $\{\phi_j\} = \{e^{ik_j x}\}$, the spectral method is immediately recognized as a truncated Fourier series:

$$\hat{u} = u_0 + \sum_{j=1}^{N} a_j e^{ik_j x}, \tag{3.3}$$

which can be inverted to give

$$a_j = \int e^{-ik_j x} (u - u_0)\, dx. \tag{3.4}$$

The pseudospectral expansion, on the other hand, corresponds to the Discrete Fourier Transform (DFT):

$$\hat{u}_i = \hat{u}(x_i) = u_0 + \sum_{j=1}^{N} a_j e^{ik_j x_i} \tag{3.5}$$

which has the inversion formula

$$a_j = \sum_{i=1}^{N} (\hat{u}_i - u_0)\, e^{-ik_j x_i} \tag{3.6}$$

which corresponds to using the trapezoidal rule for the integral in Eq. (3.3). The difference between these equations is important since Eqs. (3.5)–(3.6) may be accomplished directly via the Fast Fourier Transform (FFT) [38, 39, 40, 41] whereas Eqs. (3.3)–(3.4) may not.

3.2 An Example: Burger's Equation

Burger's equation is the the one-dimensional analog of the Navier-Stokes equation. Let u be the fluid velocity. Then Burger's equation may be written as

$$\frac{\partial u}{\partial t} + u\frac{\partial u}{\partial x} = \nu\frac{\partial^2 u}{\partial x^2}. \tag{3.7}$$

As with our treatment of the drift wave problem, we'll assume periodic boundary conditions. We'll use $2N$ Fourier modes and we'll set the period to 2π.

3.2.1 The Spectral Method

First we'll take a look at the spectral method. We define the following inner product

$$\langle f, g\rangle = \frac{1}{2\pi}\int_{-\pi}^{\pi} f(x)g^*(x)\,dx, \tag{3.8}$$

where g^* denotes the complex conjugate of g. The expansion functions are chosen to be the Fourier modes $\{e^{ikx}\}$ where[1] $-N+1 \leq k \leq N$. These eigenmodes obey the following orthogonality condition

$$\langle \phi_j, \phi_k\rangle = \delta_{j,k}, \tag{3.9}$$

where $\delta_{j,k}$ is the Kronecker δ-function. Then we let[2]

$$\hat{u}(x,t) = \sum_{k=-N}^{N} a_k(t)e^{ikx}. \tag{3.10}$$

Substituting Eq. (3.10) into the linear terms in Eq. (3.7) gives the results

$$\left\langle \frac{\partial \hat{u}}{\partial t}, e^{ikx}\right\rangle = a_k'(t), \tag{3.11}$$

$$\left\langle \nu\frac{\partial^2 \hat{u}}{\partial x^2}, e^{ikx}\right\rangle = -\nu k^2 a_k(t). \tag{3.12}$$

---

[1] It may seem somewhat odd at first to use this asymmetric transform space. For efficient evaluation of the transform, however, it is necessary to use an even number of modes. Note that the $k = N$ mode must be real and is referred to as the phase-less mode.

[2] For notational convenience I will write the sums as though there were really $2N+1$ modes. This may either be interpreted by remembering that $a_{-N} = 0$ or by adopting the more symmetric convention that $a_{-N} = a_N$ where both must be real (so there is only one mode's worth of information in the two modes).

The nonlinear term is less trivial. Differentiating Eq. (3.10) with respect to x gives

$$\frac{\partial \hat{u}}{\partial x} = \sum_{p=-N}^{N} ipa_p(t)e^{ipx},$$

and thus

$$\hat{u}\frac{\partial \hat{u}}{\partial x} = \sum_{p=-N}^{N}\sum_{q=-N}^{N} ipa_p(t)a_q(t)e^{i(p+q)x}. \tag{3.13}$$

Taking the inner product of this with e^{ikx} gives

$$\begin{aligned} \left\langle \hat{u}\frac{\partial \hat{u}}{\partial x}, e^{ikx} \right\rangle &= \frac{1}{2\pi}\sum_{p=-N}^{N}\sum_{q=-N}^{N} ipa_p(t)a_q(t)\int_{-\pi}^{\pi} e^{i(p+q-k)x}\,dx \\ &= \sum_{p=-N}^{N}\sum_{q=-N}^{N} ipa_p(t)a_q(t)\delta_{p+q,k} \\ &= \sum_{\substack{|p|,|q|\leq N \\ p+q=k}} ipa_p(t)a_q(t). \end{aligned} \tag{3.14}$$

Thus, the spectral coefficients obey the following mode coupling equation

$$\frac{\partial a_k}{\partial t} + \nu k^2 a_k(t) = \sum_{\substack{|p|,|q|\leq N \\ p+q=k}} ipa_p(t)a_q(t). \tag{3.15}$$

Energy Conservation

Suppose we define a measure of the energy in the system by the integral

$$E = \int_{-\pi}^{\pi} u^2(x,t)\,dx. \tag{3.16}$$

If we take the partial derivative of Eq. (3.16) with respect to time, and make use of Eq. (3.7), we get the following energy conservation equation:

$$\frac{\partial E}{\partial t} = -\nu\int_{-\pi}^{\pi} u_x^2\,dx. \tag{3.17}$$

The nonlinearity is annihilated by this integral since it is a total derivative and the domain is periodic. Using Parseval's Theorem for Fourier series, we can also write the above equation as

$$\frac{\partial E}{\partial t} = \frac{\partial}{\partial t} \sum_{k=-\infty}^{\infty} |a_k|^2 = -\nu \sum_{k=-\infty}^{\infty} k^2 |a_k|^2. \tag{3.18}$$

A very important property of the spectral method is that it retains the same conservation law, even though the Fourier series has been truncated. To see this we multiply the mode coupling equation, Eq. (3.14), by a_k^* and sum over all k. Consider the nonlinear term:

$$\begin{aligned}
\sum_{k=-N}^{N} a_k^* \left\{ \sum_{\substack{|p|,|q| \leq N \\ p+q=k}} ipa_p(t)a_q(t) \right\} \\
&= \sum_{\substack{|p|,|q|,|k| \leq N \\ p+q=k}} ipa_p(t)a_q(t)a_{-k}(t) \\
&= \sum_{\substack{|p|,|q|,|k| \leq N \\ p+q+k=0}} ipa_p(t)a_q(t)a_k(t) \\
&= \sum_{\substack{|p|,|q|,|k| \leq N \\ p+q+k=0}} i\frac{(p+q+k)}{3} a_p(t)a_q(t)a_k(t) \\
&= 0,
\end{aligned}$$

where we have used the property that $a_k^* = a_{-k}$ since $\hat{u}$ must be real. Thus, even if we truncate the Fourier series, we still get an energy conservation equation very similar to the one given above:

$$\frac{\partial E}{\partial t} = \frac{\partial}{\partial t} \sum_{k=N}^{N} |a_k|^2 = -\nu \sum_{k=N}^{N} k^2 |a_k|^2. \tag{3.19}$$

Why is this an important feature? The fact that Eq. (3.19) holds guarantees us that we haven't introduced any strange, nonlinear instabilities into the problem via our approximation of the spatial operators. As we shall see, this property does not hold for the pseudospectral approximation.

3.2.2 The Pseudospectral Method

As with the spectral method above, we use the exponential eigenfunctions $\{e^{ikx}\}$. Now, however, we also choose a grid in real space on which to evaluate these eigenfunctions. The appropriate grid is a uniformly spaced grid of $2N+1$ points, given by

$$x_j = \frac{2\pi j}{N}, \qquad j = -N, \ldots, -1, 0, 1, \ldots, N. \tag{3.20}$$

The discrete Fourier transform (DFT) defines a map between quantities defined on this grid and quantities defined in the transform space, as illustrated in Eqs. (3.5)–(3.6).

The appropriate inner product is

$$\langle f, g \rangle = \frac{1}{2N} \sum_{j=-N+1}^{N} f_j g_j^*. \tag{3.21}$$

With this inner product, the orthogonality condition is

$$\langle \phi_j, \phi_k \rangle = \delta_{j,k\mathrm{mod}2N} = \begin{cases} 1 & \text{if } j = k \bmod 2N \\ 0 & \text{otherwise.} \end{cases} \tag{3.22}$$

As we did for the spectral method, we write out our expansion as

$$\hat{u}_j \equiv \hat{u}(x_j, t) = \sum_{k=-N}^{N} a_k(t) e^{ikx_j}, \tag{3.23}$$

where the coefficients are advanced with the following equations:

$$\frac{\partial \hat{u}_j}{\partial t} + u_j \left[\frac{\partial u}{\partial x}\right]_j = \nu \frac{\partial^2 u_j}{\partial x^2}, \qquad j = -N+1, \ldots, -1, 0, 1, \ldots, N. \tag{3.24}$$

The pseudospectral philosophy is to do everything where it is easiest: Evaluate the spatial derivatives in the transform space (where they are local operators) and evaluate the nonlinearities and inhomogeneities on the physical grid (where *they* are local). This is an attractive philosophy for two reasons: First, it is extremely simple to implement and understand. We just use the DFT in the same manner we would use the Fourier transform as an analytic tool. Second, it is very efficient because the DFT can be performed in $\mathcal{O}(N \log_2 N)$ operations using the FFT [38], rather than the $\mathcal{O}(N^2)$ operations required to perform the convolution sum in Eq. (3.15).

The relation between Eq. (3.24) and Eq. (3.15) is illuminated by transforming Eq. (3.24) to Fourier space. The linear terms transform in a straightforward manner. Let us examine the nonlinear term. Differentiating Eq. (3.23) with respect to x gives

$$\frac{\partial \hat{u}_j}{\partial x} = \sum_{p=-N}^{N} ipa_k(t)e^{ipx_j}.$$

Multiplying this by $\hat{u}$ gives

$$\hat{u}_j \left[\frac{\partial \hat{u}_j}{\partial x}\right]_j = \sum_{p=-N}^{N} \sum_{q=-N}^{N} ipa_p(t)a_q(t)e^{i(p+q)x_j}. \tag{3.25}$$

So far this looks exactly like Eq. (3.13). Now we take the inner product with e^{ikx_j}:

$$\begin{aligned} \left\langle \hat{u}_j \left[\frac{\partial \hat{u}}{\partial x}\right]_j, e^{ikx_j} \right\rangle &= \sum_{p=-N}^{N} \sum_{q=-N}^{N} ipa_p(t)a_q(t) \sum_{j=-N+1}^{N} e^{i(p+q-k)x_j} \\ &= \sum_{p=-N}^{N} \sum_{q=-N}^{N} ipa_p(t)a_q(t)\delta_{p+q,k\mathrm{mod}2N} \\ &= \sum_{\substack{|p|,|q|\leq N \\ p+q=k\mathrm{mod}2N}} ipa_p(t)a_q(t). \end{aligned} \tag{3.26}$$

The mode coupling equation corresponding to Eq. (3.15) is then

$$\frac{\partial a_k}{\partial t} + \nu k^2 a_k(t) = \sum_{\substack{|p|,|q|\leq N \\ p+q=k\mathrm{mod}2N}} ipa_p(t)a_q(t),$$

or, more explicitly

$$\begin{aligned} \frac{\partial a_k}{\partial t} + \nu k^2 a_k(t) = &\sum_{\substack{|p|,|q|\leq N \\ p+q=k}} ipa_p(t)a_q(t) \\ &+ \sum_{\substack{|p|,|q|\leq N \\ p+q=k+2N}} ipa_p(t)a_q(t) + \sum_{\substack{|p|,|q|\leq N \\ p+q=k-2N}} ipa_p(t)a_q(t). \end{aligned} \tag{3.27}$$

The last two terms in Eq. (3.27) are called the *aliasing* terms [39, 29, 42]. They arise from the fact that, if two quantities have wavenumbers as high as N, then their product will have wavenumbers as high as $2N$. However wavenumbers $k > N$ cannot be interpreted correctly when sampled on our $2N$-point grid. When such a high mode is sampled on this grid, the beat-mode energy gets misplaced into the mode $k - 2N$ rather than k (this is why they are called *aliases*—they cannot be distinguished when sampling on our fixed grid).

Are these terms *errors*? Not necessarily [28]. The above scheme is consistent with the original differential equation. Thus if it were stable, it would converge. But there is a possible source of trouble here. If we try to derive an energy conservation equation for Eq. (3.27) we quickly learn that the last two terms cannot be annihilated. The lack of energy conservation opens the door to a nonlinear numerical instability known as the *aliasing instability* [28, 42]. The aliasing instability usually disappears if the dissipation spectrum is very well resolved, i.e. as N gets very large for fixed ν [36]. However if $\nu = 0$ then there is no finite dissipation region and instability does not go away with increasing N.

3.2.3 A Fast Spectral Method

For our purposes, we have found that the aliasing instability is very difficult and expensive to remove, if not impossible. Thus we wish to implement the spectral method in an efficient fashion. This can be done as follows [29]: Suppose that $a_k = 0$ for $|k| \geq \frac{2}{3}N$. Then it is impossible to write $k + 2N = p + q$. To see this suppose we can find k, p, q satisfying these conditions. Then we may write

$$2N = p + q - k \leq |p| + |q| + |k| < 3(\frac{2}{3}N) = 2N$$

which is a contradiction. A similar result holds true for $k - 2N = p + q$. Thus the two aliasing sums vanish. Only the first term survives, and it is just the spectral mode coupling sum. However, after one iteration there will be modes excited with $\frac{2}{3}N < |k| < N$. The trick is to just set those modes equal to zero. If we only consider the modes with $|k| < \frac{2}{3}N$ and continually set the rest of the modes to zero (this process is known as *dealiasing*, for the obvious reason), we find that the coefficients satisfy the same equation as the spectral coefficients for a spectral approximation with only 2/3 as many points.

The above scheme is often referred to as a dealiased pseudospectral method. Actually this is just a fancy term for a spectral method, as we have shown above that they are one and the same. Note that there is some overhead incurred in that we no longer have use of the full resolution of the grid. The work that must be done still scales like $N \log_2 N$ even though we're only getting 2/3 the resolution. But for N large this is still vastly superior to the $(2N/3)^2$ work that would be required to directly evaluate the convolution sum on the same effective grid.

There are more efficient methods to implement a spectral method [29, 28]. They all use the FFT and their operation counts all scale like $N \log_2 N$, but with a smaller coefficient in front. The disadvantages of these schemes stem from their complexity. They usually involve shifted grids and much more coding. The scheme we use is fairly simple and has the advantage that it can be used as a pseudospectral code just by eliminating the dealiasing part of the algorithm.

3.3 The Drift Wave Code

The code which I have written uses a fast spectral method similar to that described above. It can be used as a pseudospectral code, though I have not had much success in doing so. The style of a pseudospectral code, however, makes the code very easy to modify. The code could easily be modified to solve any similar (quadratically nonlinear) equation with periodic boundary conditions—the 2-D Navier-Stokes equations, for instance. Also, the nonadiabatic electron piece is somewhat generic in its $\omega - \omega_{*e}$ form, and could probably be adapted to other low frequency plasma problems.

3.3.1 Testing the Code

One of the difficulties in solving a set of model equations such as ours is: how do you know the code is working right? Although there is no way to prove that a code as complex as this is correct, there are a few tests which give us some confidence that nothing major is wrong.

Energy and Enstrophy Conservation

The first test is to see how well energy and enstrophy are conserved when there is no dissipation. As in the case of Burger's equation, these moments are exact constants even after the truncation of the Fourier series. Thus the only variation we should see would be due to the time-discretization, and we should be able to make this variation small.

The code passes this test with flying colors. Many runs have been made without dissipation while studying isolated monopoles and dipoles (see Chapter 4), and the relaxation to the equipartition spectrum. In these runs, energy and enstrophy are typically conserved to 6–8 decimal places.

Incidentally, if the code is run as a pseudospectral code in these cases, it is violently unstable.

Convergence of the Dipole Vortex Solution

The Hasegawa-Mima equation possesses a family of exact solutions which are of the form of localized dipole vortices, or *modons*, traveling at a constant velocity in the diamagnetic direction: $\phi(x, y - ct)$ [43, 26]. Since they are highly localized, it should be possible to do a good job of simulating their motion using our code, with its finite, periodic grid.

Table 3.1 summarizes the initial conditions for the dipole vortex test. Here c is the vortex speed and r_0 is the radial size of the inner solution for the vortex (again, see Chapter 4). These are sufficient to specify the initial potential profile for the solution. H_x and H_y are the x and y dimensions of the domain, and T is the length of time for which the solution was integrated. Since $cT = H_y$, the final profile should be equal to the initial condition.

Figure 3.1 shows the L_2 error, ϵ_2, in the solution at time T, which is define to be:

$$\epsilon_2^2 \equiv \frac{\sum_{\mathbf{x}} \left(\phi(\mathbf{x}, T) - \phi(\mathbf{x}, 0)\right)^2}{\sum_{\mathbf{x}} \phi^2(\mathbf{x}, 0)}, \tag{3.28}$$

Table 3.1: *Standard Dipole Vortex*

Input Parameter	Value
c	2.0
r_0	6.0
H_x	20π
H_y	20π
T	10π

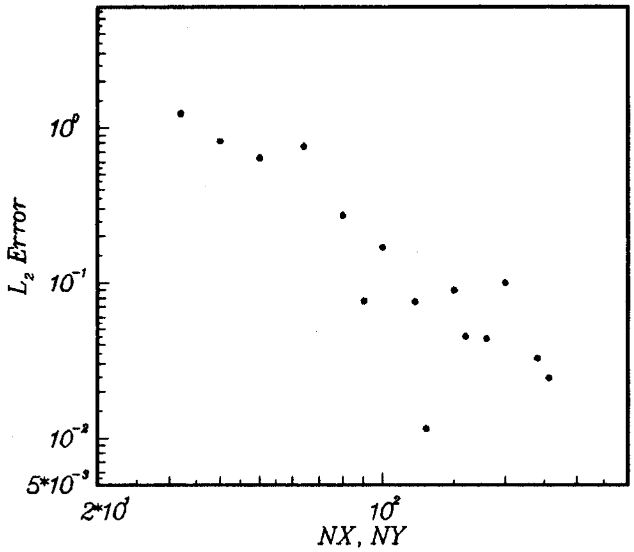

Figure 3.1: *L_2 error in calculating the trajectory of the standard dipole vortex.*

The fluctuations of ϵ_2 as N increases are inexplicable. However, the general trend has approximately a N^{-3} slope. This is the best that can be expected since the exact solution has a discontinuous third derivative. This implies that the error can go to zero no faster than N^{-4}. In fact the L_∞ error, or maximum error, cannot go to zero faster than N^{-3}. I've calculated both the L_2 and L_∞ errors, and they decrease at the same rate. Thus I believe that the code is converging at the expected rate, though I do not understand the large fluctuations.

Conservation of Density

The truncated system is not guaranteed to conserve the density, $\rho(\mathrm{x}, t)$, along the fluid element trajectory. How well this quantity is conserved gives a measure of how well our solution is tracking the correct solution. Runs have been made in which marker particles, moving at the $E \times B$ velocity, were tracked. To a good approximation, these particles are observed to move along the lines of constant ρ, which is a qualitative indication that density is being conserved.

When trapped structures form in the system, lines of constant ρ form closed curves. Conservation of density implies that the area enclosed in such curves must remain constant so long as the curve remains closed. This is also observed to hold true so long as the wavelength of the fluctuations is not too small.

The Nonadiabatic Response

The qualitative checks mentioned in the above section have also been checked in the case when the nonadiabatic electrons are included. Marker particles still tend to move primarily along the lines of constant ρ, and trapped structures still do a fairly good job of preserving their area. However the performance in this case is not as good as it is when the nonadiabatic electrons are neglected.

Unfortunately, there seems to be no good quantitative test for the nonadiabatic electron response calculations. The code has been carefully checked on numerous occasions, and I believe it to be correct. This uncertainty is complicated by the fact that the model itself is only approximate.

Chapter 4

Isolated Trapped Structures

If an isolated potential fluctuation is sufficiently large, the resulting electric field may *trap* elements (or "particles") of fluid, causing them to move in a coherent fashion along with the fluctuation. For this trapping to occur, two conditions must be satisfied: First, the electric field must be sufficiently large to overcome the natural tendency for the fluctuation to move away from the particle at the diamagnetic drift speed. Second, the fluctuation must be coherent, with a lifetime long compared with the diamagnetic drift time scale.

We shall see in Chapters 5 and 6 that trapped structures often arise naturally in the turbulent evolution of the plasma. In this chapter we look at isolated trapped structures to see if we can discern anything about their behavior which might give us some insight into their role in the turbulent system. We begin this discussion by looking at the well known dipole vortex solutions to the Hasegawa-Mima equation. Then we will look at the behavior of monopole vortices.

Note that the simulations presented in this chapter were done by solving the Hasegawa-Mima equation. The assumption made in deriving our model equation, Eq. (2.74), is essentially this: on the fast time scale, the nonadiabatic electron response has only a small perturbative effect; the "fast" scale being on the order of ω_{*e}^{-1}, or the eddy turnover time. On this time scale the Hasegawa-Mima equation is essentially correct. Since it is considerably less complex than our model, and also less expensive to simulate, I will deal only with it in this chapter and the next.

4.1 Dipole Vortices

Certain classes of nonlinear initial value problems possess exact solutions called solitons. These are highly localized traveling wave solutions with the property that soliton–soliton interactions leave the individual solitons intact. The independence of these particle-like structures allows one to use them to build up general solutions to the corresponding nonlinear problem [44, 45, 46].

The inviscid Hasegawa-Mima equation also possesses a family of exact traveling wave solutions. The simplest member of this family is a dipole vortex type solution, usually called a *modon.* Modons are not solitons, as modon–modon collisions are not elastic. However many types of collisions between modons are nearly elastic [47, 48]. Also, antisymmetric initial conditions which are vaguely shaped like a modon will tend to relax to a modon plus some noise. This apparent robustness has lead to a hope that studying modons might help in our understanding of drift wave turbulence. Indeed, theories for the turbulent spectrum have even been proposed which are based on a weakly interacting "gas" of modons [26, 49, 50, 6].

In this section we shall derive the modon solution, and then go on to discuss some of its properties. The derivation closely follows that of Meiss, *et al.* [26]. (See also [43, 51].) Several reasons shall be given as to why modons might not be an important feature in a fully turbulent system.

4.1.1 Derivation of the Modon Solution

If the Hasegawa-Mima equation is to have any exact, coherent, trapped solutions, then they must either be stationary, or move in the poloidal (y) direction. The reason for this is the constraint of conservation of the density function. This conservation law would have to be violated for the solution to move with, say, a constant x velocity. Thus we are lead to look for solutions to this equation of the form $\phi(x, y-ct)$. Substituting this into Eq. (2.57) gives:

$$\left\{x - \phi + \nabla_\perp^2\phi,\ \phi - cx\right\} = 0, \tag{4.1}$$

which is equivalent to saying that

$$\nabla_\perp^2\phi - \phi + x = F\left(\phi - cx\right), \tag{4.2}$$

where F is some function. Now, if we assume that the solution is localized, i.e. that $\phi \rightarrow 0$ as $x, y \rightarrow \infty$, then we see that by fixing x and making y very large, F must be linear:

$$F(z) = -\frac{1}{c}z, \tag{4.3}$$

leading to the equation

$$\nabla_{\perp}^{2}\phi + \left(\frac{1}{c} - 1\right)\phi = 0. \tag{4.4}$$

Equation (4.4) can only have isolated (non-oscillating) solutions if $c(c-1) > 0$, requiring that either $c > 1$ or $c < 0$.

The above analysis breaks down in the region where fluid elements are trapped. According to Eq. (2.77), a fluid element moves along lines of constant density; i.e. the *streaklines* are the contours of constant ρ. Trapping implies closed streaklines, and thus closed contours of constant ρ. Since these contours do not extend to infinity, the asymptotic analysis used above to determine the form of F is incorrect. In the trapped region, F is arbitrary. In order to get an analytical solution for the potential, we will assume the simplest case:

$$F(z) = -(1 + s^{2})z,$$

where s must be determined from the boundary conditions. Then the trapped solution must obey the following equation:

$$\nabla_{\perp}^{2}\phi + s^{2}\phi = \left(\left(1 + s^{2}\right)c - 1\right)x. \tag{4.5}$$

This equation will have a bounded solution near the origin since $s^{2} > 0$, which is why we chose this particular form for F.

Mathematically, we must solve the problem as a two region problem which has an outer solution obeying Eq. (4.4) and an inner solution obeying Eq. (4.5). The matched solution is required to be continuous and twice differentiable across the boundary between these two regions. This is the only way to obtain a general solution which is bounded near the origin and which decays rapidly away from the origin.

For simplicity, we assume that the boundary between the trapped and untrapped regions, which must itself be a streakline, is a circle of radius a. We introduce the cylindrical coordinates:

$$r^2 \equiv x^2 + (y - ct)^2 \tag{4.6}$$

$$\cos\theta \equiv x/r. \tag{4.7}$$

Under these conditions, Eqs. (4.4)–(4.5) have solutions which are a linear superposition of Bessel functions of r, multiplied by $cos(m\theta)$ for integral m. The simplest such solution is the $m = 1$ solution, given by the expression:

$$\phi = AK_1(\beta r/a)\cos\theta, \qquad r > a, \tag{4.8}$$

and

$$\phi = \frac{Br}{a}\cos(\theta) + CJ_1(\gamma r/a)\cos(\theta), \qquad r < a \tag{4.9}$$

where

$$\beta \equiv a(1 - 1/c) \tag{4.10}$$

and where γ is defined as a solution to the equation

$$\frac{K_2(\beta)}{\beta K_1(\beta)} = -\frac{J_1(\gamma)}{\gamma J_1(\gamma)}, \tag{4.11}$$

and is related to s by

$$s = \frac{\gamma^2}{a^2}.$$

The coefficients A, B, and C are found to be

$$\begin{aligned} A &= \frac{ac}{K_1(\beta)}, &(4.12)\\ B &= ac\left(1 + \frac{1}{\gamma^2}\right), &(4.13)\\ C &= -\left(\frac{\beta}{\gamma}\right)^2 \frac{ac}{J_1(\gamma)}. &(4.14) \end{aligned}$$

In these equations, J_n is the n-th order Bessel function of the first kind, and K_n is the modified n-th order Bessel function of the first kind.

Figure 4.1 shows a snapshot of the solution derived above, where $c = 2$ and $a = 6$ (c.f. Table 3.1). Figure 4.2 illustrates the evolution of this solution in time via a sequence of contour plots of the potential.

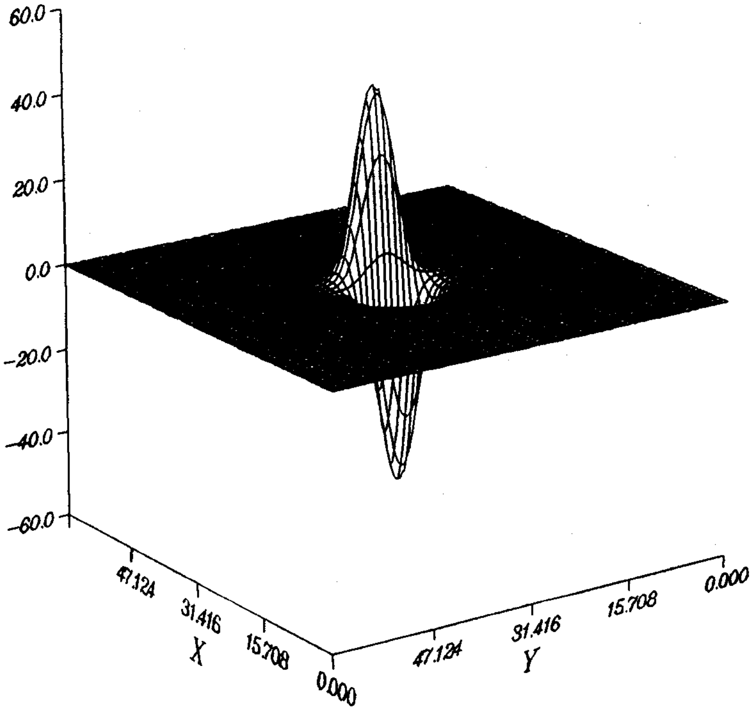

Figure 4.1: *Snapshot of the potential profile for the dipole vortex solution described above with* $c = 2$ *and* $a = 6$.

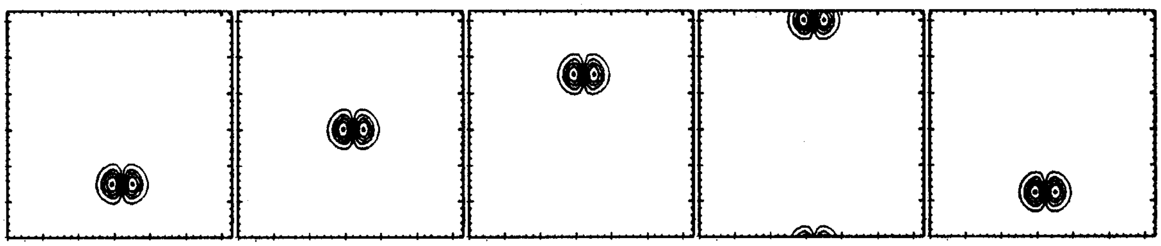

$t = 0.00$ $t = 7.54$ $t = 15.1$ $t = 22.6$ $t = 30.2$

Figure 4.2: *Evolution of the dipole vortex shown in Figure 4.1.*

4.1.2 Modon Problems

While the modon is an academically interesting structure, being an exact trapped solution to a nonlinear partial differential equation, we do not feel that it is an important element in the evolution of turbulence. This conjecture is based on several facts: the modon is energetically unfavorable in the presence of nonadiabatic electrons, its energy density and electric field are too large, and it does not appear to be stable to certain types of perturbations. This conjecture seems to be supported by the absence of dipole vortices in our turbulent simulations, as well as those of others [54].

Nonadiabatic Electrons

That dipoles are energetically unfavorable can be seen by examining the response of the nonadiabatic electrons to a structure moving with a constant velocity in the y-direction: $\phi(x, y - ct)$. In this case, the frequency spectrum is simply $|\phi_{\mathbf{k}\omega}|^2 = |\phi_{\mathbf{k}}|^2 \delta(\omega - ck_y)$, so that our energy balance equation becomes

$$\frac{dE}{d\tau} = -\sum_{\mathbf{k}} \nu_k E_{\mathbf{k}} - \delta_0 \sum_{\mathbf{k}} c\,(c-1)\, k_y^2 |\phi_{\mathbf{k}}|^2.$$

The structure is damped, even in the absence of viscosity, if $c(c-1) > 0$. This is exactly the velocity constraint which must be satisfied for a modon to exist.

Note that in this respect, the approximations made in the Terry-Horton equation are qualitatively wrong. In their model, all modes grow with the linear growth rate. Thus a dipole would also grow. Unfortunately our model cannot properly handle the damping of the modon either. Modons do damp, but they have such a high electric field that the perturbation expansion in δ_0 breaks down very quickly. This results in a numerical problem in which much energy is transferred to large k where it is very quickly damped.

Anyway, in a system in which the nonadiabatic electrons play a role, the dipole vortex solutions are energetically unfavorable. This does not, however, explain the fact that dipoles are not frequently seen in simulations in which the electrons are adiabatic.

High Energy

The most obvious problem which I have found with the modon is that it is a very high energy state. The model has a strong tendency to propagate fluctuations along at the diamagnetic drift velocity. The modon overcomes this tendency because it has a very strong electric field, resulting in a very large $\mathbf{E} \times \mathbf{B}$ velocity. One may think of the modon as two monopoles, each convecting the other forward with this high velocity.

In fact, the energy contained in a single dipole, such as the one shown in Figure 4.2, is higher than in many of the saturated turbulence runs which we'll look at in Chapter 6; and all of that energy is tied up in one trapped structure that is significantly smaller than the size of the domain. Were the domain filled with such structures, the RMS potential and electric fields would be much higher than those measured experimentally.

Instability

Because of the modon's perceived importance, a fair amount of research into the modon's behavior and stability has been done. Several people have attempted to prove that the modon solution is a particularly stable one. They have only had limited success. Laedke and Spatschek proved that the $c < 0$ vortex is linearly stable [55]. They also derived some more general linear and nonlinear stability criteria in [56], but were unable to draw any specific conclusions. Gordin and Petviashvili also prove a stability result [57], but again only for $c < 0$, and they qualify their result with the statement that it only applies to the shape of the modon, and not too its velocity vector.

We have found experimentally that the $c > 1$ modon is very unstable (most likely linearly unstable) to perturbations in its velocity vector. If we start one of these modons off with just a slight perturbation, the perturbation will quickly grow. Figure 4.3 shows part of the evolution of such a vortex.

The instability can be understood in terms of conservation of the density. The dipole initially moves an increment to the left. Since the density must be conserved during this motion, the left lobe must grow and the right lobe must shrink. But the size of the lobe is related to its circulation. Thus the left lobe now has greater circulation than the right lobe, and will begin to pull it around, increasing the angle

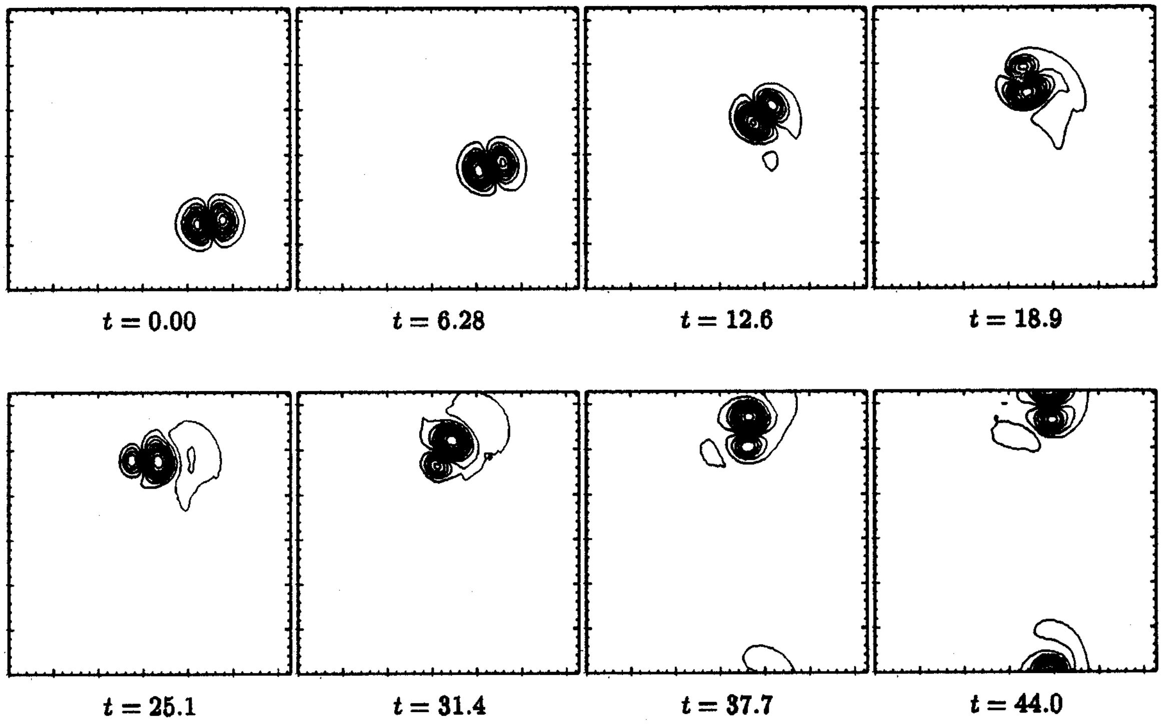

$t = 0.00$ $t = 6.28$ $t = 12.6$ $t = 18.9$

$t = 25.1$ $t = 31.4$ $t = 37.7$ $t = 44.0$

Figure 4.3: *Instability of the* $c > 1$ *modon.*

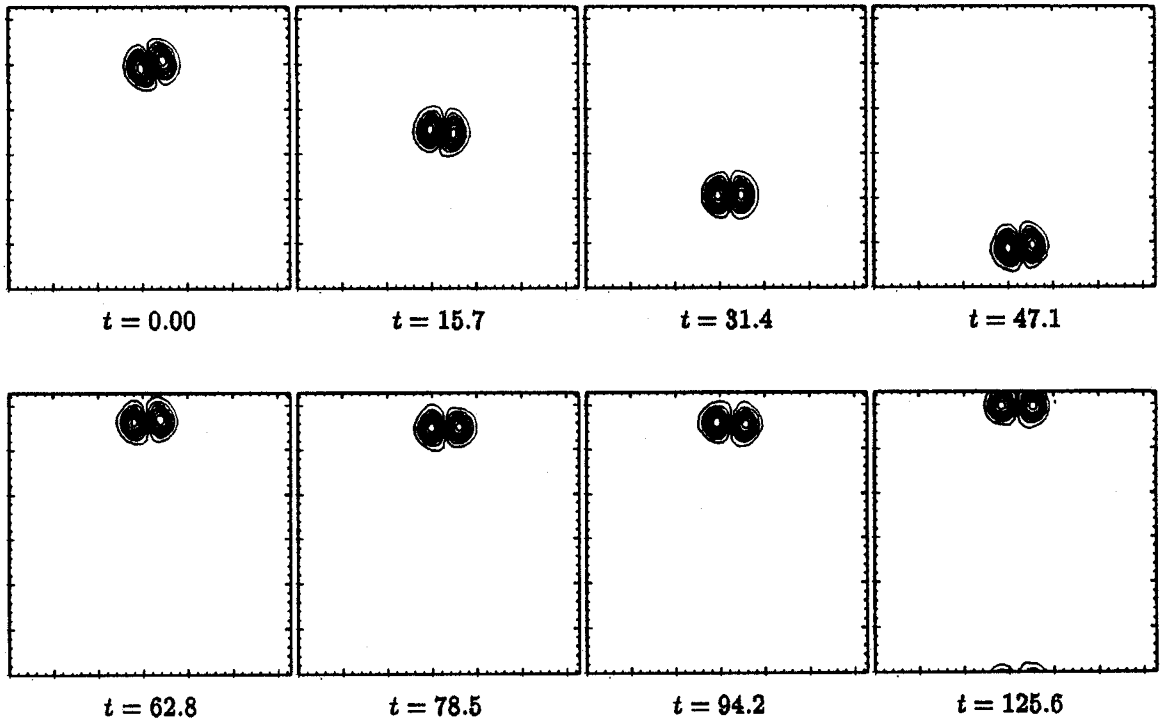

Figure 4.4: *Instability of the* $c < 0$ *modon.*

the velocity vector makes with the y-axis. This positive feedback will cause a linear instability.

On the other hand, this same argument would predict that there is negative feedback to such a perturbation to a $c < 0$ vortex. Indeed, Figure 4.4 shows that initially the vortex continues in the $-y$ direction, with an oscillating x-velocity. But there is a constant strain on the vortex that weakens the interaction between the two lobes until the electric field between the lobes is no longer strong enough and they begin to be convected "downstream". Thus it appears that this modon is linearly stable, in agreement with theory, but probably nonlinearly unstable. (Makino, *et al.*, made observations similar to these in [47], but gave only passing mention of the $c > 1$ modon, and did not discuss the implications of these observations on the role of the modon in a turbulent system.)

McWilliams, *et al.* [58] studied the problem of modon interactions with various scales of perturbations. Their observation was that modons were fairly stable to small scale (high k) perturbations, but were quickly destroyed by large scale perturbations, even if they were small in amplitude. (Their model, a barotropic β-plane model, is somewhat different from the Hasegawa-Mima equation, but does have some of the same general features in that the dominant nonlinearity is the same vector nonlinearity, and the system supports linear waves.) This is in agreement with the above observations, since a shift in the dipole's direction corresponds to a perturbation who's size is of the order of the dipole radius.

Other Problems

A further problem is that of birth. How would a dipole evolve from nothing? A $c > 0$ vortex can be formed by the coalescing of two opposing monopoles, with the negative lobe to the right and the positive lobe to the left [59]. They will drift together and form the dipole. In practice, a true dipole is extremely unlikely to result from this. There will always be some slight asymmetry, and the dipole will quickly fall apart as described above.

On the other hand, such a simple mechanism cannot even work for the $c < 0$ dipole. If we reverse the monopoles described above, giving them the polarity required to form a $c < 0$ monopole, they will drift apart. There has to be a strong force to push them together, and this seems very unlikely since nearly all of the energy in the system will have to end up in the resulting dipole.

One other problem has to do with the frequency spectrum. Due to the high energy content of individual modons, and their instability, a scenario in which the turbulence is composed of closely packed, strongly interacting modons is impossible. Rather one could only get experimentally acceptable energy levels by having a very rarefied gas of weakly interacting dipoles. What is wrong with this picture? Two things: First, it would be a very intermittent system and there seems to be no experimental evidence for such. But more importantly, this system would have a nearly discrete frequency spectrum, with delta functions at $\omega = c_i k_y$, where i indicates a particular modon. Experimentally, the frequency spectrum is found to be continuous with a width $\Delta\omega \sim \omega_{*e}$.

4.2 Monopole Vortices

The above discussion gave several reasons why dipole vortices are not likely to evolve in turbulent flows. Certainly it seems unlikely that a structure more complicated than the dipole could be any more robust. Thus, in this section, we examine the simplest type of trapped structure: a monopole vortex. In later chapters we shall see that such structures can indeed evolve in a turbulent setting.

We note that there are monopole perturbations to the modon solutions which produce stable traveling wave solutions. These "rider" perturbations may be very large and can mask the underlying dipole nature of the modon [51]. The resulting solution, however, still has all the properties and problems of the modon. In fact, it has even more energy. Thus we do not consider this type of "monopole" as being an important possibility.

4.2.1 Theory

There are no exact monopole solutions of the form $\phi(x, y - ct)$. The problem is that the linear modes in the system have phase velocities in the range $0 < \omega/k_y < 1$. The modon did not interact with these waves because its velocity complemented this range. This was made possible by the very strong interaction between the two lobes of the dipole.

An isolated monopole has no such mechanism. Thus one expects that an isolated monopole will move with $0 < c_y < 1$. This will cause it to be resonant with the linear modes in the system and thus to lose energy to them. Losing energy, in turn, implies that the structure must move in x in order to conserve the density in the trapped interior region.

The question, then, is how long would such a structure last. How fast does it give up energy to the linear waves, and move in x? Although it seems like this would be a analytically tractable problem, assuming the velocity c_x was small, it has not, to my knowledge, been solved. The fact that the solution in the outer region is an outgoing wave solution complicates the problem a great deal.

The only qualitative statement that is fairly obvious is this: As the radius of the structure increases, its lifetime should increase. Why? The process of losing energy to the waves must occur through dispersion. In fact, were it not for the dispersive term in the equation, any symmetric structure would be an exact solution to the equation since a symmetric function trivially annihilates the equation's vector nonlinearity. Making the structure large makes the dispersive term small.

4.2.2 Simulation

Figure 4.5 illustrates the evolution of an initially symmetric monopole fluctuation. Figure 4.6 illustrates the trajectories of a fluid particle trapped in that monopole. Initially there is a short relaxation period. During this time the monopole gains a small asymmetric component and its x and y velocities change slightly from their initial values (these velocities are given roughly by the average slopes of the curves in the x–t and y–t plots in Figure 4.6). After this quick adjustment, the monopole seems to settle into a quasistationary state moving with a constant x and y velocity with, in this case, $0 < c_x << c_y < 1$. There is also a trailing wake created behind the monopole as it gives up energy to the waves in a Cerenkov emission type of process.

I have simulated dozens of such monopoles, varying the monopole radius and average electric field. So long as their radius is not too small, in which case dispersion can quickly destroy them, they behave in a manner similar to that described above. I've used both Gaussian profiles and polynomial profiles for initial conditions, and found that initial conditions with roughly the same size and electric field lead to very similar histories. The x velocity is usually fairly small, and the y velocity is usually in the range $0.5 < c_y < 1.0$. The fact that the x velocity is quite small means that the monopole lifetime, though not infinite, will be very long (roughly ϕ_{max}/c_x).

After awhile the box, due to the periodic boundary conditions, begins to fill up with waves excited by the monopole. When these waves get sufficiently large they will, of course, interfere with the monopole's evolution.

There are a couple of general trends: The monopole lifetime increases (i.e. c_x decreases) as its radius increases, and as the average electric field increases. These trends are illustrated in Figure 4.7 and Figure 4.8. The first trend was hypothesized above. The second is not so easy to understand, except to note that this means that the inner particles are trapped more strongly.

(Similar long lived monopoles were studied by McWilliams and Flierl [60] for a two-zone quasi-geostrophic β-plane model. This model is considerably different from the Hasegawa-Mima equation, but does have some of the same general features in that

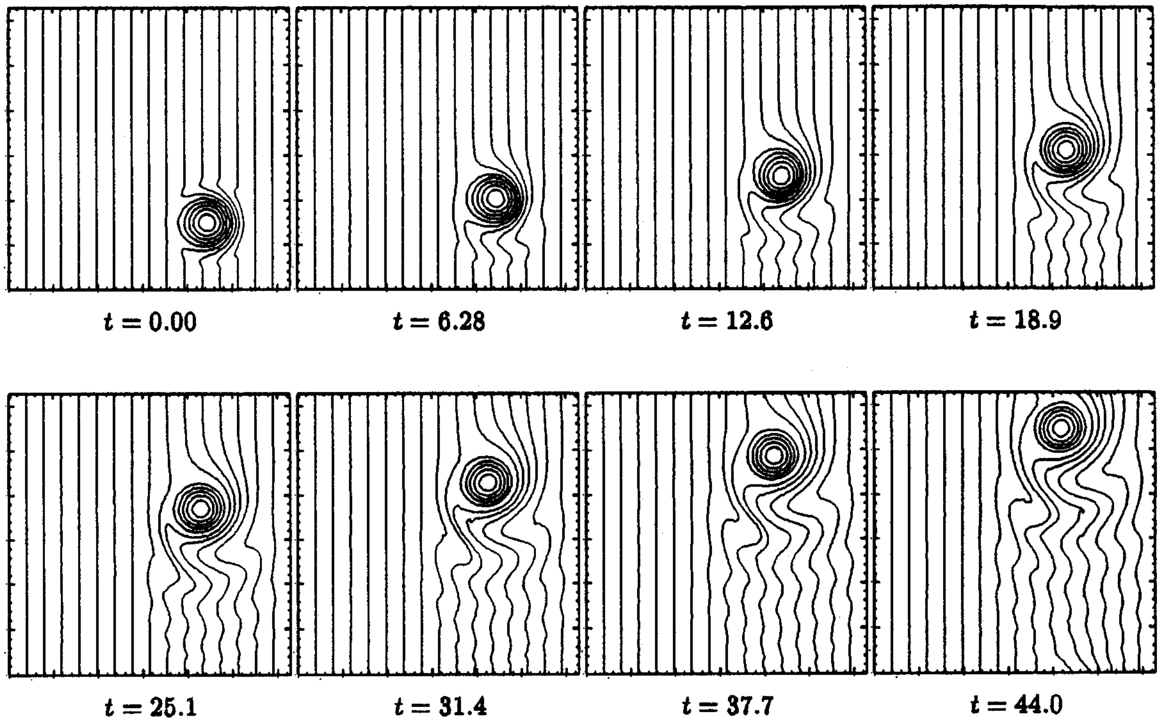

$t = 0.00$ $t = 6.28$ $t = 12.6$ $t = 18.9$

$t = 25.1$ $t = 31.4$ $t = 37.7$ $t = 44.0$

Figure 4.5: *Evolution of a monopole perturbation.*

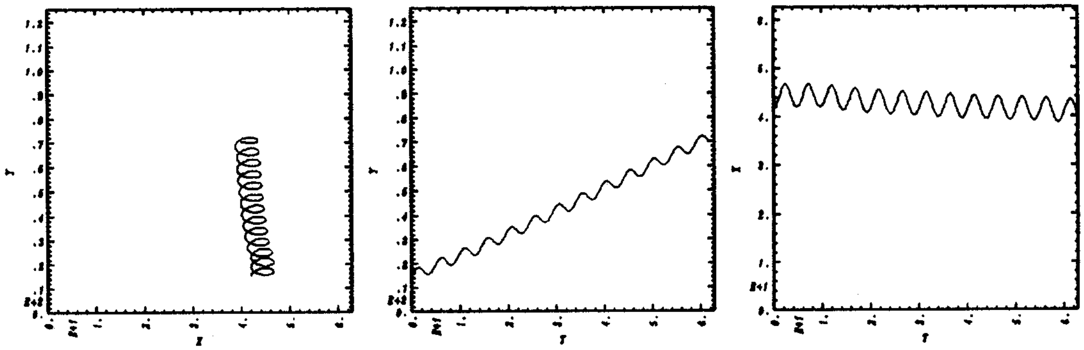

Figure 4.6: *Trapped particle trajectory for a fluid particle trapped in the monopole shown in Figure 4.5.*

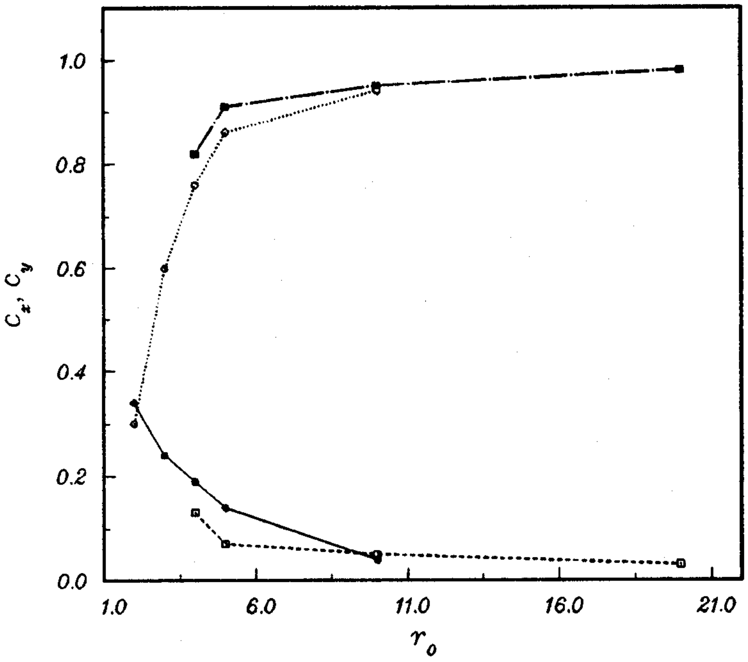

Figure 4.7: *Effect of the initial radius on the monopole evolution.*

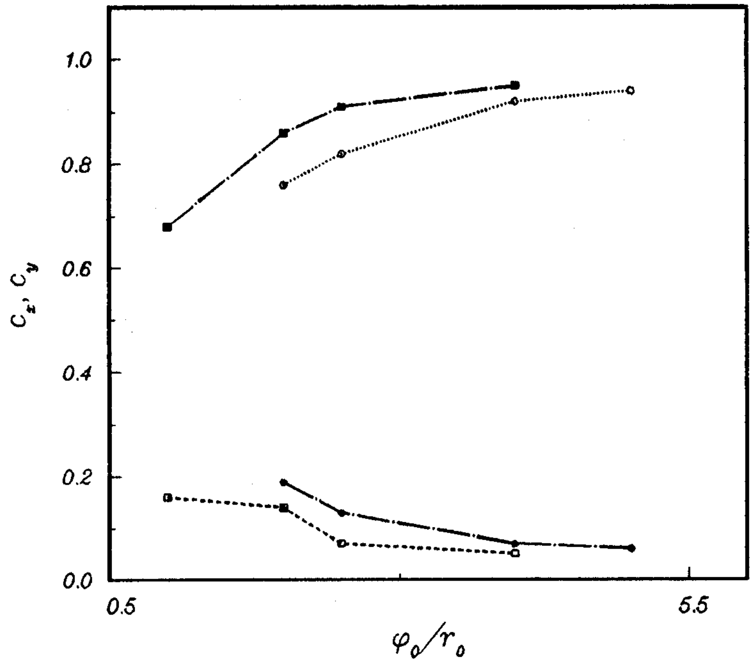

Figure 4.8: *Effect of the average electric field on the monopole evolution*

the dominant nonlinearity is the same vector nonlinearity, and the system supports linear waves.)

In summary, the monopole solution can be very long lived and appears to be quite robust. I have studied various perturbations such as viscosity, nonadiabatic electrons, and various levels of random noise. The isolated monopole is only weakly affected by these various perturbations.

Chapter 5

Turbulence of the Hasegawa-Mima Equation

In Chapter 4 we studied some of the properties of isolated trapped structures. There we showed that the lifetime of an isolated monopole vortex could be much longer than the diamagnetic drift time scale (ω_{*e}^{-1}). How might such vortices arise in a turbulent flow? In this chapter we'll attempt to understand this question via the Hasegawa-Mima equation.

It was shown in Chapter 2 that the Hasegawa-Mima equation possesses two quadratic constants of motion: the energy, E, and the generalized enstrophy, Ω. Furthermore, it was shown in Chapter 3 that these constants are *rugged* in the sense that they survive the truncation of the system to a finite number of degrees of freedom. Hasegawa reviewed several nonlinear systems having multiple rugged invariants, and found that these have a tendency to evolve towards *self-organized* states [54]. If the energy in the system is sufficiently large, these self-organized states will be trapped structures.

5.1 Equilibrium Turbulence

5.1.1 Theory

The first implication of the existence of two constants of motion is the tendency of energy to be transferred to longer wavelengths. This may be simply demonstrated as follows. First recall that the energy and enstrophy are defined as

$$E = \sum_k E_k$$

and

$$\Omega = \sum_k k^2 E_k$$

where $E_k = (1 + k^2)|\phi_{\mathbf{k}}|^2$. We define an average k vector as

$$\langle k \rangle = E^{-1} \sum_k k E_k.$$

Now, suppose we start the system off with some narrow spectrum. Intuitively we expect that the spectrum will be broadened by the nonlinear coupling. Thus we may write

$$\frac{\partial}{\partial t} \left\langle (k - \langle k \rangle)^2 \right\rangle > 0.$$

However

$$\begin{aligned}
\left\langle (k - \langle k \rangle)^2 \right\rangle &= E^{-1} \sum (k - \langle k \rangle)^2 E_k \\
&= E^{-1} \sum \left(k^2 - 2k \langle k \rangle + \langle k \rangle^2\right) E_k \\
&= \frac{\Omega}{E} - \langle k \rangle^2 .
\end{aligned}$$

Now, since Ω and E are constant, this means that

$$\frac{\partial}{\partial t} \left\langle (k - \langle k \rangle)^2 \right\rangle = -\frac{\partial}{\partial t} \langle k \rangle^2 > 0,$$

or

$$\frac{\partial}{\partial t} \langle k \rangle^2 < 0.$$

If the energy spectrum broadens, its average wave number must decrease.

This behavior may be put on a firmer foundation using the powerful tool of equilibrium statistical mechanics. This theory has been discussed at length in Kraichnan and Montgomery's review paper on two-dimensional turbulence [61], and applications to various two dimensional systems may be found in [54, 62, 63, 64, 65, 66, 67] and others. Here we will only summarize its predictions without attempting to give a rigorous derivation of the results.

Two factors make the statistical mechanics treatment possible: First, as mentioned above, the energy and enstrophy moments remain exact constants of motion for the system even after the Fourier space has been truncated to a finite number of modes. Second, one may define a phase space whose coordinates are the real and imaginary parts of the potential and it may be shown that this phase space is incompressible (see the reviews by Orszag and by Kraichnan [21, 61], and references therein).

Once the system has evolved to its equilibrium state, it may be described by a macrocanonical ensemble [68]. We denoting the state of the system by a set Fourier coefficients: $\zeta = \{\phi(\mathbf{k}_1), \phi(\mathbf{k}_2), \ldots\}$. The density distribution may be written as

$$\begin{aligned} P(\zeta) &= c e^{-(\alpha E + \beta \Omega)} \\ &= c \exp\left(-\sum \left(1+k^2\right)\left(\alpha + \beta k^2\right) |\phi(\mathbf{k})|^2\right). \end{aligned} \tag{5.1}$$

where c is a normalizing constant, and α and β are the inverse *temperatures* corresponding to the energy and enstrophy constants.

Using Eq. (5.1), various ensemble averages may be calculated. The average of the k-spectrum is

$$\langle |\phi_{\mathbf{k}}| \rangle = \frac{1}{(1+k^2)(\alpha + \beta k^2)}. \tag{5.2}$$

The average isotropic energy spectrum is then given by

$$E(k) = \frac{2\pi k}{\alpha + \beta k^2}. \tag{5.3}$$

Similarly, the average isotropic enstrophy spectrum is

$$\Omega(k) = \frac{2\pi k^3}{\alpha + \beta k^2}. \tag{5.4}$$

These isotropic spectra are defined such that the total energy and enstrophy are given by

$$E = \int E(k)dk$$

and

$$\Omega = \int \Omega(k)dk.$$

Given the total energy and enstrophy of a given system, these expressions may be solved for α and β.

If the energy and enstrophy are such that $k_E^2 = \Omega/E << 1$, which is frequently the case (as will be discussed in the next section), then the energy temperature, α, will be negative and most of the energy in the system will reside in the longest wavelength possible [63]. Also note that for large k, the enstrophy spectrum increases linearly with k. Thus we see that the system has an apparent tendency to transfer the energy to the longest wavelengths in the system while simultaneously transferring the enstrophy to the shortest. This is the *dual cascade* phenomenon of two-dimensional turbulence.

We should also note that these spectra are completely non-physical. Indeed, they are not integrable in the limit as $k_{max} \to \infty$. They serve only as an indication of the direction in which the system would like to evolve.

5.1.2 Simulation

In Figure 5.1 we show a comparison of the spectra predicted above and that calculated by our code. The initial conditions for this case were

$$\phi_{\mathbf{k}}(t=0) = \begin{cases} \phi_0 e^{-i\alpha(\mathbf{k})} & k_l < k < k_u \\ 0 & \text{otherwise.} \end{cases}$$

where $\alpha(\mathbf{k})$ is a uniformly distributed random number in the range $0 < \alpha(\mathbf{k}) < 2\pi$. The various parameters describing this run, which we shall refer to as Run 5.1, are summarized in Table 5.1. In the table, H_x and H_y are the x and y dimensions of the domain, and k_{max} is the maximum component of the $\mathbf{k}$-vector along either axis (i.e. the $k_{max} = \pi/\Delta x$). At high-k, we observe that the spectrum does approach the equilibrium prediction. It may also be approaching the predicted value at low-k, but if it is, it is proceeding at a very slow rate.

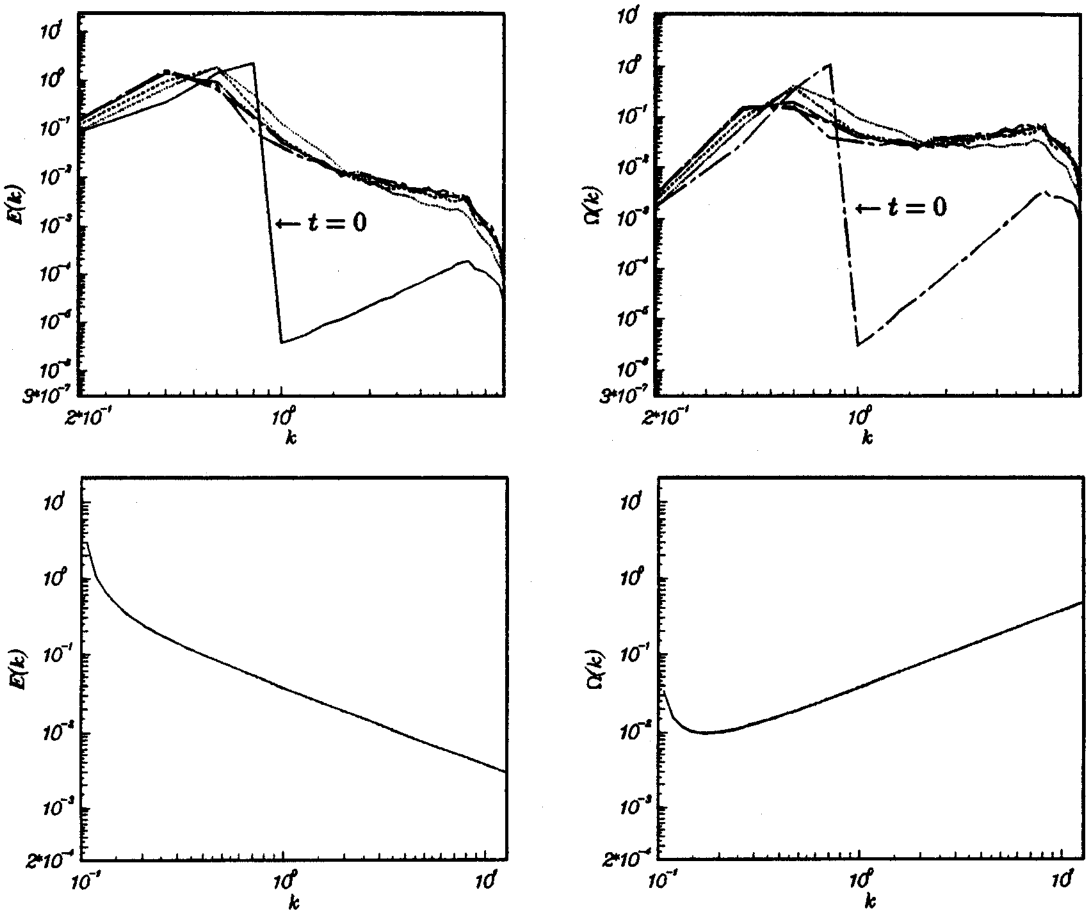

Figure 5.1: *Energy and Enstrophy spectra for Run 5.1 (top) and as predicted by equilibrium theory (bottom).*

Table 5.1: *Equilibrium Turbulence, Run 5.1*

Input Parameter	Value
$H_x = H_y$	20π
k_{max}	6.3
ϕ_0	0.2
k_l	0.0
k_u	0.8
E	4.35
Ω	1.56
α	-0.84
β	8.4

5.2 Decaying Turbulence

5.2.1 Course Grained Entropy and Selective Decay

How are these results modified by viscosity? Since the viscosity is small for small k, it will have little effect in the region where the bulk of the energy is being transferred. Thus we might expect that there would still be a tendency for energy to accumulate in the longest wavelengths. However at high k the very strong viscosity will quickly damp the enstrophy which the system is putting there. This leads us to the so-called *selective decay* model—that the system tends to a state in which the energy remains basically constant but the enstrophy is minimized.

One can calculate the approximate final state of the system via a variational principle based on the selective decay model. Minimizing the enstrophy while fixing the energy may be accomplished via the following variational principle:

$$\delta L \equiv \delta\Omega - \lambda\delta E = 0. \tag{5.5}$$

Viscosity is necessary for this arguement to hold in our truncated Fourier space. The resulting variational principle, however, is independent of the viscosity. In fact, the selective decay arguement is just a special case of a much more general arguement (which is independent of the viscosity): that the course grained entropy of the system will be maximized. This arguement has been used in the Vlasov problem to predict the existence of phase space density holes [69].

Let us consider, for the moment, the inviscid Hasegawa-Mima equation in an infinite domain. In this case, enstrophy will continue to flow out to infinite k—the reflection which led to the equilibrium solution predicted above will never occur. Rather the turbulence will create ever finer scales since, in the absence of viscosity, the density must be conserved along the particles' chaotic orbits. No information is lost—it is just *mixed* to finer and finer scales. These scales will quickly become so small that they are impossible to resolve. The real observable quantity which we should calculate, then, is a course grained average of the density.

The conservation of the actual density gave rise to an infinite family of integral invariants:

$$I_F[\rho] = \int F(\rho)\, d^2x$$

for any function F. Let us define

$$\hat{I}_F[\bar{\rho}] \equiv \int F(\bar{\rho})\, d^2x,$$

where $\bar{\rho}$ is the course grained average of the density. These functionals will not be conserved. We will make this quantity stationary subject to the constraints of conservation of energy and of the average x position. This leads to the following variational principle:

$$\delta L \equiv \delta I_F + \frac{\lambda}{2}\delta E - \lambda c \delta X = 0. \tag{5.6}$$

Using the expressions in Eq. (2.79) for the energy and X moment gives

$$\delta L = \int \left[F'(\bar{\rho})\delta\bar{\rho} + \frac{\lambda}{2}\left(2\bar{\phi}\delta\bar{\phi} + 2\nabla_\perp\bar{\phi}\cdot\nabla_\perp\delta\bar{\phi}\right) - \lambda c x \delta\bar{\phi}\right]$$

or, using the facts that

$$\int x\nabla_\perp^2 f = 0,$$

$$\int \nabla_\perp\bar{\phi}\cdot\nabla_\perp\delta\bar{\phi} = -\int \bar{\phi}\nabla_\perp^2\delta\bar{\phi},$$

Table 6.2: *Effect of input parameters on saturation energy, enstrophy, and electric field*

ν_4	γ^L_{max}	k_n	E	Ω	$\nabla\phi$
0.05	0.04	∞	10.0	2.3	1.5
0.05	0.04	1.0	11.0	5.7	2.4
0.05	0.04	0.4	18.0	7.8	3.2
0.05	0.040	∞	10.0	2.3	1.50
0.05	0.075	∞	3.6	2.2	1.55
[1] 0.05	0.100	∞	2.4	1.9	1.35
0.05	0.025	1.0	17.5	5.5	2.7
0.05	0.040	1.0	11.0	5.7	2.4
0.05	0.075	1.0	6.1	4.5	2.2
[2] 0.05	0.100	1.0	4.7	4.1	2.0
0.05	0.025	0.4	25.0	9.0	3.4
0.05	0.040	0.4	18.0	7.8	3.2
0.05	0.075	0.4	15.0	8.0	3.1
0.025	0.04	∞	7.0	2.2	1.8
0.050	0.04	∞	10.0	2.3	1.5
0.075	0.04	∞	13.0	2.0	1.8
0.100	0.04	∞	14.0	1.6	1.7
0.010	0.04	1.0	9.2	6.7	2.6
0.025	0.04	1.0	10.5	6.2	2.6
0.050	0.04	1.0	11.0	5.7	2.4
[3] 0.075	0.04	1.0	11.0	4.7	2.4
0.100	0.04	1.0	11.5	4.5	2.4
0.010	0.04	0.4	19.0	11.0	3.3
0.025	0.04	0.4	18.0	8.8	3.0
0.050	0.04	0.4	18.0	7.8	3.2
[4] 0.075	0.04	0.4	17.5	6.8	3.2
0.100	0.04	0.4	17.0	6.7	3.0

[1–4] See Tables 6.4–6.7, respectively

and

$$\delta\bar{\rho} \equiv \nabla_\perp^2 \delta\bar{\phi} - \delta\bar{\phi},$$

we get

$$\delta L = \int \delta\bar{\rho}\left[F'(\bar{\rho}) - \lambda\left(\bar{\phi} - cx\right)\right]. \tag{5.7}$$

Thus the equilibrium solution must satisfy the following Euler equation:

$$F'(\bar{\rho}) = \lambda\left(\bar{\phi} - cx\right),$$

or, defining $G(\xi) \equiv F'^{-1}(\lambda\xi)$

$$\bar{\rho} = G(\bar{\phi} - cx). \tag{5.8}$$

This is precisely the equation derived in Chapter 4 for a steady state traveling wave solution, Eq. (4.2)! Exactly the same type of result obtained by Dupree in calculating the relaxation of a Vlasov plasma to a phase space density hole [69]. There it was shown that the course grained average of the phase space density would relax to a steady state solution of the Vlasov equation—a Bernstein-Green-Kruskal (BGK) mode. In fact, Dupree has shown that $\hat{I}_F[\bar{\rho}]$ may be thought of as a generalized entropy functional [70].

In the case that $F(\rho) \sim \rho^2$, one gets the result

$$\bar{\rho} = \lambda(\bar{\phi} - cx).$$

This is the equation which we solved for the dipole modon. Note that this is also the Euler equation that comes from the selective decay arguement if we add the constraint of conservation of the x moment. This might seem to support the position that dipole modons should be important since they are the only localized solutions to the above equations. The key word here is localized. In a turbulent system the fluctuations are not necessarily localized. For instance, if we take a linear function for G: $G(\xi) = -\xi/c$, then we get Eq. (4.4):

$$\nabla_\perp^2\bar{\phi} + \left(\frac{1}{c} - 1\right)\bar{\phi} = 0.$$

This can have monopole solutions with speed $c < 1$, but the solutions won't vanish at infinity. An isolated monopole with $c < 1$ *is not* a solution. However a finite number of such monopoles might very well be. In this case the boundary condition for each individual monopole involves connecting on to the other monopoles and this is not something that is analytically tractable except in very special cases. For instance, in a box with sides of length L, the function

$$\bar{\phi} = \phi_0 \cos\left(\frac{2\pi x}{L}\right) \cos\left(\frac{2\pi y}{L}\right)$$

is an exact solution traveling with speed

$$c = \frac{1}{1+\kappa^2}$$

where the wavenumber $\kappa = 2\pi L^{-1}$. This solution consists of four monopoles in equilibrium with each other.

We shall see that, in the simulations, the system will relax quickly to semi-localized monopole trapped structures. We conjecture that these are actually near-stationary states of the Hasegawa-Mima equation. This conjecture is supported by Dupree's entropy arguements. In fact, it can be shown that the initial quick relaxation will be to structures having size $k \sim 1$. After that, the driving force towards the ultimate equilibrium state becomes much weaker [70]. This is also in agreement with our observations.

5.2.2 Inertial Range

The three dimensional Navier-Stokes equations have only a single rugged invariant, the energy, which is cascaded to high k where it is dissipated by viscosity. In 1941, Kolmorogov postulated that at very high Reynold's numbers there would be a range of scales small compared to the energy containing scales, but large compared to the dissipation scales, which could be considered to be in equilibrium with each other. He proposed that the energy spectrum in this regime would be independent of the viscosity, ν, and depend only on the scale size, k, and the total energy dissipation rate. Based on dimensional arguments, the form of this relation must be [32]

$$E(k) \sim k^{-5/3}. \tag{5.9}$$

This conjecture has been shown to be basically true in many experiments and numerical simulations, and it is considered an acid test for any turbulence theory proposing to explain high Reynold's number fluid turbulence.

In two dimensional fluid turbulence, similar arguments may be made as well, although it is not so clear when they should apply. There are now two invariants to deal with, however, which leads to a second inertial range:

$$E(k) \sim k^{-3}. \tag{5.10}$$

Computer experiments have shown that under certain circumstances these two laws can indeed be observed [64]. The usual setup is to force the equations in some narrow band of wave numbers $k \sim k_0$. Then, when the viscosity is sufficiently small, an energy inertial range will be set up for $k << k_0$ (according to Eq. (5.9)), and an enstrophy inertial range will be set up for $k >> k_0$ (according to Eq. (5.10)). Kraichnan gives an detailed account of this phenomenon for two-dimensional fluid turbulence in [62].

The evidence for the dual inertial range is not, however, conclusive. A high resolution, high Reynold's number simulation of two-dimensional isotropic fluid turbulence done by McWilliams indicated that the high-k energy spectrum went more like k^{-5} [71]. They also observed that the enstrophy evolved to a very intermittent state, composed of a small number of monopole vortices whose sizes were small compared to the domain. They suggested that the steepening of the energy spectrum at high-k is related to this intermittent state. However they also note that there was significant enstrophy dissipation in moderate scale sizes and that this might be responsible for the steepening of the k spectrum (i.e. their Reynold's number was not high enough). Although there are some theories for the steepening of the k^{-3} spectrum, the subject is not well understood, and numerical experiments have not, to date, provided conclusive evidence against the k^{-3} spectrum [61].

5.2.3 Artificial Viscosity

One other important question is what happens as the viscosity is decreased (i.e. the viscous Reynold's number is increased). As far as solutions to the exact equation are concerned, this is still an unanswered question [21].

For the truncated mode system, however, there is a smooth transition to the equilibrium solution. The first evidence of trouble is that the edge of the enstrophy spectrum will start to peak up, going linearly with k, as predicted above. This effect can only be eliminated by either increasing k_{max}, or increasing ν. Thus we see that a large viscosity may be necessary to get meaningful numerical solutions, even though this is not consistent with the actual problem.

In this spirit, we have done most of our simulations using a *hyper-viscosity*, with the damping rate going like k^6 rather than k^4. This raises the effective viscous Reynold's number over the regular viscosity without requiring more modes [71].

5.2.4 Simulation

Run 5.2, described by Table 5.2, is a typical decay run. The initial conditions were again given by Eq. (5.1.2). Figure 5.2 shows the energy and enstrophy histories for this run. We see exactly what we expect from the above discussion. The energy drops by a moderate fraction of its initial value while the enstrophy drops nearly to zero.

Table 5.2: *Input Parameters, Runs 5.2–5.3*

Input Parameter	Value
$H_x = H_y$	20π
k_{max}	6.3
ϕ_0	0.15
k_l	2.0
k_u	2.5
ν_4	0.003

Figure 5.3 illustrates the evolution of the energy spectrum for Run 5.2. First of all, we can clearly see that there was a rapid transfer of energy from the original high-k annulus to very low k. Second, we observe that the slope of the energy spectrum is

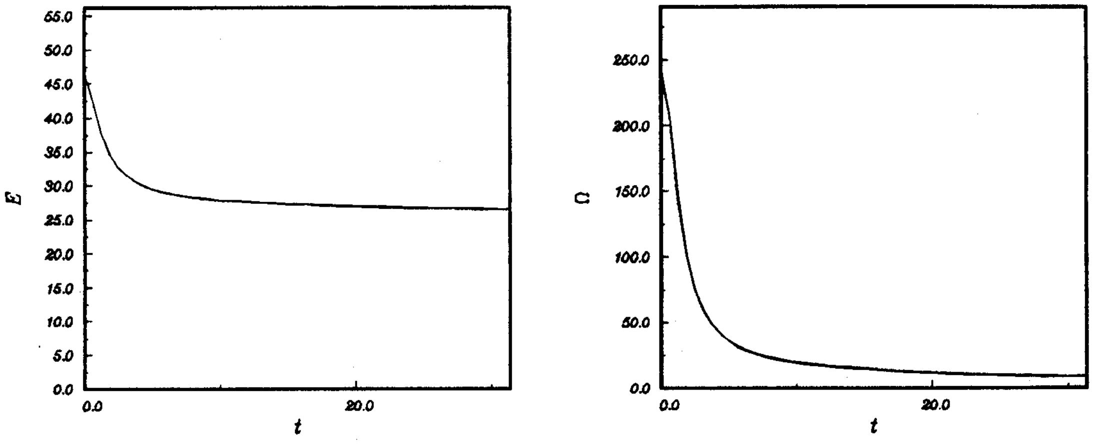

Figure 5.2: *Energy and enstrophy relaxation for Run 5.2.*

steeper than k^{-3}, in fact, a bit steeper than k^{-5}. The low k spectrum never reaches a steady shape. Energy continues to build up at the lowest wavenumbers while the remaining modes are slowly being diminished.

Figure 5.4 shows contours of constant ρ at several times during this run. Regions of closed contours may be seen in these plots. These regions represent prospective trapped structures. Their coherence is checked by placing marker particles, which move with the fluid velocity, in these regions and integrating the particle trajectories simultaneously with the fields. Figure 5.5 shows the evolution of the density contours and the positions of 6 marker particles, indicated by the $*$'s. Figure 5.6 illustrates the trajectories of two of these particles. Note that several of the stronger trapped structures can easily be traced through most of Fig. 5.4, and thus have lifetimes on the order of $100\omega_{*e}^{-1}$.

The Effect of the Density Gradient

The existence of the density gradient places some important constraints on the solutions of the Hasegawa-Mima equation, such as the conservation of the average x and the lack of exact isolated monopole solutions. It is thus of interest to compare the above decay run with an identical run, Run 5.3, in which there was no density gradient. The Hasegawa-Mima equation then becomes

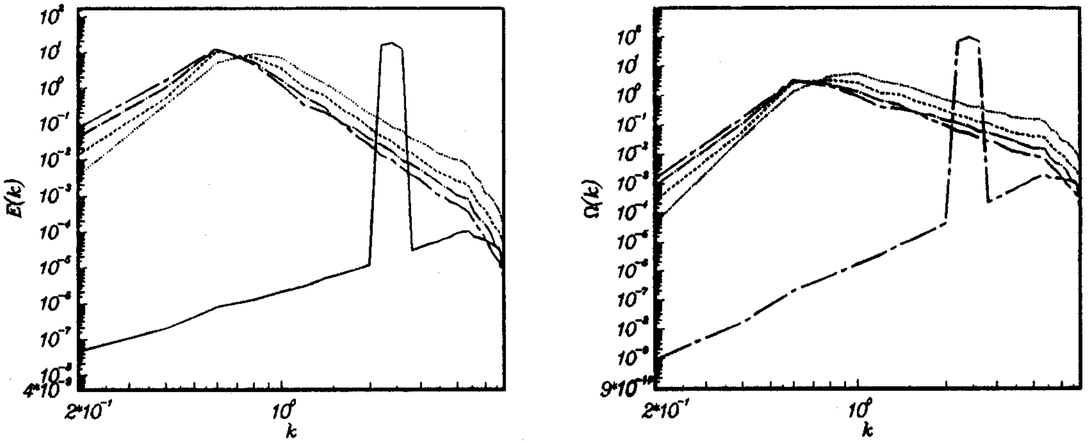

Figure 5.3: *Evolution of the isotropic energy and enstrophy spectra for Run 5.2.*

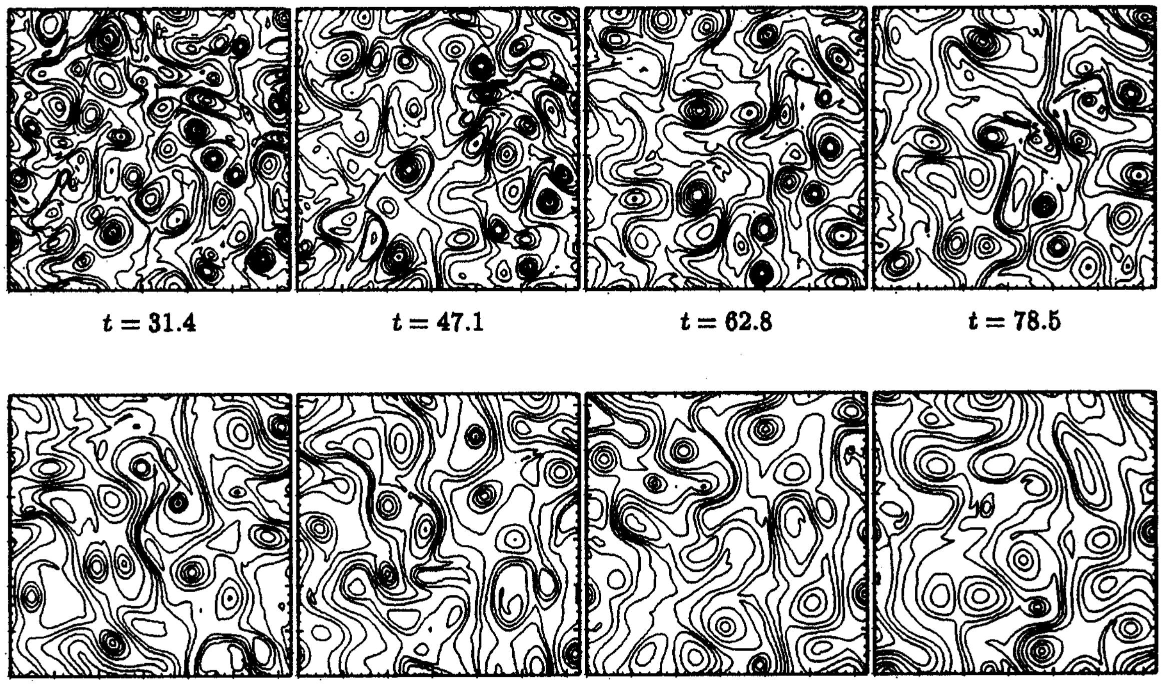

$t = 31.4$ $t = 47.1$ $t = 62.8$ $t = 78.5$

$t = 94.2$ $t = 110.$ $t = 126.$ $t = 141.$

Figure 5.4: *Density contours for Run 5.2.*

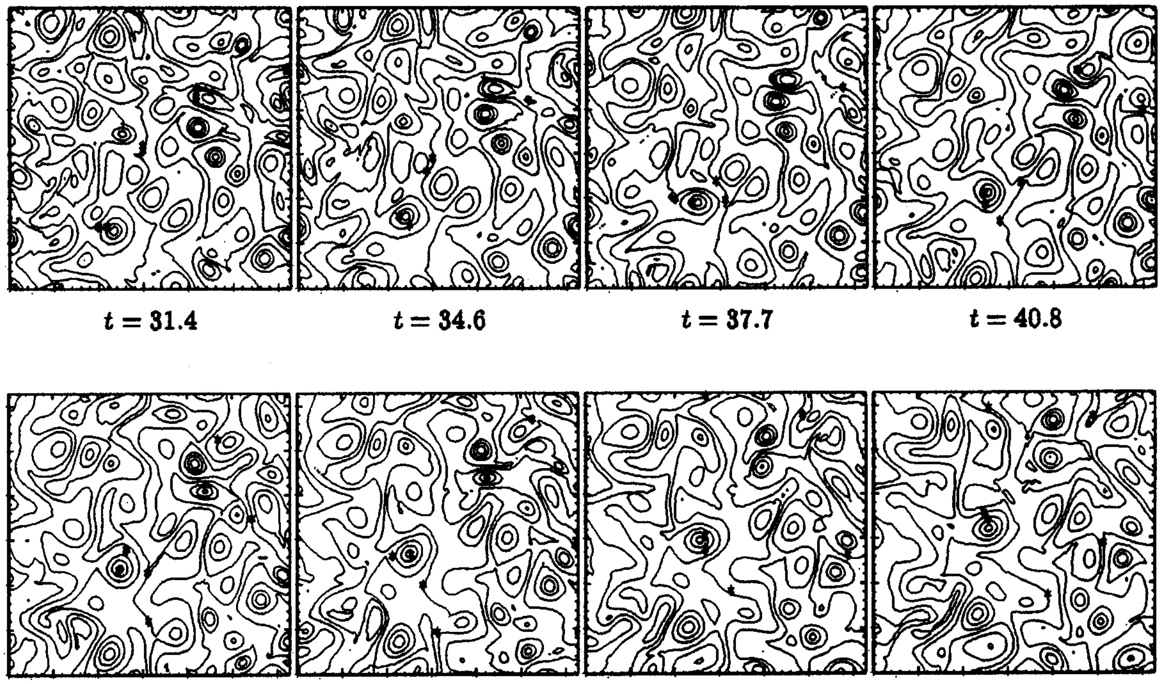

$t = 31.4$ $t = 34.6$ $t = 37.7$ $t = 40.8$

$t = 44.0$ $t = 47.1$ $t = 50.3$ $t = 53.4$

Figure 5.5: *Density contours for Run 5.2, including marker particles (indicated by the* $*$ *symbols).*

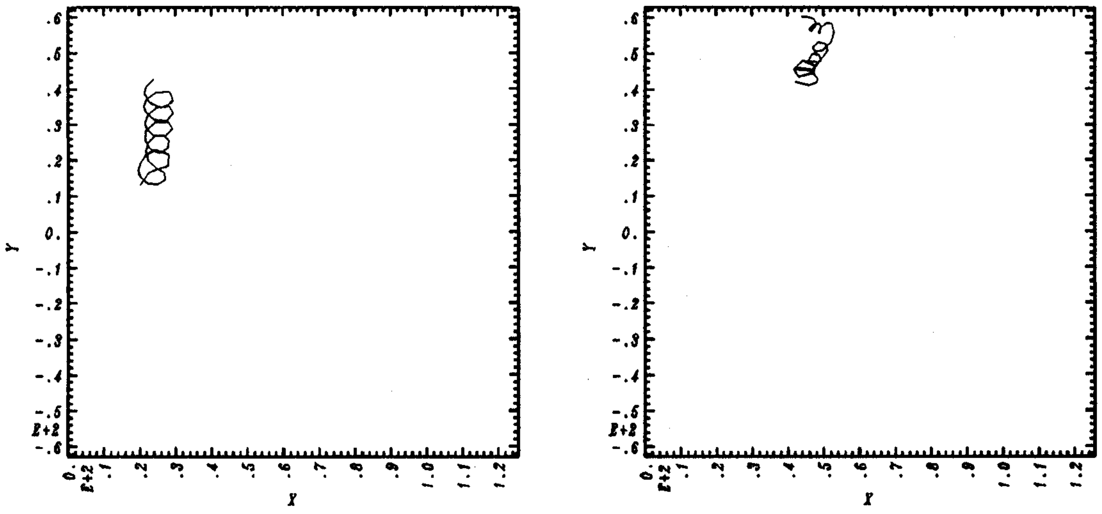

Figure 5.6: *Trajectories of a two trapped marker particles.*

$$\left(\frac{\partial}{\partial t} + \hat{\mathbf{z}}\times\nabla_\perp\phi\cdot\nabla_\perp\right)\left(\phi - \nabla_\perp{}^2\phi\right) + \nu\nabla_\perp{}^4\phi = 0. \tag{5.11}$$

Figure 5.7 shows the evolution of the energy and enstrophy for Run 5.3. Comparing it to Figure 5.2 we see that the runs are virtually identical in this regard. Figure 5.8 shows the isotropic energy spectrum. Here there is a difference—the energy spectrum for Run 5.3, being slightly steeper than k^{-6}, falls off even more quickly than it did in Run 5.2.

An important statistic in studying possibly intermittent fluctuations is the kurtosis. The kurtosis for the potential and for the true vorticity, $\nabla_\perp{}^2\phi$, are defined to be:

$$\kappa_\phi \equiv \frac{L^2 \int \phi^4 d^2x}{\left(\int \phi^2 d^2x\right)^2}, \tag{5.12}$$

$$\kappa_\psi \equiv \frac{L^2 \int \left(\nabla_\perp{}^2\phi\right)^4 d^2x}{\left(\int \left(\nabla_\perp{}^2\phi\right)^2 d^2x\right)^2}, \tag{5.13}$$

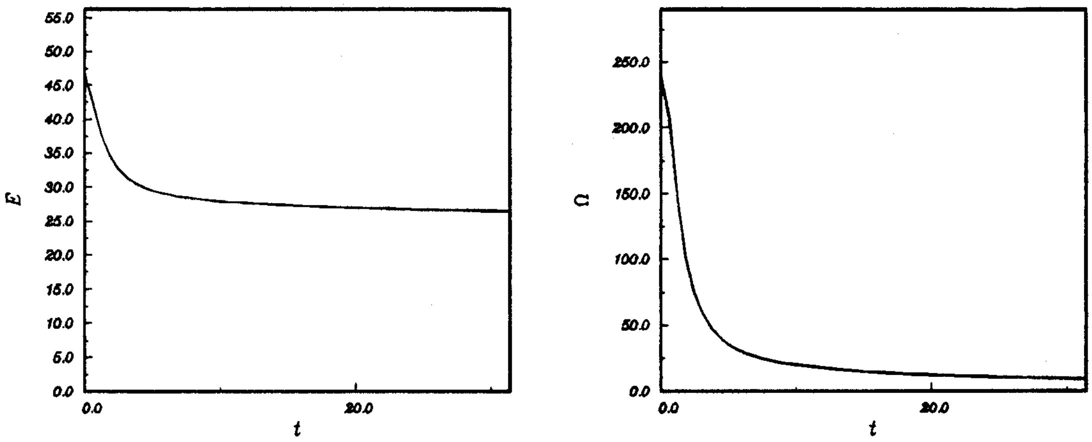

Figure 5.7: *Energy and enstrophy relaxation for Run 5.3.*

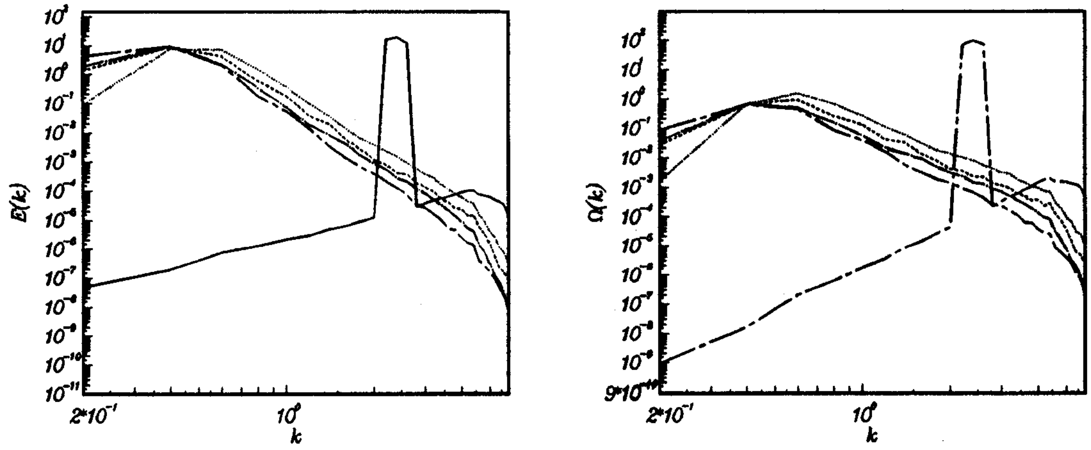

Figure 5.8: *Evolution of the isotropic energy spectrum for Run 5.3.*

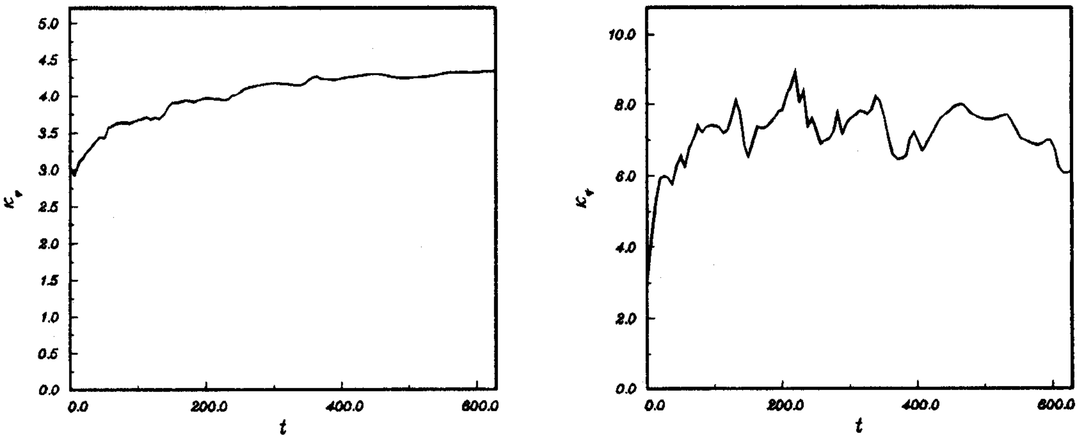

Figure 5.9: *Potential and vorticity kurtosis for Run 5.3.*

where L^2 is the area of the domain. If the spatial scale of the fluctuations had a Gaussian distribution, then the kurtosis would be equal to three. The kurtosis is greater than three if the distribution of fluctuations has a long tail, which results in a larger than Gaussian probability of seeing a very large structure. For instance, an intermittent field with a few widely separated, large fluctuations will have a kurtosis much larger than three.

Figure 5.9 shows the spatial kurtosis of the potential and the true vorticity, $\nabla_\perp^2\phi$, for Run 5.3. We see a trend similar to that noticed by McWilliams [71]—the kurtotisis of the stream function (the potential, in our case) remain close to three, while the kurtosis of the vorticity grows significantly larger than three. For comparison, Figure 5.10 shows the same quantities plotted for Run 5.2. The kurtosis of the potential again remains near three throughout the simulation. The kurtosis of the vorticity initially grows, similarly to the zero-gradient case. However it comes crashing back down to around 4 after awhile, and seems to want to stay there.

Figure 5.11 shows the contours of the vorticity function at the end of these runs. We see that they are, indeed, quite different. The vorticity for Run 5.3 is concentrated in localized vortex structures, while the vorticity for Run 5.2 is much less well organized.

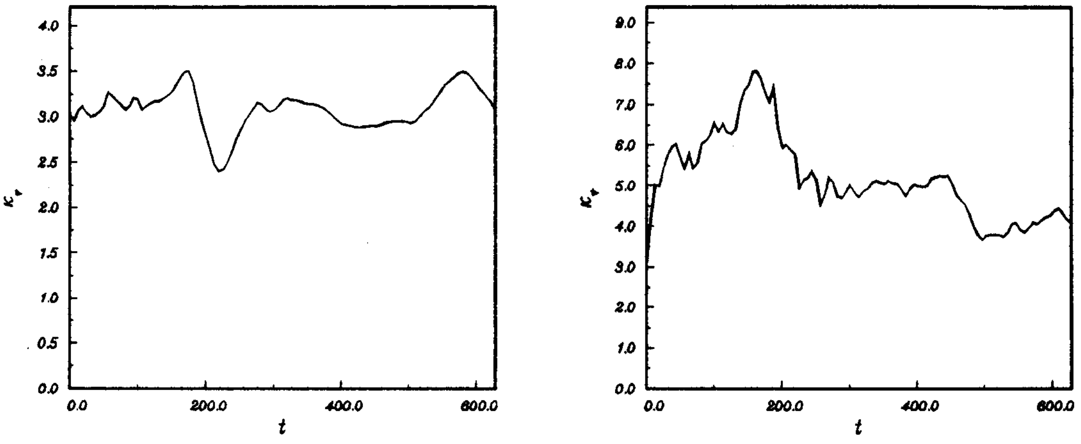

Figure 5.10: *Potential and vorticity kurtosis for Run 5.2.*

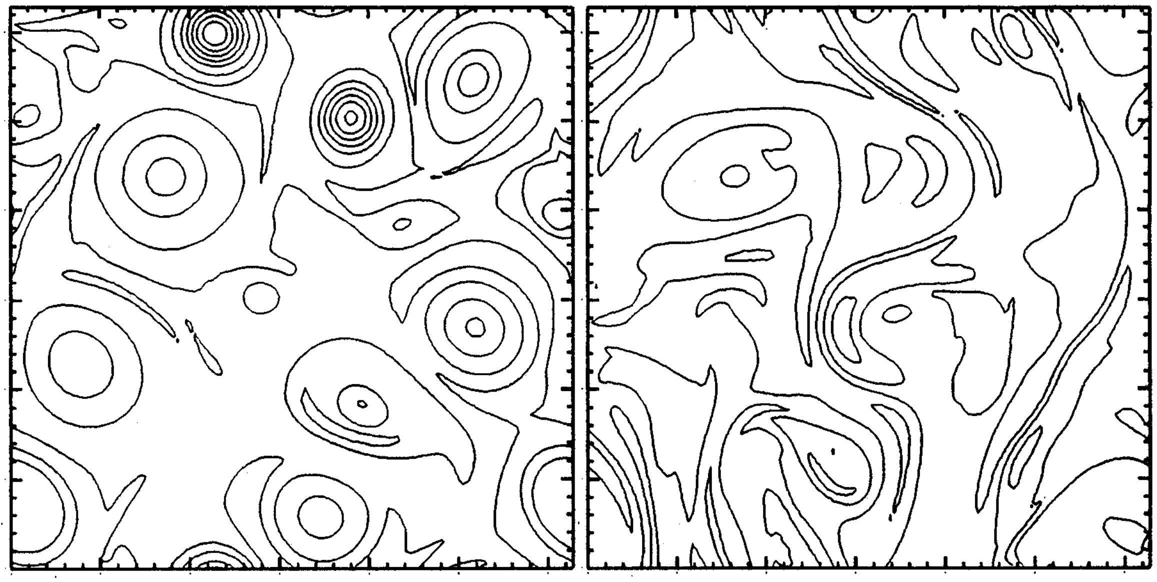

Figure 5.11: *Comparison of the vorticity contours for Run 5.3 (left) and Run 5.2 (right).*

The vorticity, however, is not the correct quantity to measure if we are seeking to identify trapped structures. It is useful, as it gives us an indication of where energy is being dissipated. But with regard to trapped structures, the density function, ρ, is really the more meaningful quantity as its contours represent the actual streaklines along which particles move. For the zero-gradient runs, this quantity is just

$$\rho = \nabla_{\perp}^{2}\phi - \phi.$$

Figure 5.12 shows the contours of ρ for both runs. In neither case is the field terribly intermittent. Indeed, the kurtosis for the function $\nabla_{\perp}^{2}\phi - \phi$, which in both cases represents the fluctuation in the density, always tends to be very near three. This is not surprising since the average k-vector tends to be relatively small, making $\nabla_{\perp}^{2}\phi << \phi$, so that the statistics of ρ will be very similar to those of ϕ. Thus we see that the trapped structures in both cases tend to not be very isolated. However we definitely see more trapped structures in Run 5.3. Perhaps this is due to the fact that, with a finite gradient, trapped structures can become untrapped simply by moving in the x direction, a degree of freedom which the zero-gradient model lacks.

Higher Resolution

Table 5.3 gives the input parameters describing Runs 5.4–5.5, which are basically identical to Runs 5.2–5.3, except that the resolution is twice as high, and the viscosity coefficient has been reduced by an order of magnitude. Fig. 5.13 shows the energy and enstrophy for one of these runs (again, these come out virtually identical). Comparing this figure to Fig. 5.2, we see that the lower viscosity has resulted in much less of an energy drop during the initial stage of the turbulence. The enstrophy, however, still drops by a substantial amount. Since the energy did not fall as far as it did in Runs 5.2–5.3, the quasistationary state has a much higher energy, electric field, etc.

Figures 5.14 and 5.15 show the evolution of the isotropic energy and enstrophy spectra for these runs. This time the two look quite similar, both having approximately k^{-5} behavior at high-k. Figures 5.16 and 5.17 show the density contours for each of these runs. This time, due to the much higher electric field, the two figures look quite similar.

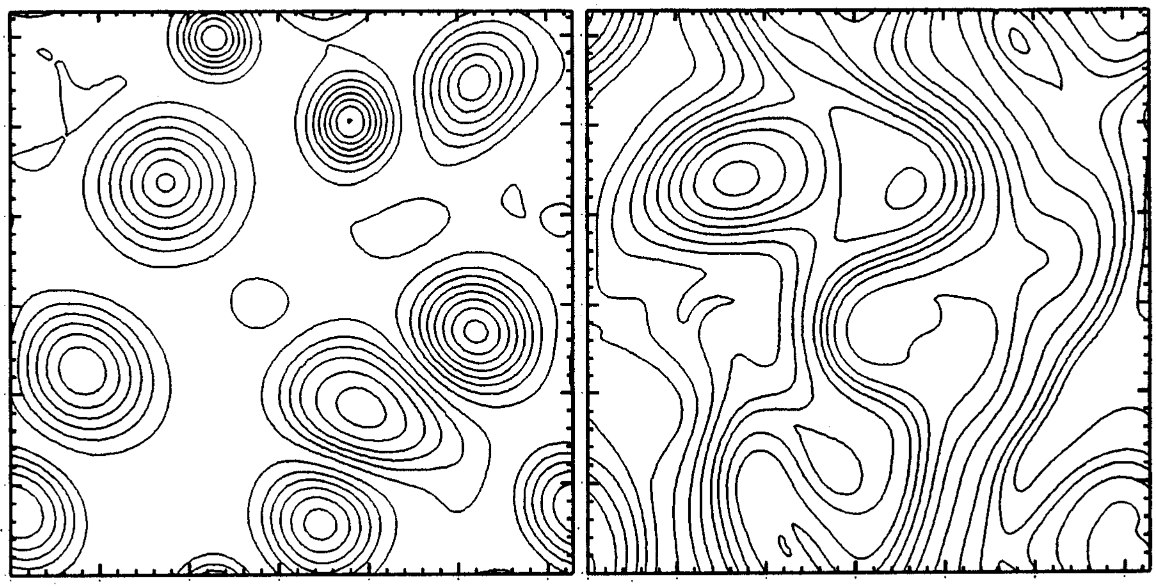

Figure 5.12: *Comparison of the density contours for Run 5.3 (left) and Run 5.2 (right).*

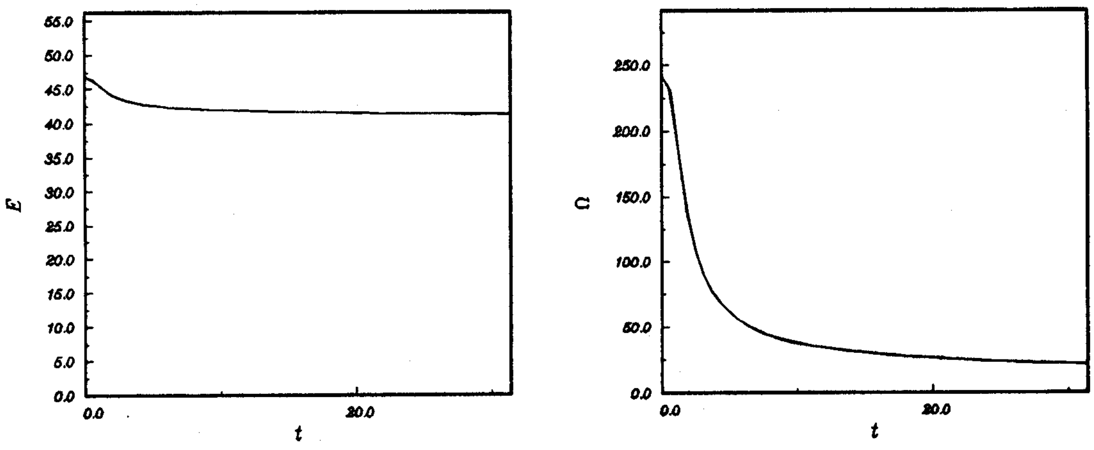

Figure 5.13: *Energy and enstrophy relaxation for Run 5.5.*

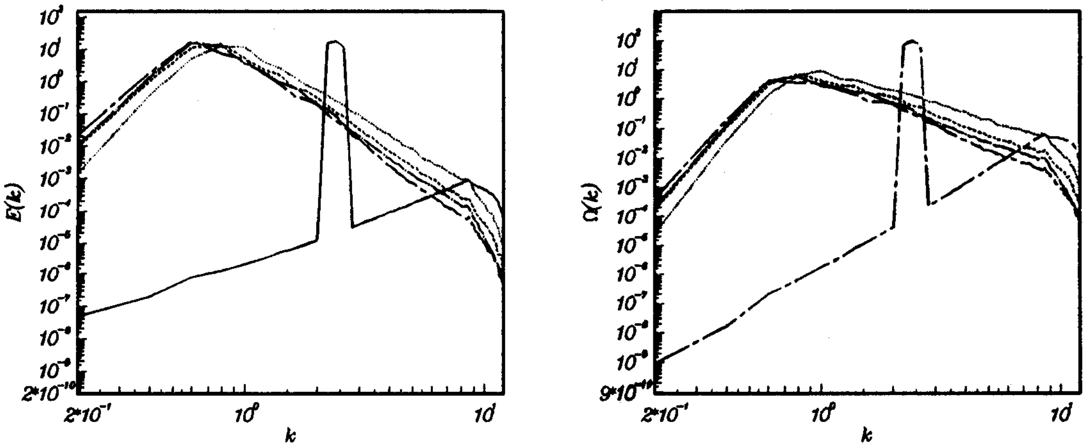

Figure 5.14: *Evolution of the isotropic energy spectrum for Run 5.4.*

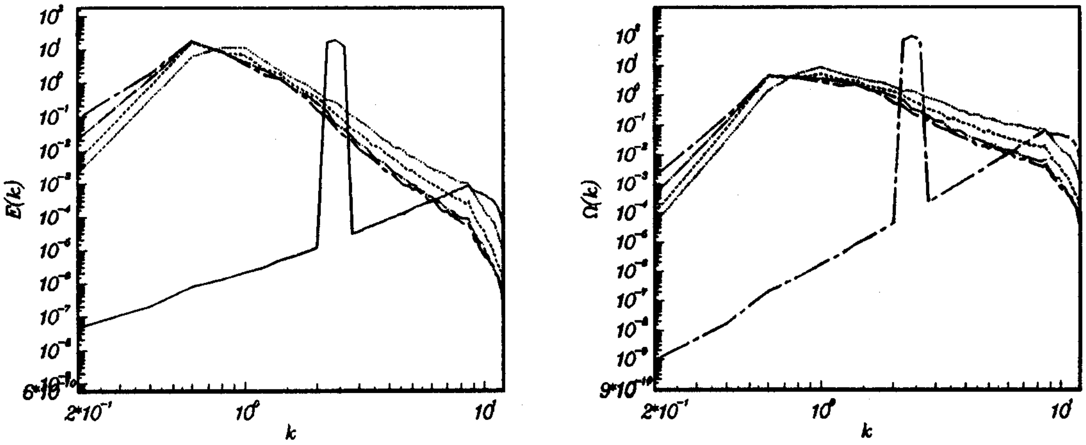

Figure 5.15: *Evolution of the isotropic energy spectrum for Run 5.5.*

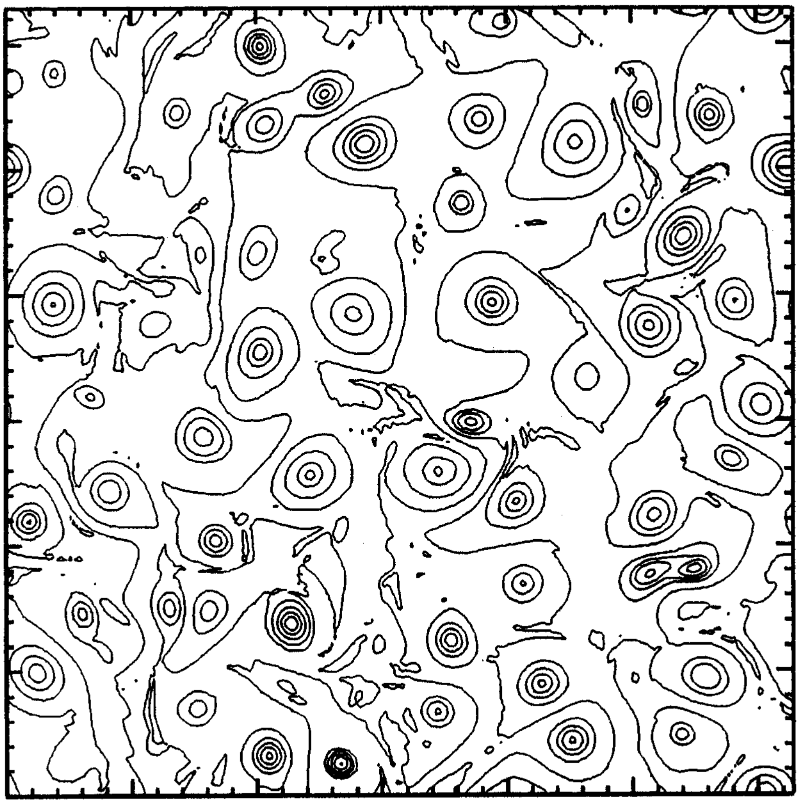

Figure 5.16: *Density contours for Run 5.4.*

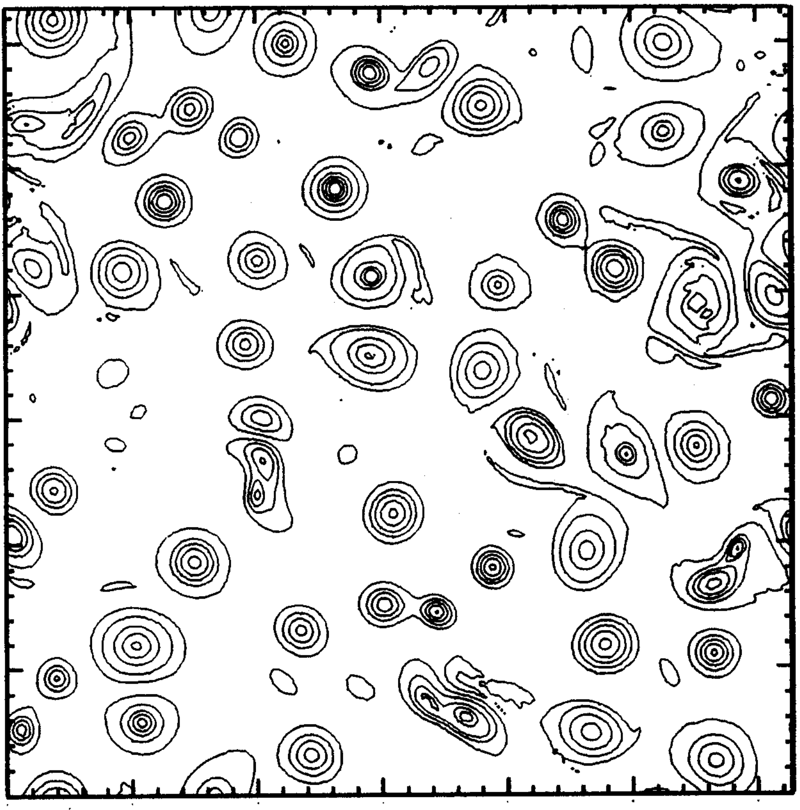

Figure 5.17: *Density contours for Run 5.5.*

Table 5.3: *Input Parameters, Runs 5.4–5.5*

Input Parameter	Value
$H_x = H_y$	20π
k_{max}	12.7
ϕ_0	0.15
k_l	2.0
k_u	2.5
ν_4	0.0003

The Frequency Spectrum

Unfortunately the frequency spectrum cannot be quantatively measured for these decay runs since the average quantities are changing much too quickly. (Actually, it probably could be measured for a high Reynold's number run, like Runs 5.4–5.5. This would be extremely expensive.) However we can make some qualitative comments. Basically, the frequency spectrum appears to be quite narrow. As noted above, the decay runs tend to be characterized by localized structures, slowly interacting, coalescing, and moving to larger scales. During this slow evolution, the motion of the various large vortices is very uniform. They all move with a y-velocity very near

$$\frac{E}{E+\Omega} = \frac{1}{1+\Omega/E} = \frac{1}{1+k_E^2},$$

and with very little x motion. Except during a rare interaction, they remain basically circular. This motion is extremely coherent, and deviations from this coherent motion happen on a time scale much longer than ω_{*e}. Qualitatively speaking, the width of the frequency spectrum is much smaller than the frequency: $\Delta\omega << \omega$.

5.3 Summary

These simulations, and many other similar ones, give us the following picture of the turbulent evolution of the system: First the system quickly relaxes from the initial random phase state to a much more coherent state. During this relaxation there is a quick change in the shape of the energy spectrum, with the average k vector decreasing rapidly. When the average k vector gets below one, the relaxation slows dramatically. A quasisteady state is achieved, with smaller vortices slowly merging to form larger vortices, moving the average k vector slowly towards k_{min}.

In this quasisteady regime, the high k part of the spectrum basically is shape preserving, with a slope of around k^{-4}–k^{-6}. Although this shape, as well as the other observations, does not seem to be tremendously sensitive to the magnitude of the viscosity, our runs had a fairly low viscous Reynold's number and so it is not clear proof that the k^{-3} spectrum is incorrect.

For $k \leq 1$ the spectrum does not really attain a steady shape. Energy continues to build up at the lowest wave numbers while the rest of the spectrum slowly dies away. This may be an indication of the low k spectrum trying to move towards the equilibrium state. However it appears to be happening at a relatively slow rate.

We also observed that the fluctuation in the density function were qualitatively similar to an identical run using a model with no density gradient. However there were fewer trapped structures in the finite density gradient case, and the vorticity field for these two cases was quite different. Our interpretation of this is that the tendency of trapped structures to evolve is very similar to the fluid dynamics case. However the constraints placed on the system by the existence of the density gradient modify the manner in which these vortices can interact, giving them a new means by which to be come untrapped, and modifying the way in which energy is dissipated.

Finally, the frequency spectrum, although not quantitatively measurable in this decaying regime, appeared to be fairly narrow. This is a very important observation because it is strongly at odds with the experimental facts. It is also somewhat at odds with the intuitive feeling that a strongly nonlinear system, which we certainly have here, will always be characterized by a broad frequency spectrum.

We shall see in the next chapter that the introduction of nonadiabatic electron effects will modify this observation. It is not at all obvious that the trapped structures which we have studied in this chapter and the last will survive this broadening of the spectrum. We shall see that, in certain circumstances, they will.

Chapter 6

Saturated Turbulence

In the previous two chapters we have made a fairly detailed study into the behavior of the Hasegawa-Mima equation, both in turbulent and non-turbulent situations. Our motivation for studying this equation was that it was simple, relatively inexpensive to simulate, and to lowest order, correct. We can expect that the short time scale behavior will not be strongly affected by the introduction of the nonadiabatic electrons.

These simulations led to some interesting observations: that very long lived trapped structures could develop in decaying turbulence, and that the frequency spectrum of the fluctuations was quite narrow. Both of these observations are long time scale observations, however, and thus we should expect the nonadiabatic electrons to have a strong effect on them.

In this chapter we study the saturated turbulence which develops when the nonadiabatic electrons are included in the problem. Our main focus will be to see if the trapped structures which were so prominent earlier still play a role, and to see what type of effect our nonadiabatic electron term has.

6.1 Modified Nonadiabatic Model

Recall that the nonadiabatic electron density, derived in Chapter 2, could be written as

$$\hat{n}_{\mathbf{k}_\omega} = i\delta_0 \left(\omega - k_y\right) \phi_{\mathbf{k}_\omega}.$$

Assuming that this term was small, we derived Eq. (2.74). This equation is quite complex. In particular, the effect of the nonadiabatic electrons at high-k is not at all clear. In order to expedite numerical solution of this model, I have introduced a modified nonadiabatic electron response of the following form:

$$\hat{n}_{\mathbf{k}_\omega} = i\delta_k \left(\omega - k_y\right) \phi_{\mathbf{k}_\omega}, \tag{6.1}$$

where

$$\delta_k \equiv \delta_0 e^{-k^2/k_n^2}. \tag{6.2}$$

We can adjust k_n so that only the low-k modes contribute to the nonadiabatic response, and the high-k modes are strongly damped. In this way we are assured that the equations are well behaved as k increases. Lowering k_n also lowers the value of k at which the linear growth rate peaks, and thus we might expect that this would make the simulation less expensive, since the k-spectrum ought to peak at a lower-k. The latter prediction, however, will be seen to be only partially correct.

6.2 Frequency Spectrum and Energy Saturation

A slow time scale energy balance equation, Eq. (2.107), was derived in Chapter 2. Taking into account our modified nonadiabatic electron response, this equation may be written as

$$\frac{dE}{d\tau} = -\sum_{\mathbf{k}} \nu_k E_{\mathbf{k}} - \sum_{\mathbf{k}} \delta_k \sum_{\omega} \omega \left(\omega - k_y\right) |\phi_{\mathbf{k}_\omega}|^2. \tag{6.3}$$

This may also be written as follows

$$\frac{dE}{d\tau} = -\sum_{\mathbf{k}} \left(\nu_k - \gamma_{\mathbf{k}}^{NL}\right) E_{\mathbf{k}} \tag{6.4}$$

where $\gamma_{\mathbf{k}}^{NL}$ is a nonlinear growth rate defined by

$$\gamma_{\mathbf{k}}^{NL} \equiv -\frac{\delta_k}{E_k} \sum_{\omega} \omega \left(\omega - k_y\right) |\phi_{\mathbf{k}_\omega}|^2. \tag{6.5}$$

The frequency spectrum may be characterized by an average frequency, $\bar{\omega}$, and a frequency spread, $\Delta\omega$, defined by

$$\bar{\omega}_{\mathbf{k}} \equiv \frac{1}{|\phi_{\mathbf{k}}|^2} \sum_{\omega} \omega |\phi_{\mathbf{k}_\omega}|^2, \tag{6.6}$$

$$\Delta\omega_{\mathbf{k}}{}^2 \equiv \frac{1}{|\phi_{\mathbf{k}}|^2} \sum_{\omega} \left(\omega - \bar{\omega}_{\mathbf{k}}\right)^2 |\phi_{\mathbf{k}_\omega}|^2. \tag{6.7}$$

In terms of these, the nonlinear growth rate may be written as

$$\gamma_{\mathbf{k}}^{NL} = -\frac{\delta_k}{1+k^2}\left[\Delta\omega_{\mathbf{k}}{}^2 + \bar{\omega}_{\mathbf{k}}\left(\bar{\omega}_{\mathbf{k}} - k_y\right)\right]. \tag{6.8}$$

In the linear and weak turbulence regimes, $\bar{\omega}_{\mathbf{k}} \approx \omega_{\mathbf{k}}$ and $\Delta\omega_{\mathbf{k}} \approx 0$, and $\gamma_{\mathbf{k}}^{NL}$ reduces to the linear growth rate. The Terry-Horton description for the nonadiabatic electron response is appropriate in these regimes. If the turbulence is strong, however, both $\Delta\omega_{\mathbf{k}}$ and $\bar{\omega}_{\mathbf{k}}$ may change significantly from their linear values. Equation (6.8) shows how these changes will affect the energy balance: if the spectrum is broadened, or if the $\bar{\omega}_{\mathbf{k}}$ is shifted up past k_y, the nonadiabatic electrons will become a sink of energy, rather than a source.

Although the above analysis is not exact for our model equation, these effects are definitely included in an approximate way. This fact greatly complicates our view of what is happening. In the Terry-Horton model, the picture is fairly clear—there is a source of energy at low k due to the nonadiabatic electrons, and there is a sink of energy at high k due to ion viscosity. This allowed Terry and Horton to make a rather general prediction of the circumstances under which the system would saturate. Arguing that if the energy grew large enough, the system would approach equipartition, they showed [3, 4, 5] that the system would saturate if

$$\gamma_t \equiv \sum_{\mathbf{k}} \left(\hat{\gamma}_{\mathbf{k}}^L - \nu_{\mathbf{k}}\right) < 0.$$

Thus as one increases δ_0, approaching the critical value where $\gamma_t = 0$, the saturation energy is expected to increase without bound.

Such a simple picture does not work for our model. Increasing δ_0 affects not only the linear growth rate. It increases the strength of the nonadiabatic electron term in general, which may be a sink as well as a source, and it also modifies the spectrum, and thus $\bar{\omega}_{\mathbf{k}}$ and $\Delta\omega_{\mathbf{k}}$.

Table 6.1 illustrates this point quite dramatically. This table compares four runs whose only difference in input was the value of γ^L_{max}, the maximum linear growth rate (which is directly proportional to δ_0). There are two notable results: First, as γ^L_{max} was increased, the saturation energy *decreased*! Second, the RMS electric field was relatively constant due to the fact that, as the energy went down, the average k vector went up.

Table 6.1: *Runs 6.1a–6.1d.*

Input Parameter	Run 6.1a	Run 6.1b	Run 6.1c	Run 6.1d
γ^L_{max}	0.025	0.04	0.075	0.10
$H_x = H_y$	20π			
k_{max}	3.9			
ν_4	0.05			
k_n	1.0			
Output				
E	17.5	11.0	6.1	4.7
Ω	5.5	5.7	4.5	4.1
$k_* = \sqrt{\Omega/E}$	0.56	0.72	0.85	0.92
$(\nabla\phi)_{rms}$	2.7	2.4	2.3	2.2

The relatively weak dependence of the electric field on γ^L_{max} is further explored in Table 6.2. These runs are identical to those listed in Table 6.1 except for the variations of γ^L_{max}, ν_4, and k_n shown. We see that the electric field also depends only weakly on the viscosity. The only input value upon which the saturated electric field depends strongly is the nonadiabatic cutoff, k_n.

The strong dependence of the saturation level on k_n is understandable. The high-k modes tend to have very broad frequency spectra, and thus to have negative nonlinear growthrates. By limiting the effect of the nonadiabatic electrons to low-k, we are removing a sink of energy.

In order to further study the effect of k_n, we show more detailed spectral information for four of these runs in Tables 6.4–6.7. These runs correspond to the footnoted runs in Table 6.2. Their differences are summarized in Table 6.3. They are presented in order of increasing average (RMS) electric field. Shown are the mode energy, E_k, linear frequency, ω_k, line width, $\Delta\omega$, frequency shift,

$$\delta\omega \equiv \bar{\omega}_{\mathbf{k}} - \omega_{\mathbf{k}},$$

and a measure of the nonlinear growth rate,

$$\gamma_{\mathbf{k}}^{NL}/\delta_{\mathbf{k}} = -\frac{1}{1+k^2}\left(\Delta\omega^2 + \bar{\omega}\left(\bar{\omega} - k_y\right)\right).$$

The factor $\delta_{\mathbf{k}}$ is scaled out so that this is purely a measure of the frequency width and shift, depending only on $\delta_{\mathbf{k}}$ through the changes it causes to the spectrum. Values are given for a sampling of k-vectors in the energy containing part of the spectrum.

Table 6.3: *Input differences for Runs 6.2a–6.2d*

Input Parameter	Run 6.2a	Run 6.2b	Run 6.2c	Run 6.2d
γ_{max}^{L}	0.10	0.10	0.040	0.040
ν_4	0.05	0.05	0.075	0.075
k_n	∞	1.00	1.000	0.400

Run 6.2a had the lowest electric field of all those shown in Table 6.2. In this case we see that the frequency spectrum is fairly narrow relative to the mode frequency. For the strongest mode in the system, which is highlighted in Table 6.4, $\Delta\omega/\omega < 10\%$. Also, the spectral characteristics are quite anisotropic. The k-spectrum is much larger along the k_y-axis, which we might expect since the linear growth rate is largest there. But the line widths tend to be broader near the k_x-axis, even though the energy in these modes is smaller. These observations are reflected in the nonlinear growth rate, which is positive along the k_y-axis, and negative along the k_x-axis. The deviations of this growth rate from the linear one are mostly due to the broadening term—the shift $\delta\omega$ is not sufficiently large to have much of an effect. The average frequency, $\bar{\omega}_{\mathbf{k}}$, appears to drop off somewhat faster than the linear growth rate, but it is difficult to

Table 6.4: *Frequency Characteristics for Run 6.2a.*

(k_x, k_y)	$E_{\mathbf{k}}$	$\omega_{\mathbf{k}}$	$\Delta\omega$	$\delta\omega$	$\gamma_{\mathbf{k}}^{NL}/\delta_0$
(0.0,0.1)	.001	.10	.035	-0.0016	-0.0010
(0.0,0.3)	.004	.28	.075	-0.0004	0.0011
(0.0,0.5)	.030	.40	.055	0.021	0.024
(0.0,0.6)	.076	.44	.042	0.030	0.043
(0.0,0.7)	.038	.47	.070	0.021	0.066
(0.0,0.9)	.015	.50	.129	-0.018	0.102
(0.0,1.1)	.007	.50	.205	-0.097	0.108
(0.1,0.0)	.006	0	.039	0.004	-0.0016
(0.3,0.0)	.006	0	.098	-0.0008	-0.0088
(0.5,0.0)	.008	0	.133	-0.004	-0.014
(0.6,0.0)	.009	0	.144	0.009	-0.015
(0.7,0.0)	.010	0	.156	-0.006	-0.016
(0.9,0.0)	.006	0	.235	-0.011	-0.030
(1.1,0.0)	.002	0	.343	0.001	-0.053
(0.2,0.5)	.018	.39	.083	0.025	0.023
(0.4,0.4)	.008	.30	.140	0.002	0.007
(0.5,0.2)	.008	.16	.145	-0.012	-0.010
(0.6,0.6)	.011	.35	.154	0.0005	0.037

draw any firm conclusions since the precise value of this average becomes difficult to determine when the spectrum is very broad.

Run 6.2b is identical to Run 6.2a except that k_n was decreased to $k_n = 1$. We see that the corresponding increase in the average electric field has resulted in broader line widths, with the strongest mode now having $\Delta\omega/\omega \approx 50\%$, and a more isotropic k-spectrum. This is again reflected in the nonlinear growth rate, which is generally smaller than before.

For Run 6.2c, the maximum linear growth rate was decreased to $\gamma_{max}^{L} = 0.04$ and the viscosity was increased slightly. This resulted in an average total energy of over twice that in Run 6.2b. The electric field, however, changed only slightly. The line width for the strongest mode has dropped back to around 20%. The higher-k modes are still fairly broad. The k-spectrum is slightly more isotropic than it was for Run 6.2b, but not much different. The narrowing of the frequency spectrum has caused some of the nonlinear growth rate terms to increase.

Table 6.5: *Frequency Characteristics for Run 6.2b*

(k_x, k_y)	$E_{\mathbf{k}}$	$\omega_{\mathbf{k}}$	$\Delta\omega$	$\delta\omega$	$\gamma_{\mathbf{k}}^{NL}/\delta_{\mathbf{k}}$
(0.0,0.1)	.004	.10	.062	-0.0060	-0.0031
(0.0,0.3)	.010	.28	.137	-0.0009	-0.011
(0.0,0.5)	.024	.40	.171	-0.0015	0.009
(0.0,0.6)	.030	.44	.188	-0.0081	0.027
(0.0,0.7)	.033	.47	.207	-0.031	0.048
(0.0,0.9)	.034	.50	.235	-0.105	0.079
(0.0,1.1)	.016	.50	.309	-0.167	0.072
(0.1,0.0)	.011	0	.064	0.0001	-0.0040
(0.3,0.0)	.010	0	.182	0.001	-0.030
(0.5,0.0)	.012	0	.256	-0.009	-0.053
(0.6,0.0)	.014	0	.268	0.012	-0.053
(0.7,0.0)	.018	0	.271	0.003	-0.049
(0.9,0.0)	.019	0	.284	-0.006	-0.045
(1.1,0.0)	.010	0	.347	-0.011	-0.054
(0.2,0.5)	.020	.39	.209	0.002	-0.0002
(0.4,0.4)	.019	.30	.229	0.007	-0.019
(0.5,0.2)	.015	.16	.248	-0.006	-0.042
(0.6,0.6)	.028	.35	.242	-0.044	0.018

Finally, k_n was decreased to 0.4 for Run 6.2d, resulting in an average electric field of over 3.0. The line width of the strongest mode is now slightly over 33%, and the high-k modes are quite broad. The k-spectrum has become nearly isotropic.

The nonlinear growth rate is an excellent measurement of the characteristics of the frequency spectrum since it ties in directly with the energy balance for the model. Tables 6.4–6.7 gave measurements of the nonlinear growth rate for only a few modes as it is very expensive to calculate the frequency spectrum. However we can use Parseval's Theorem to calculate the nonlinear growth rate directly in the simulation code:

$$\begin{aligned}
\gamma_{\mathbf{k}}^{NL} &= -\frac{\delta_{\mathbf{k}}}{E_{\mathbf{k}}} \sum_{\omega} \omega \left(\omega - k_y\right) \left|\phi_{\mathbf{k}_\omega}\right|^2 \\
&= -\frac{\delta_{\mathbf{k}}}{E_{\mathbf{k}}} \sum_{\omega} i\omega \phi_{\mathbf{k}_\omega}^{*} \left(-i\omega + ik_y\right) \phi_{\mathbf{k}_\omega}
\end{aligned}$$

Table 6.6: *Frequency Characteristics for Run 6.2c*

(k_x, k_y)	$E_\mathbf{k}$	$\omega_\mathbf{k}$	$\Delta\omega$	$\delta\omega$	$\gamma_\mathbf{k}^{NL}/\delta_\mathbf{k}$
(0.0,0.1)	.018	.10	.031	-0.0009	-0.0008
(0.0,0.3)	.085	.28	.065	-0.0007	0.0025
(0.0,0.5)	.194	.40	.079	-0.0036	0.028
(0.0,0.6)	.135	.44	.113	-0.024	0.047
(0.0,0.7)	.095	.47	.146	-0.050	0.065
(0.0,0.9)	.030	.50	.253	-0.120	0.074
(0.0,1.1)	.007	.50	.400	-0.181	0.040
(0.1,0.0)	.038	0	.03	0.001	-0.0009
(0.3,0.0)	.052	0	.08	0.004	-0.007
(0.5,0.0)	.112	0	.10	0.009	-0.009
(0.6,0.0)	.096	0	.13	-0.002	-0.013
(0.7,0.0)	.063	0	.17	-0.0003	-0.019
(0.9,0.0)	.016	0	.30	-0.009	-0.048
(1.1,0.0)	.004	0	.40	-0.003	-0.071
(0.2,0.5)	.153	.39	.097	-0.012	0.029
(0.4,0.4)	.136	.30	.106	-0.009	0.015
(0.5,0.2)	.118	.16	.108	-0.004	-0.003
(0.6,0.6)	.033	.35	.238	-0.082	0.019

$$= -\frac{\delta_\mathbf{k}}{E_\mathbf{k}}\frac{1}{T}\sum_{t=0}^{T}\frac{\partial\phi_\mathbf{k}^*}{\partial t}\left(\frac{\partial\phi_\mathbf{k}}{\partial t}+ik_y\phi_\mathbf{k}\right) \tag{6.9}$$

$$\tag{6.10}$$

Equation (6.9) is used in the code to calculate the nonlinear growth rate. Figs. 6.1–6.4 show the average nonlinear growth rate for Runs 6.2a–6.2d. Fig. 6.1 shows just how strong a damping force the nonadiabatic electrons can be—the nonlinear growth rate at the edge of the spectrum is so large ($\approx$ 5–20) that the details of the low-k growth rate are completely invisible on the same scale. In Figs. 6.2–6.3, the peak growth rate is not much different from the linear value. In Fig. 6.4 it is moderately lower than the linear value. Another important feature of these plots is the large anisotropy at small to moderate wave numbers, with strong damping at low-k along the k_x-axis, and a positive growth rate extending out to fairly high-k along the k_y axis.

Table 6.7: *Frequency Characteristics for Run 6.2d*

(k_x, k_y)	$E_{\mathbf{k}}$	$\omega_{\mathbf{k}}$	$\Delta\omega$	$\delta\omega$	$\gamma^{NL}_{\mathbf{k}}/\delta_{\mathbf{k}}$
(0.0,0.1)	.058	.10	.042	0.0026	-0.0020
(0.0,0.3)	.152	.28	.115	0.012	-0.009
(0.0,0.5)	.248	.40	.142	-0.021	0.020
(0.0,0.6)	.252	.44	.158	-0.043	0.041
(0.0,0.7)	.120	.47	.222	-0.046	0.046
(0.0,0.9)	.028	.50	.465	-0.14	-0.013
(0.0,1.1)	.008	.50	.603	-0.25	-0.068
(0.1,0.0)	.062	0	.049	-0.0004	-0.002
(0.3,0.0)	.077	0	.147	-0.007	-0.020
(0.5,0.0)	.171	0	.163	-0.003	-0.021
(0.6,0.0)	.194	0	.166	-0.006	-0.020
(0.7,0.0)	.114	0	.205	0.003	-0.028
(0.9,0.0)	.027	0	.325	-0.007	-0.059
(1.1,0.0)	.007	0	.418	-0.001	-0.079
(0.2,0.5)	.217	.39	.157	-0.025	0.019
(0.4,0.4)	.198	.30	.162	-0.026	0.006
(0.5,0.2)	.182	.155	.160	-0.017	-0.013
(0.6,0.6)	.044	.35	.307	-0.020	-0.003

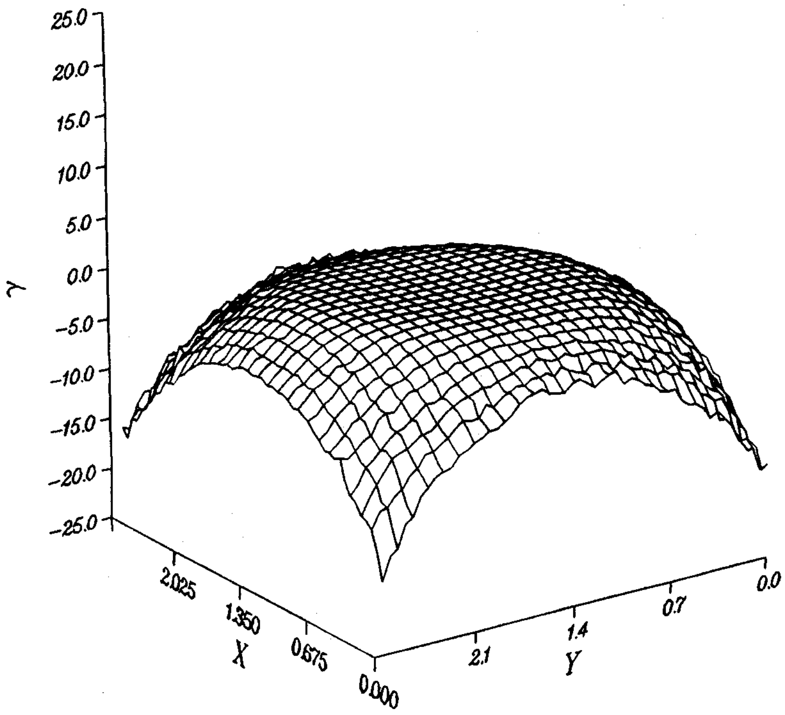

Figure 6.1: *Nonlinear growthrate, $\gamma_{\mathbf{k}}^{NL}$, for Run 6.2a.*

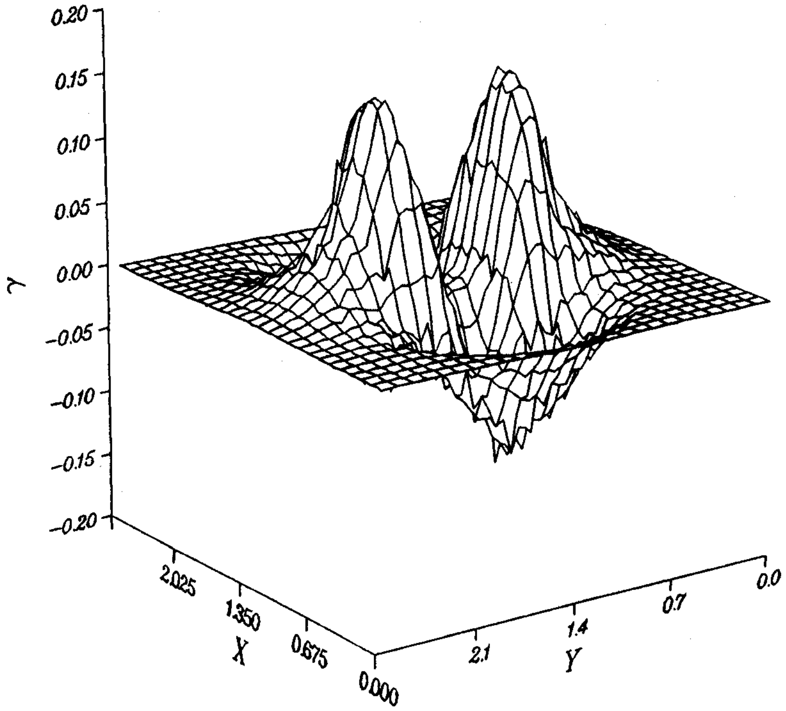

Figure 6.2: *Nonlinear growthrate,* $\gamma_{\mathbf{k}}^{NL}$*, for Run 6.2b.*

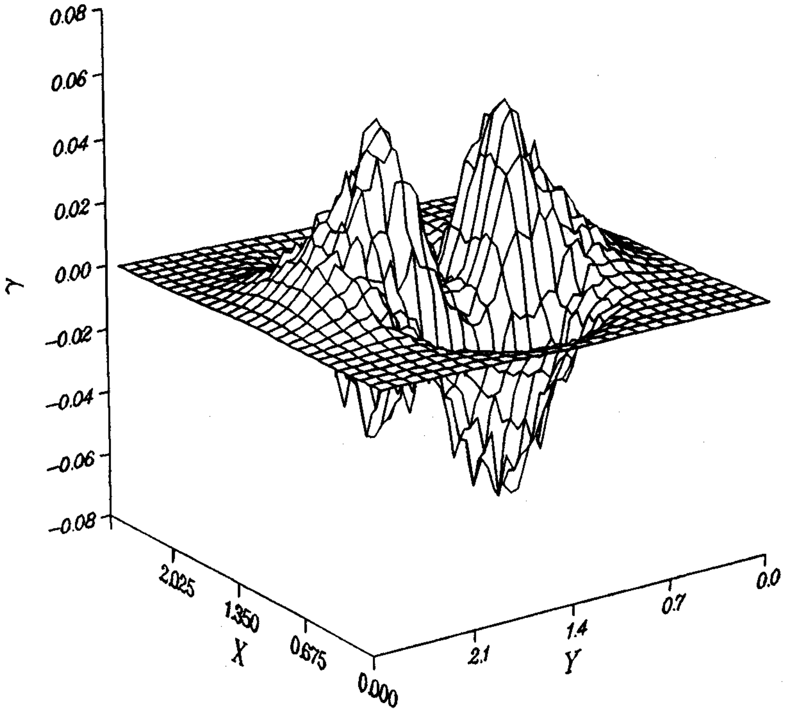

Figure 6.3: *Nonlinear growthrate, $\gamma_{\mathbf{k}}^{NL}$, for Run 6.2c.*

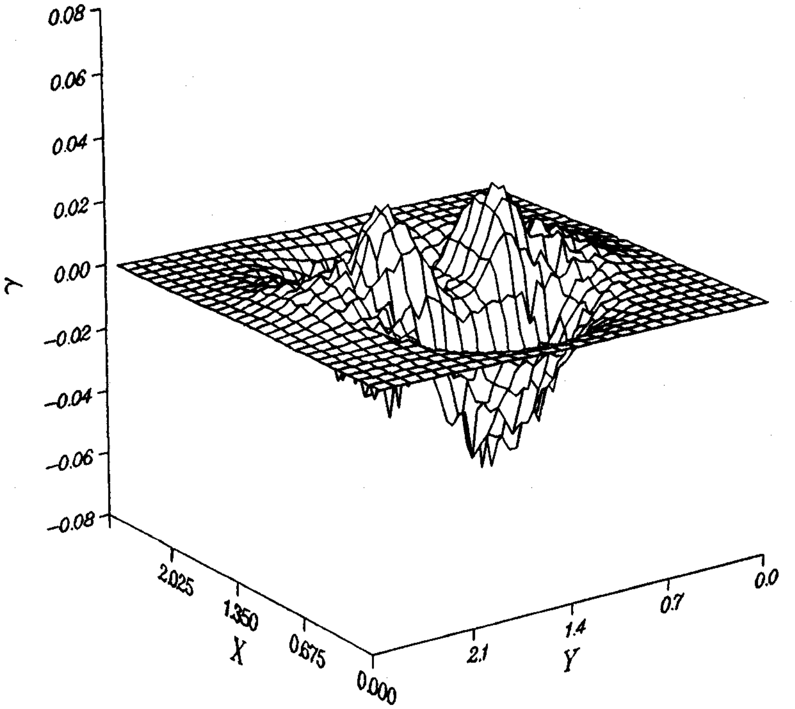

Figure 6.4: *Nonlinear growthrate,* $\gamma_{\mathbf{k}}^{NL}$, *for Run 6.2d.*

6.2.1 Comparison with Experimental Observations

The spectral data reviewed in the last section indicated that the line widths for the strongest modes were only moderately broad, with the width increasing as the electric field and the linear growth rate were increased. These widths are not consistent with experimental data taken from tokamaks where the frequency spectrum is often characterized by $\Delta\omega \geq \omega$.

Such broad widths are not possible with this nonadiabatic electron model. Let us calculate the frequency broadening required to stabilize a mode, assuming that the shift is negligible (which is supported by the above data). We then have

$$\gamma_{\mathbf{k}}^{NL} = -\frac{\delta_{\mathbf{k}}}{1+k^2}(\Delta\omega_{\mathbf{k}}{}^2 + \bar{\omega}_{\mathbf{k}}(\bar{\omega}_{\mathbf{k}} - k_y)) = 0,$$

or, setting $\bar{\omega}_{\mathbf{k}} = \omega_{\mathbf{k}}$,

$$\begin{aligned}\Delta\omega_{\mathbf{k}}{}^2 &= -\omega_{\mathbf{k}}(\omega_{\mathbf{k}} - k_y) \\ &= -\frac{k_y}{1+k^2}\left(\frac{k_y}{1+k^2} - k_y\right) \\ &= k^2\omega_{\mathbf{k}}^2\end{aligned}$$

Thus we see that a mode will be damped if $\Delta\omega_{\mathbf{k}} > k\omega_{\mathbf{k}}$. Our simulations show that the energy containing modes usually have $0.5 < k < 1.0$. Some of these modes must have a positive growth rate in order for the system to reach a saturated state. These modes, then, cannot have the broad spectrum characteristic of the experiments.

It is important to note that the problem here lies with our model for the nonadiabatic electrons, not with our treatment of the ions. The results are, indeed, very sensitive to changes in the nonadiabatic electron model, as is reflected by the strong dependence of the saturated state on the value of k_n. It is not difficult to imagine that a completely different electron model might lead to the broad spectra observed in the experiments.

6.3 Trapped Structures

The frequency and wavenumber spectra tell us nothing explicit about whether or not monopole trapped structures exist in the system. Both monopoles and waves have dispersion relations which are very similar:

$$\begin{array}{ll} \omega_{\mathbf{k}} = k_y/1 + k^2 & \text{linear waves} \\ \omega_{\mathbf{k}} = ck_y & \text{monopole vortices} \end{array}$$

where $c \sim 1/(1+\bar{k}^2)$, $\bar{k}$ being some kind of average wave vector for the monopole (see Section 5.2.1). The ω-spectrum of an isolated monopole is discrete, but if the system has many monopoles, each having a different velocity and size, then the frequency spectrum will be broadened. The broadening is further enhanced by monopole–monopole interactions. The difference between a broad spectrum of waves and a chaotic system of monopoles lies in the phase coherence of the modes. This information is completely absent from the spectrum.

The moderately broad spectra observed in Runs 6.2a–6.2d thus do not preclude the existence of trapped structures. One would expect, however, that the monopole lifetime would decrease as the spectrum broadened.

Fig. 6.5 shows the evolution of the density, ρ, for Run 6.2a, over a short period of time long after the turbulence has saturated. This run had an RMS electric field of only 1.5, which is reflected by the near lack of closed contours. Clearly, the majority of the fluid is not trapped in this case. Note, however, that there are also very large nontrapped perturbations to the density (or at least there are no closed contours visible at the resolution of our contour plot). Some of these perturbations seem to last for a fairly long time, even if they don't trap a lot of particles. A clump type turbulence theory might be well suited to this type of turbulence, although the long coherence time of some of the fluctuations might invalidate the renormalized calculation of the relative diffusion coefficient.

The * markers show positions of marker particles which are evolved (at great computational expense) with the flow. Four of the particles were purposely placed near closed contours, and the other two were placed away from closed contours. Three of the particles remained trapped for the length of the run. Fig. 6.6 shows the trajectory of two of the particles. Note that this is not indicative of the system in

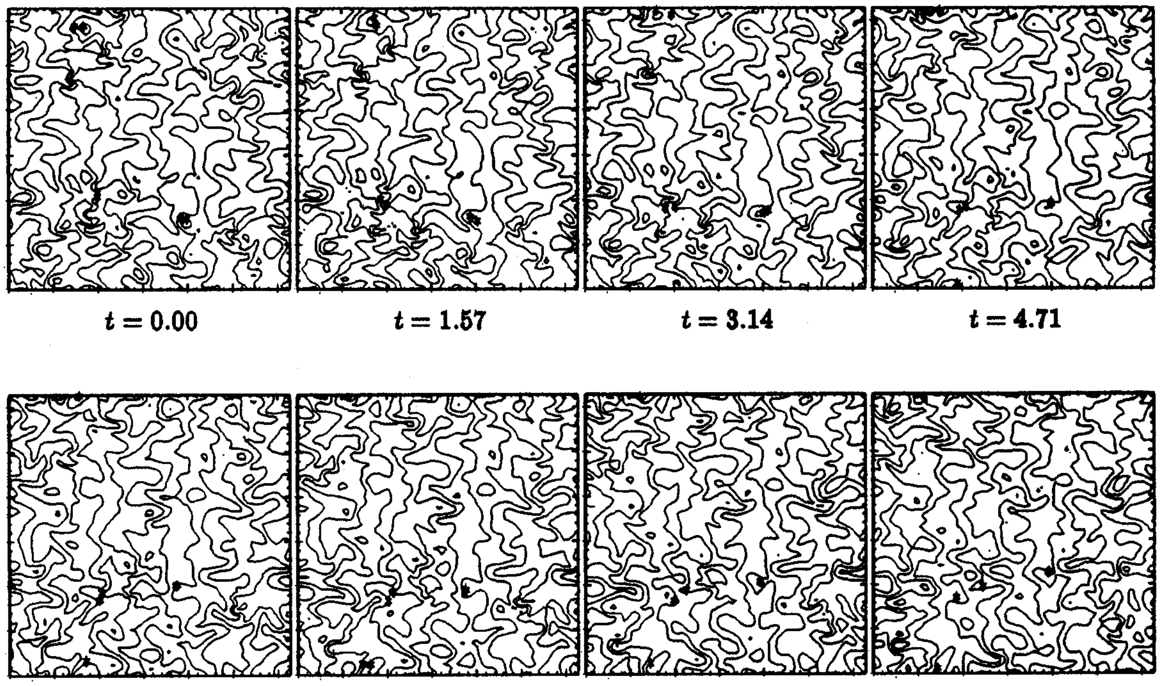

$t = 0.00$ $t = 1.57$ $t = 3.14$ $t = 4.71$

$t = 6.28$ $t = 7.85$ $t = 9.42$ $t = 12.5$

Figure 6.5: *Density evolution with marker particles (∗) for Run 6.2a.*

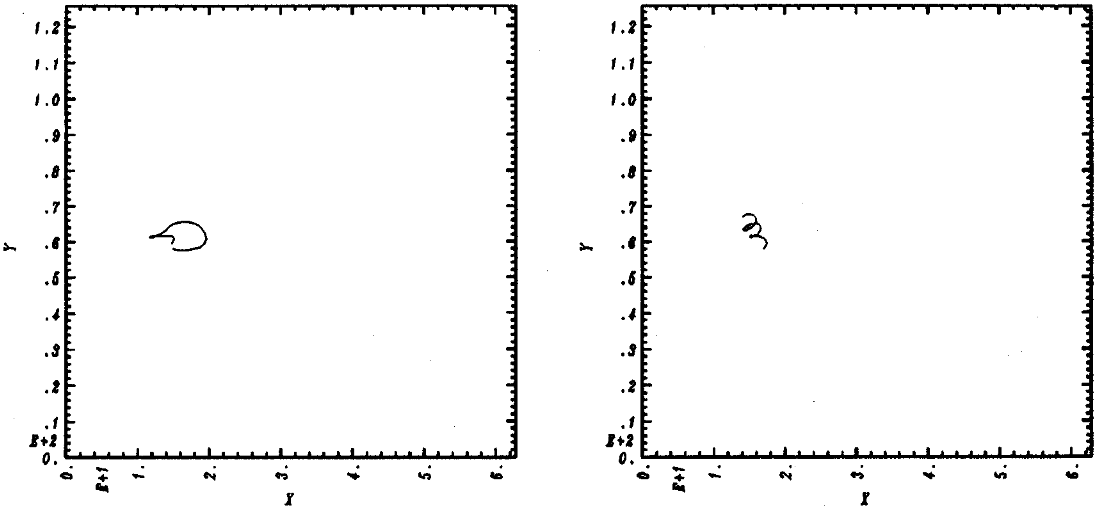

Figure 6.6: *Trapped particle trajectory for Run 6.2a.*

general—I have purposely set it up so that we'd see the trapped particles. It is obvious from Fig. 6.5 that most of the fluid particles are not trapped.

Figures 6.7–6.12 show the same information for Runs 6.2b–6.2d. As the electric field increases, the portion of the flow which is trapped obviously increases. Not only are there more trapped structures, but they are also considerably larger. It is quite clear that a renormalized turbulence theory would not be appropriate for the runs with the strongest electric field.

In each of the four runs we have found trapped structures which lasted for the full-length of the run (15.7 drift periods). The evolution of these structures is much different from the purely damped case, however. The structures change shape, and wander about in the x direction during the course of the run. Also, the trapped particle orbits are much less regular than in the cases of an isolated monopole or decaying turbulence. Certainly this is related to the increased line width in the frequency spectrum. One is tempted to say that the structure lifetime should be given by $\tau_s \approx 2\pi/\Delta\omega_{\mathbf{k}}$. For the strongest modes in Runs 6.2a–6.2d $\tau_s \approx$ 26–150. Unfortunately, our simulations did not run this long, and doing so would have been impractical. Examination of Fig. 6.11 shows that the structures can be very robust, however, surviving very strong interactions with other vortices. We have, in fact,

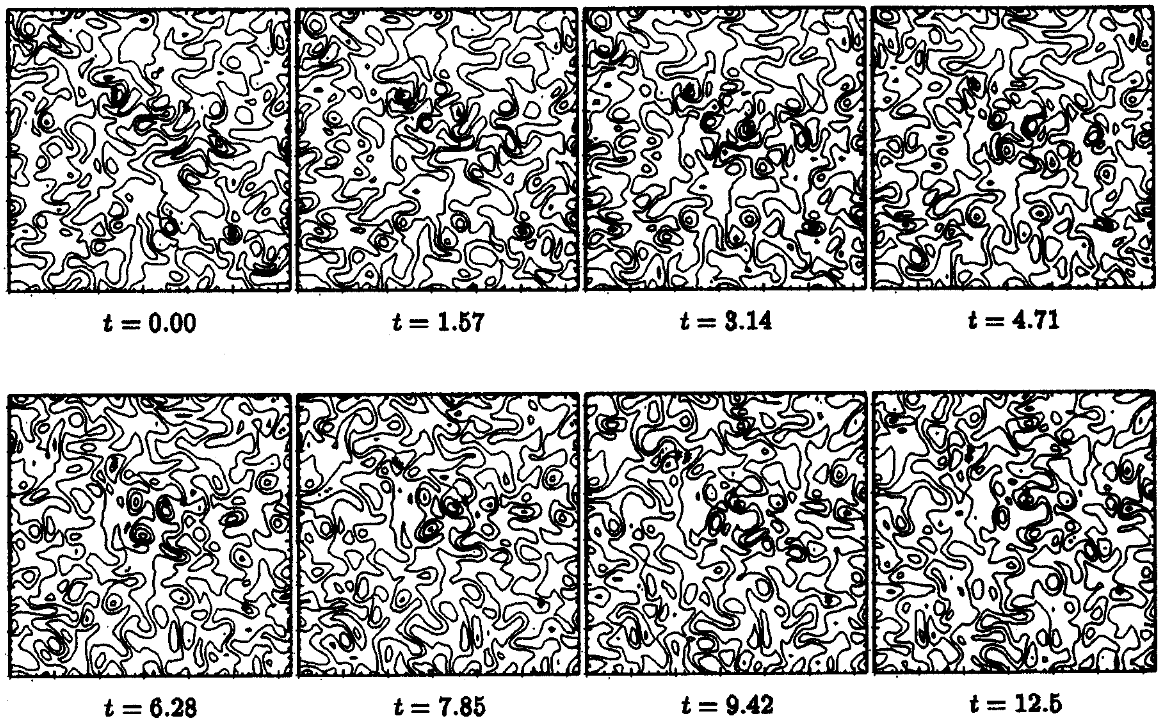

$t = 0.00$ $t = 1.57$ $t = 3.14$ $t = 4.71$

$t = 6.28$ $t = 7.85$ $t = 9.42$ $t = 12.5$

Figure 6.7: *Density evolution with marker particles (∗) for Run 6.2b.*

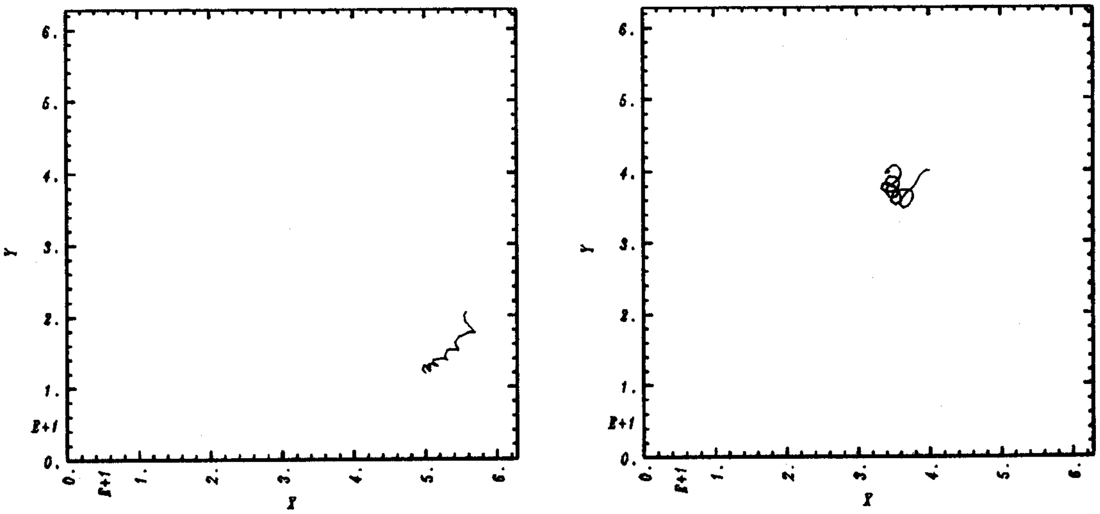

Figure 6.8: *Trapped particle trajectory for Run 6.2b.*

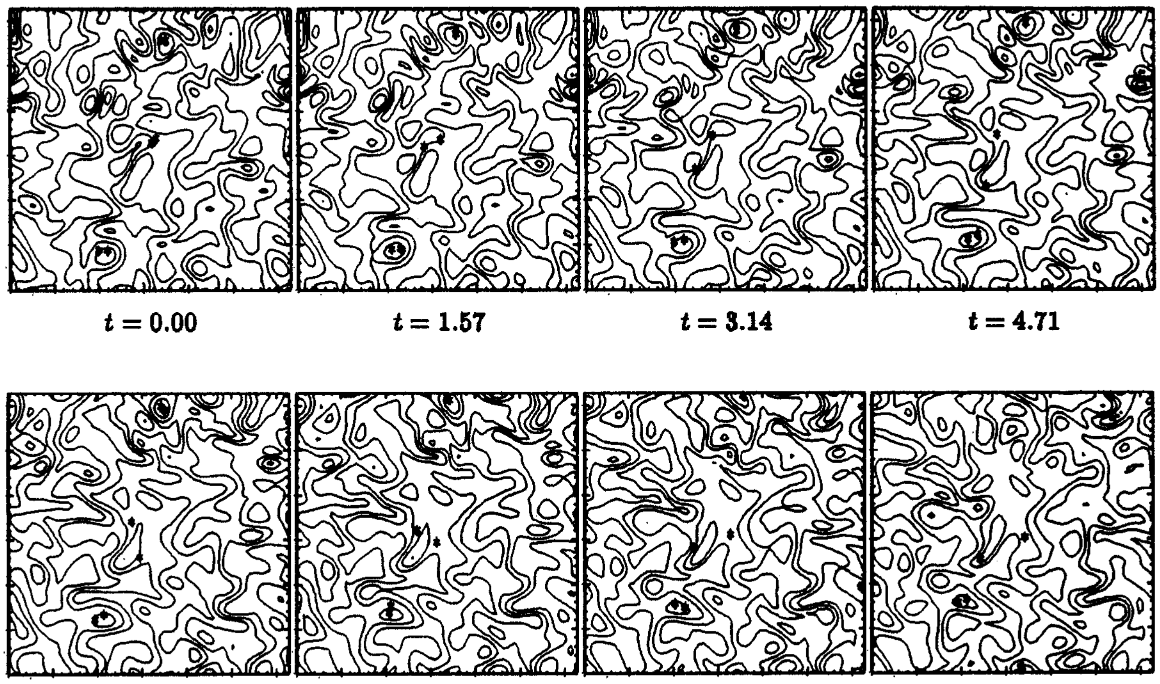
$t = 0.00$ $t = 1.57$ $t = 3.14$ $t = 4.71$

$t = 6.28$ $t = 7.85$ $t = 9.42$ $t = 12.5$

Figure 6.9: *Density evolution with marker particles (*) for Run 6.2c.*

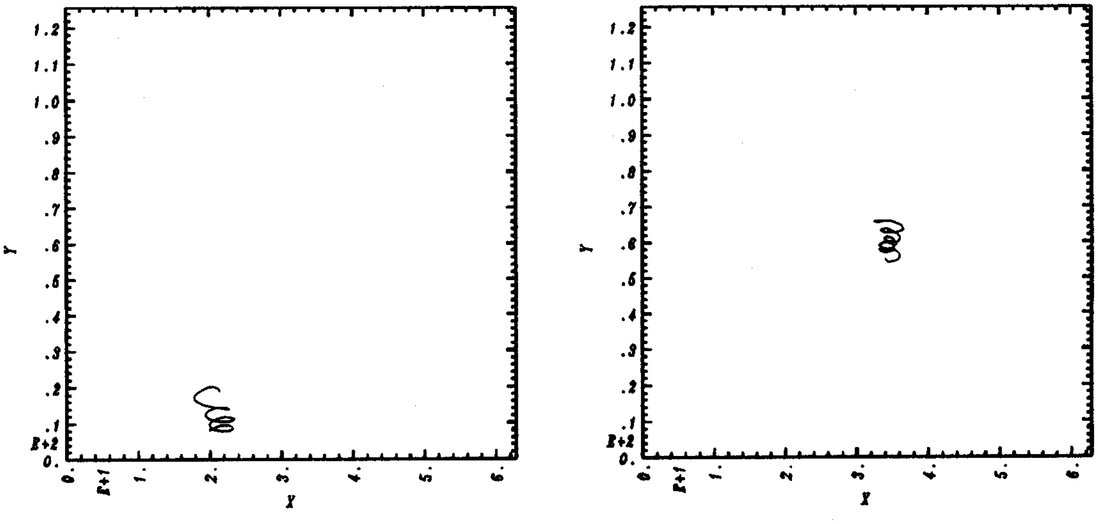

Figure 6.10: *Trapped particle trajectory for Run 6.2c.*

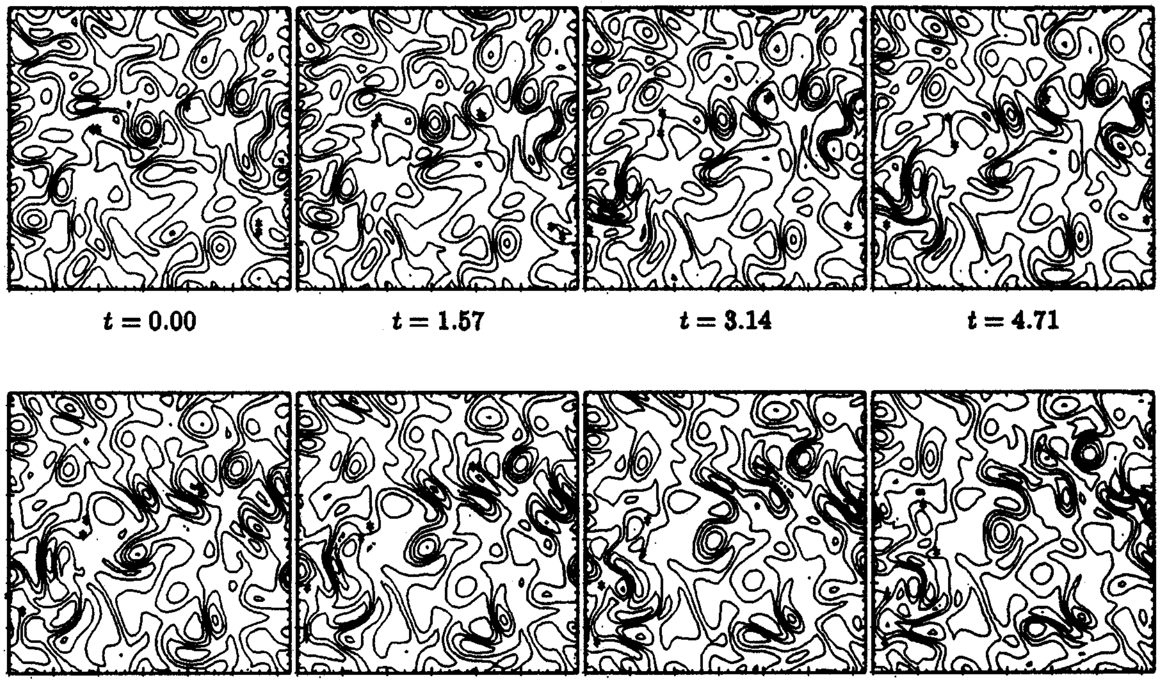

$t = 0.00$ $t = 1.57$ $t = 3.14$ $t = 4.71$

$t = 6.28$ $t = 7.85$ $t = 9.42$ $t = 12.5$

Figure 6.11: *Density evolution with marker particles (*) for Run 6.2d.*

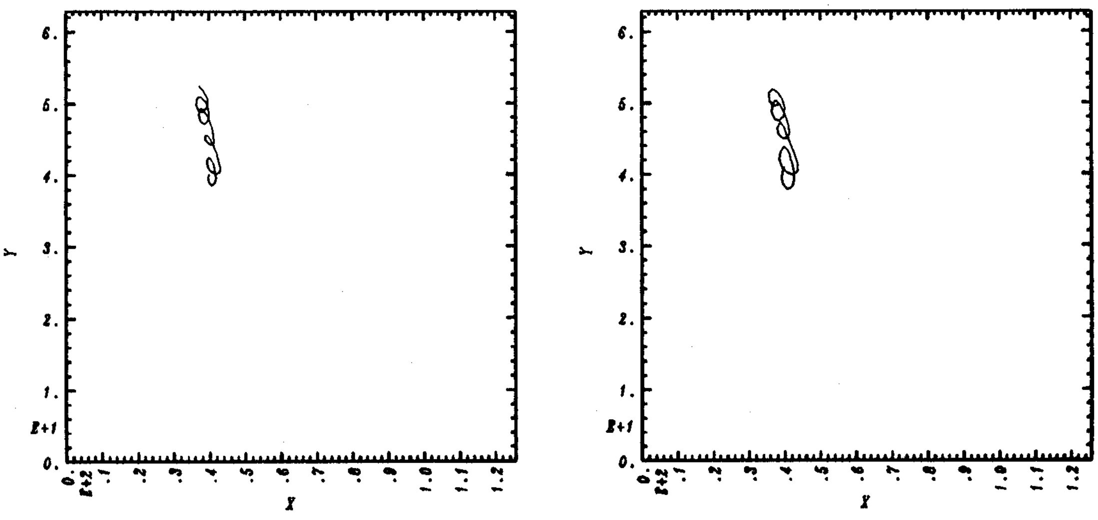

Figure 6.12: *Trapped particle trajectory for Run 6.2d.*

observed particles trapped for more than 20 trapping times for a run very similar to Run 6.2d. In these runs, where the electric field is quite strong, the width of the frequency spectrum seems to be more related to the time scale over which the vortices get perturbed than the vortex life time. However, longer runs, preferably with higher resolution, are needed to confirm this hypothesis.

6.4 Conclusions

The addition of the nonadiabatic electron model developed in Chapter 2 has several important effects on the evolution of the turbulence. The nonadiabatic electrons contribute in an important way to the saturation of the turbulence. This saturated state is characterized by a broader frequency spectrum than in the case of decaying turbulence. In spite of this broader spectrum, however, long lived trapped structures still evolve in the flow.

The most significant effect of the nonadiabatic electrons seems to be the strong dissipation they provide for high-k modes and modes along the k_x-axis. This dissipation mechanism is quite complex and is responsible for the somewhat nonintuitive result that increasing the strength of the nonadiabatic electron term, which is usually thought of as a source term, results in a decrease in the saturation energy. This is a good example of how our intuition based on linear theory can lead us far astray when trying to understand a strongly nonlinear problem. Although I don't make any pretense of trying to explain tokamak transport with this model, it could be just such nonlinear effects as these which are responsible for certain nonintuitive observations about anomalous transport, such as the increase in the neo-Alcator energy confinement time with density.

Although the frequency spectra were found to be quite broad at high-k, in the energy containing region, $k < 1$, the spectral line widths were only narrow to moderately broad. This result is qualitatively different from experimental observations taken from tokamaks. It was shown that this result is an inherent shortcoming of the model—a stationary state cannot be maintained with all the modes having $\Delta\omega \geq \omega$.

A few additional trends were noticed: The saturation levels depend only weakly on the magnitude of the hyperviscosity coefficient, ν_4. This is a comforting result, since the viscous models for this problem are really quite unjustifiable. Most of the saturation values depended strongly on the maximum linear growthrate, γ^L_{max}, except for the RMS electric field. This quantity was found to depend only on the nonadiabatic cutoff, k_n. Thus, for a given k_n, the system seems to have a critical electric field that is very important in the saturation process.

In all cases, the saturated electric field was sufficiently high for trapping to occur and, in spite of the broadened frequency spectrum, coherent trapped structures were observed in many runs. This is counter to speculation by some authors that driving the system in the energy containing region would destroy any coherent structures that might otherwise develop [54, 71].

Although trapping occurred in all of the runs, it was not a dominant effect in all cases—specifically, those with $k_n = \infty$. However the density contours still exhibited very strong nontrapped perturbations. As the electric field increased, so did the dominance of trapped structures. A clump type turbulence theory might be well suited to the turbulence of the runs which had only a small amount of trapping, although the long coherence time of some of the nontrapped fluctuations might invalidate the renormalized calculation of the relative diffusion coefficient. For the runs with a stronger electric field, and much more trapping, it is clear that the renormalization should be invalid.

The observation that saturation occurs at a relatively constant electric field level, independent of γ^L_{max} and ν_4, and large enough to support trapping, could indicate that the formation of coherent structures plays an important role in the saturation of the turbulence. However more work is required to support this hypothesis.

The fact that the nonadiabatic electron model plays such an important role in the qualitative nature of the turbulence shows that close attention should be paid to how such effects are included. In some ways this makes my model inconsistent, since several effects were neglected which might be just as important as the nonadiabatic electron terms which we have tried to simulate.

Simulation of a real system was not the goal of this thesis, though. Rather we were interested in studying trapped structures in a driven-damped system with the most realistic nonadiabatic electron model that we could derive in two dimensions. Our model was perfectly suitable for this task. Indeed it would be interesting to compare renormalized turbulence theories to this model, especially for runs such as Run 6.2d which exhibited very strong trapping along with a fairly broad frequency spectrum. We leave this problem to future work.

Appendix A

Fourier Transform Conventions

The following conventions are used to in this thesis: The Fourier transform of a field $\phi(\mathbf{x}, t)$ is given by

$$\hat{\phi}(\mathbf{k}, \omega) = \sum_{\mathbf{x},t} \phi(\mathbf{x}, t) e^{-i\mathbf{k}\cdot\mathbf{x}+i\omega t}, \tag{A.1}$$

and the inverse transform is

$$\phi(\mathbf{x}, t) = \sum_{\mathbf{k},\omega} \hat{\phi}(\mathbf{k}, \omega) e^{i\mathbf{k}\cdot\mathbf{x}-i\omega t}. \tag{A.2}$$

Here $\sum$ is shorthand for the appropriate set of integral/summations. For example, if we are working on a square domain

$$-L \leq x, y \leq L$$

then

$$\hat{\phi}(m, n, t) = \int_{-\infty}^{\infty} \left(\int_{-L}^{L} \int_{-L}^{L} \phi(x, y, t) e^{-i(k_m x + k_n y - \omega t)}\, dy\, dx \right) dt, \tag{A.3}$$

where

$$k_j = 2\pi j / L, \qquad j = -\infty, \ldots, -1, 0, 1, \ldots, \infty. \tag{A.4}$$

Similarly the inverse is

$$\phi(x, y, t) = \int_{-\infty}^{\infty} \left(\sum_{m,n=-\infty}^{\infty} \hat{\phi}(m, n, t) e^{i(k_m x + k_n y - \omega t)} \right) dt. \tag{A.5}$$

For compactness we will often denote the Fourier transform of $\phi(\mathbf{x}, t)$ by $\phi_{\mathbf{k},\omega}$.

Bibliography

[1] Akira Hasegawa and Kunioki Mima. Stationary spectrum of strong turbulence in magnetized nonuniform plasma. *Phys. Rev. Lett.*, 39(4):205–208, July 1977.

[2] Akira Hasegawa and Kunioki Mima. Pseudo-three-dimensional turbulence in magnetized nonuniform plasma. *Phys. Fluids*, 21(1):87–92, January 1978.

[3] Paul Terry and Wendell Horton. Stochasticity and the random phase approximation for three electron drift waves. *Phys. Fluids*, 25(3):491–501, March 1982.

[4] P. W. Terry and W. Horton. Drift wave turbulence in low-order k space. *Phys. Fluids*, 26(1):106–112, January 1983.

[5] Wendell Horton. Statistical properties and correlation functions for drift waves. *Phys. Fluids*, 29(5):1491–1503, May 1986.

[6] W. Horton. Drift wave vortices and anomalous transport. Technical Report IFSR #312, Institute for Fusion Studies, The University of Texas at Austin, April 1988.

[7] R. E. Waltz. Numerical study of drift-wave turbulence with simple models for wave-wave nonlinear coupling. *Phys. Fluids*, 26(1):169–179, January 1983.

[8] Paulett C. Liewer. Measurements of microturbulence in tokamaks and comparison with theories of turbulence and anomalous transport. *Nuc. Fusion*, 25(5):543–621, 1985.

[9] Thomas H. Dupree. A perturbation theory for strong plasma turbulence. *Phys. Fluids*, 9(9):1773–1782, September 1966.

[10] T. H. Dupree. Nonlinear theory of drift-wave turbulence and enhanced diffusion. *Phys. Fluids*, 10(5):1049–1055, May 1967.

[11] Robert H. Kraichnan. The structure of isotropic turbulence at very high Reynolds numbers. *J. Fluid Mech.*, 5:497–543, 1959.

[12] B. B. Kadomtsev. *Plasma Turbulence.* Academic Press, London - New York, 1965.

[13] Thomas H. Dupree. Theory of phase space density granulation in plasma. *Phys. Fluids*, 15(2):334–344, February 1972.

[14] Thomas H. Dupree. Role of clumps in drift-wave turbulence. *Phys. Fluids*, 21(5):783–792, May 1978.

[15] Thomas H. Dupree and David J. Tetreault. Renormalized dielectric function for collisionless drift wave turbulence. *Phys. Fluids*, 21(3):425–433, March 1978.

[16] Teymour Boutros-Ghali and Thomas H. Dupree. Theory of two-point correlation function in Vlasov plasma. *Phys. Fluids*, 24(10):1839–1858, October 1981.

[17] Teymour Boutros-Ghali and Thomas H. Dupree. Theory of nonlinear ion-electron instability. *Phys. Fluids*, 25(5):874–883, May 1982.

[18] John A. Krommes and Robert G. Kleva. Aspects of a renormalized weak plasma turbulence theory. *Phys. Fluids*, 22(11):2168–2177, November 1979.

[19] Robert H. Kraichnan. Dynamics of nonlinear stochastic systems. *J. Math. Phys.*, 2:124–148, 1961.

[20] Steven A. Orszag and Robert H. Kraichnan. Model equations for strong turbulence in a Vlasov plasma. *Phys. Fluids*, 10(8):1720–1736, August 1967.

[21] Steven A. Orszag. Lectures on the statistical theory of turbulence. In R. Balian and J.-L. Peube, editors, *Fluid Dynamics: Les Houches 1973*, pages 235–374, New York, 1974. Gordon and Breach.

[22] C. M. Surko and R. E. Slusher. Waves and turbulence in a tokamak fusion plasma. *Science*, 221:817–822, August 1983.

[23] C. M. Surko. Scale length in microturbulence in tokamak plasmas. *Comments Plasma Phys. and Cont. Nucl. Fusion*, 10(6):265–269, 1987.

[24] F. L. Hinton and C. W. Horton, Jr. Amplitude limitation of a collisional drift wave instability. *Phys. Fluids*, 14(1):116–123, January 1971.

[25] B. D. Fried and S. D. Conte. *The Plasma Dispersion Function.* Academic, New York, 1961.

[26] J. D. Meiss and W. Horton. Solitary drift waves in the presence of magnetic shear. *Phys. Fluids*, 26(4):990–997, April 1983.

[27] V. I. Petviashvili and O. A. Pokhotelov. Solitary vortices in plasmas. *Sov. J. Plasma Phys.*, 12(9):651–661, September 1986.

[28] Steven A. Orszag. Numerical simulation of incompressible flows within simple boundries: accuracy. *Journal of Fluid Mechanics*, 49(1):75–112, 1971.

[29] Steven A. Orszag. Numerical simulation of incompressible flows within simple boundries. I. Galerkin (spectral) representations. *Studies in Applied Mathematics*, L(4):293–327, December 1971.

[30] David Gottlieb and Steven A. Orszag. *Numerical Analysis of Spectral Methods: Theory and Application.* SIAM, Philadelphia, Pennsylvania, 1977.

[31] David Gottlieb, M. Yousuff Hussaini, and Steven A. Orszag. Theory and applications of spectral methods. In Robert G. Voigt, David Gottlieb, and M. Yousuff Hussaini, editors, *Spectral Methods for Partial Differential Equations*, pages 1–54, Philadelphia, 1984. ICASE, SIAM.

[32] G. K. Batchelor. *The Theory of Homogenous Turbulence.* Cambridge University Press, Cambridge, England, 1953.

[33] D. C. Leslie. *Developments in the Threory of Turbulence.* Oxford University Press, London, England, 1973.

[34] Steven A. Orszag. Numerical methods for the simulation of turbulence. *Phys. Fluids Supplement II*, 12:250–257, 1969.

[35] Steven A. Orszag and G. S. Patterson, Jr. Numerical simulation of three-dimensional homogeneous isotropic turbulence. *Phys. Rev. Lett.*, 28(2):76–79, January 1972.

[36] Douglas G. Fox and Steven A. Orszag. Pseudospectral approximation to two-dimensional turbulence. *Journal of Computational Physics*, 11:612–619, 1973.

[37] C. A. J. Fletcher. *Computational Galerkin Methods.* Springer-Verlag, New York, 1984.

[38] James W. Cooley and John W. Tukey. An algorithm for the machine calculation of complex Fourier series. *Math. Comp.*, 19:297–301, 1965.

[39] J. W. Cooley, P. A. Lewis, and P. D. Welch. Application of the Fast Fourier Transform to computation of Fourier integrals, Fourier series, and convolution integrals. *IEEE Trans. Audio Electroacoust.*, AU-15(2):79–84, June 1967.

[40] J. W. Cooley, P. A. Lewis, and P. D. Welch. The Finite Fourier Transform. *IEEE Trans. Audio Electroacoust.*, AU-17(2):77–85, June 1969.

[41] J. W. Cooley, P. A. Lewis, and P. D. Welch. The Fast Fourier Transform algorithm: programming considerations in the calculation of sine, cosine, and Laplace transforms. *J. Sound Vib.*, 12(3):315–337, 1970.

[42] Steven A. Orszag. Comparison of pseudospectral and spectral approximation. *Studies in Applied Mathematics*, LI(3):253–259, September 1972.

[43] V. D. Larichev and G. M. Reznik. Nonnlinear Rossby waves on a large-scale current. *Oceanologia*, 15:113–116, 1975.

[44] G. L. Lamb, Jr. *Elements of Soliton Theory.* Pure and Applied Mathematics. Wiley Interscience, New York, 1980.

[45] Mark J. Ablowitz and Harvey Segur. *Solitons and the Inverse Scattering Transform.* SIAM Studies in Applied Mathematics. SIAM, Philadelphis, PA, 1981.

[46] Shalom Eliezer. A stroll through soliton theory (lecture notes). Technical Report IFSR #164, Institute for Fusion Studies, Univ. of Texas, Austin, January 1985.

[47] M. Makino, T. Kamimura, and T. Taniuti. Dynamics of two-dimensional solitary vortices in a low-β plasma with convection motion. Technical Report IPPJ-496, Institute for Plasma Physics, Nagoya University, Nagoya Japan, December 1980.

[48] James C. McWilliams and Norman J. Zabusky. Interaction of isolated vortices I: Modons colliding with modons. *Geophys. Astrophys. Fluid Dynamics*, 19:207–227, 1982.

[49] J. D. Meiss and W. Horton. Fluctuation spectra of a drift wave soliton gas. Technical Report IFSR #45, Institute for Fusion Studies, 1982.

[50] J. D. Meiss. Solitons in turbulent flow. Technical Report IFSR #82, Institute for Fusion Studies, 1983.

[51] G. R. Flierl, V. D. Larichev, J. C. McWilliams, and G. M. Reznik. The dynamics of baroclinic and barotropic solitary eddies. *Dynamics of Atmospheres and Oceans*, 5:1–41, 1980.

[52] V. D. Larichev and G. M. Reznik. Strongly nonlinear Rossby waves. *Oceanologia*, 15:213–217, 1975.

[53] V. D. Larichev and G. M. Reznik. Strongly nonlinear, two-dimensional isolated Rossby waves. *Oceanologia*, 16:547–550, 1976.

[54] Akira Hasegawa. Self-organization processes in continuous media. *Advances in Physics*, 34(1):1–42, 1985.

[55] E. W. Laedke and K. H. Spatschek. Dynamical properties of drift vortices. *Phys. Fluids*, 28(3):1008–1010, March 1985.

[56] E. W. Laedke and K. H. Spatschek. Drift vortices in inhomogeneous plasmas: Stationary states and stability criteria. *Phys. Fluids*, 31(6):1492–1498, June 1988.

[57] V. I. Gordin and V. I. Petviashvili. Lyapunov-stable quasigeostrophic vortices. *Sov. Phys. Dokl*, 30(12):1004–1006, December 1986.

[58] J. C. McWilliams, G. R. Flierl, V. D. Larichev, and G. M. Riznik. Numerical studies of barotropic modons. *Dynamics of Atmospheres and Oceans*, 5:219–238, 1981.

[59] James C. McWilliams. Interactions of isolated vortices II: Modon generation by monopole collision. *Geophys. Astrophys. Fluid Dynamics*, 24:1–22, 1983.

[60] James C. McWilliams and Glenn R. Flierl. On the evolution of isolated, nonlinear vortices. *J. Phys. Oceanography*, 9:1155–1182, November 1979.

[61] Robert H. Kraichnan and David Montgomery. Two-dimensional turbulence. *Rep. Prog. Phys.*, 43:547–619, 1980.

[62] Robert H. Kraichnan. Inertial ranges in two-dimensional turbulence. *Phys. Fluids*, 10(7):1417–1423, July 1967.

[63] C. E. Seyler, Jr. et al. Two-dimensional turbulence in inviscid fluids or guiding center plasmas. *Phys. Fluids*, 18(7):803–813, July 1975.

[64] David Fyfe and David Montgomery. Statistical formulation of one-dimensional electron fluid turbulence. *Phys. Fluids*, 21(3):316–326, March 1978.

[65] Lawrence C. Kells and Steven A. Orszag. Randomness of low-order models of two-dimensional inviscid dynamics. *Phys. Fluids*, 21(2):162–168, February 1978.

[66] David Fyfe and David Montgomery. Possible inverse cascade behavior for drift-wave turbulence. *Phys. Fluids*, 22(2):246–248, February 1979.

[67] David Montgomery and Leaf Turner. Two-dimensional electrostatic turbulence with variable density and pressure. *Phys. Fluids*, 23(2):264–268, February 1980.

[68] Richard C. Tolman. *The Principles of Statistical Mechanics.* Dover, New York, 1938.

[69] Thomas H. Dupree. Theory of phase-space density holes. *Phys. Fluids*, 25(2):277–289, February 1982.

[70] Thomas H. Dupree. To be published. General discussion of entropy in nonequilibrium systems., 1989.

[71] James C. McWilliams. The emergence of isolated coherent vortices in turbulent flow. *J. Fluid Mech.*, 146:21–43, 1984.